ESC-TR-97-063

Project Report
STK-249
Volume II

# Proceedings of the 1997 Space Control Conference

L.B. Spence
Editor

DTIC QUALITY INSPECTED

25–27 March 1997

## Lincoln Laboratory

MASSACHUSETTS INSTITUTE OF TECHNOLOGY

*LEXINGTON, MASSACHUSETTS*

19971023 013

This technical report has been reviewed and is approved for publication.

FOR THE COMMANDER

Gary Tatungian
Administrative Contracting Officer
Directorate of Contracted Support Management

## MASSACHUSETTS INSTITUTE OF TECHNOLOGY
### LINCOLN LABORATORY

## PROCEEDINGS OF THE 1997
## SPACE CONTROL CONFERENCE

PROJECT REPORT STK-249
VOLUME II

25–27 MARCH 1997

The fifteenth Annual Space Control Conference (formerly called Space
Surveillance Workshop) held on 25–27 March 1997 was co-hosted by
MIT Lincoln Laboratory and Phillips Laboratory and provided a forum
for space control issues. This *Proceedings* documents some of the presen-
tations, with minor changes where necessary.

LEXINGTON                                                    MASSACHUSETTS

# PREFACE

The Fifteenth Annual Space Control Conference sponsored by ESC was held on 25, 26 and 27 March 1997. The purpose of this series of conferences is to provide a forum for the presentation and discussion of space surveillance issues.

These *Proceedings* document presentations from this conference. Volume I contains those papers that were received in time for pre-conference publication. Volume II contains those papers that were not received in time for pre-conference publication. The papers contained were reproduced directly from copies supplied by their authors (with minor mechanical changes where necessary). It is hoped that these publications will enhance the utility of the conference.

Dr. Lee B. Spence
Editor

# TABLE OF CONTENTS

An Overview of the Space Surveillance Performance Analysis Tool (SSPAT)

R.B. Teets (SenCom Corporation), J.G. Miller (MITRE Corporation)

# Introduction

SSPAT is a prototype set of tools developed jointly by SenCom and MITRE Corporations to exploit, manipulate and display a large amount of Space Surveillance historical data captured and stored each day on the 1CACS local network of SGI workstations. These data include the satellite catalog data, radar cross section (rcs) data, observations, element sets, sensor tasking, solar flux, and a myriad of data derived from these raw data.

SSPAT is intended to enable an analyst to retrieve and display data which provide insight into the workings and performance of the various parts of the Space Surveillance Network. Much emphasis was placed on developing data which could help answer the traditionally tough questions frequently asked:

1.  What is the quality and how complete is the space catalog?
2.  How good are the observation data provided by the space surveillance sensors, quality as well as quantity?
3.  How much does a sensor contribute to the space catalog?
4.  What is the impact of a single sensor on the overall space surveillance process?
5.  How well does a sensor respond to its metric tasking?
6.  How good (appropriate) is the sensor tasking produced by the SPADOC Tasker and how does the tasking affect the space catalog?

SSPAT provides the analyst with data to uncover problems with individual satellite element sets, or satellites grouped by orbit class. The analyst is provided with several lists of objects requiring manual intervention.

SSPAT also provides feedback on the observation routing process, identifying problems with either sensor or SPADOC identification of the appropriate object number for a track of observations. The analyst can use the information to correctly file up those mis-routed observations improving the age and accuracy of those elements.

SSPAT uses the latest element set and hundreds of observations to measure the accuracy of each element set in the space catalog every day. It compares these data with the standard accuracy for each object which is an average taken over tens of recent element sets using hundreds of observations on each. Thresholds are computed for accuracy, error tolerance, error growth rates and observation fit spans (in days). Current element sets failing these limits are listed for analyst attention. Average accuracies are computed daily by orbit class and for the entire catalog as well as for the near earth and deep space subsets.

SSPAT compiles and saves daily a large number of statistics for the total sensor network and by individual sensor. Total counts for each and all sensors on all objects tracked and the deep space subset are available for observations (obs), tracks, objects, associated obs, unassociated obs, retagged obs, mistagged obs, detagged obs, misfiled obs, astat (association status) 0 through 4 obs, obs within 2, 5 10, 25, 50, and 150 Km of the position predicted by the element set, obs on elsets with ages less than 2, 5, 10, 20, and 30 days, and obs on attention or lost list objects.

SPADOC's daily tasking is saved in SSPAT, and the track response for each sensor is computed and also saved for detailed satellite analysis. Daily track and object response for each sensor is aggregated by category and by cataloged and analyst satellites, and is saved for sensor analysis. The daily object response is also aggregated by tasking group and saved for analysis of SPADOC's tasking. The two main tasking control parameters, elset epoch age and error growth rate, are also saved for analysis of the space catalog and SPADOC's tasking.

In this brief overview of SSPAT capabilities, we will show only a few of the possible displays and data analyses that can be produced. Indeed these are not the only ways to perform these particular analyses; they are just samples of what can be done. There is a wealth of data available and waiting for an analyst with imagination to manipulate and take advantage of it. In the first section we show some ways to measure the quantity of data contributed by the sensors to the maintenance of the space catalog. The next section illustrates a few ways the data can be used to describe the accuracy of the catalog and compared to the requirements. Next, the design of the sensor tasking portion of the database is discussed. It is followed by a brief discussion of orbit classes, tasking groups and the deep space tasking philosophy employed by SPADOC to manage our limited deep space resources. Finally, tasking related data were queried to search for reasons why a large number of pieces from the recent Pegasus breakup have been so hard to maintain with good accuracy.

## Quantity of Contributions by Sensor

Space Surveillance operators and decision makers are continuously asked to quantify sensors' contribution to help justify the money spent maintaining them. The question has always been difficult, especially when asked to rank sensors. All the sensors contribute significantly in different ways. When one statistic is used as a measure it tends to emphasize the value of the sensors that are better equipped to respond and appears to belittle sensors that are unable to respond with the same volume in that area even though they may be better equipped in another area. This is what makes the problem so difficult, and is why we

must refrain from using only one or a few measuring sticks when attempting to measure a sensor's contribution to Space Surveillance. Nevertheless, decision makers demand numbers. The best we can do is ask "what for" and carefully choose our measuring sticks from the data available to fairly represent the capabilities in question. We can also cite reasons for a sensors ranking and point out when their capabilities lie in different areas.

In an attempt to measure some relevant areas of a sensor's contribution, SSPAT has collected a variety of statistics derived from the observations provided to the Space Control Center each day. The number of observations, the number of tracks (defined by time separation of more than 1 hour), and the number of unique objects tracked each day by each sensor are some of the data already tabulated for the last 3 years. The total numbers for the network are the sum of the numbers for the individual sensors. All these data are stored in an Oracle Database and can be retrieved, summed, averaged and displayed in a variety of ways. Data for years prior to 1994 can be compiled from the raw data (which is available back to 1960) at the cost of approximately 10 minutes of computer run time per day of data.

Figure 1 shows three different ways to measure quantity contributions from each sensor for the year 1996. The top chart shows the percentage of unique objects tracked daily by each sensor averaged over the year. This method of counting gives no credit to a sensor that tracks the same object or a small group of objects (like only active payloads) over and over again many times in the same day. The middle chart shows each sensor's percentage of total tracks provided to the Space Control Center for the year. The contribution by NAVSPASUR stands out in this measure because each and every time any object passes through their fence they provide a one-ob-track whether tasked or not. Other sensors usually attempt only tasked objects and provide 3 to 5 obs or more in each track. The bottom chart shows each sensor's percentage of total observations provided to the Space Control Center for the year. All three charts show that Eglin, Cavalier and NAVSPASUR are the 3 main contributors when it comes to quantity of data provided to the Space Control Center for overall catalog maintenance of near earth and deep space objects. Because most of the space catalog consists of small near earth objects, the data presented in figure 1 tends to place more importance on near earth sensors that have a large capacity to track the smaller objects.

Figure 2 shows the same quantity measures but only for near earth sensors tracking only near earth objects. The picture is pretty similar to the one painted in figure 1 for the overall catalog because nearly 80% of catalog consists of near earth objects.

Figure 3 shows the same quantity measures for deep space sensors tracking only deep space objects. For good reason, deep space has been arbitrarily defined as any orbit with a period above 225 minutes. Most near earth sensors cannot track objects above 225 minute periods. Therefore, deep space sensors with the capability to track objects at those ranges must do the job. Here, contributions by deep space sensors in their primary mission area begin to stand out. Eglin and NAVSPASUR, because they track a large number of semi-synchronous objects, stand out as the largest contributors to deep space. Cavalier, who was a big contributor in the overall picture, does not track anything in deep space. The next largest contributors are the GEODSS sites at Socorro, Maui and Diego Garcia. Combined they contribute more than any one sensor in deep space. They are the workhorses for tracking at geosynchronous ranges and beyond.

## Quantity of Objects Tracked by Sensor in 1996



## Quantity of Tracks Provided by Sensor in 1996



## Quantity of Obs Provided by Sensor in 1996
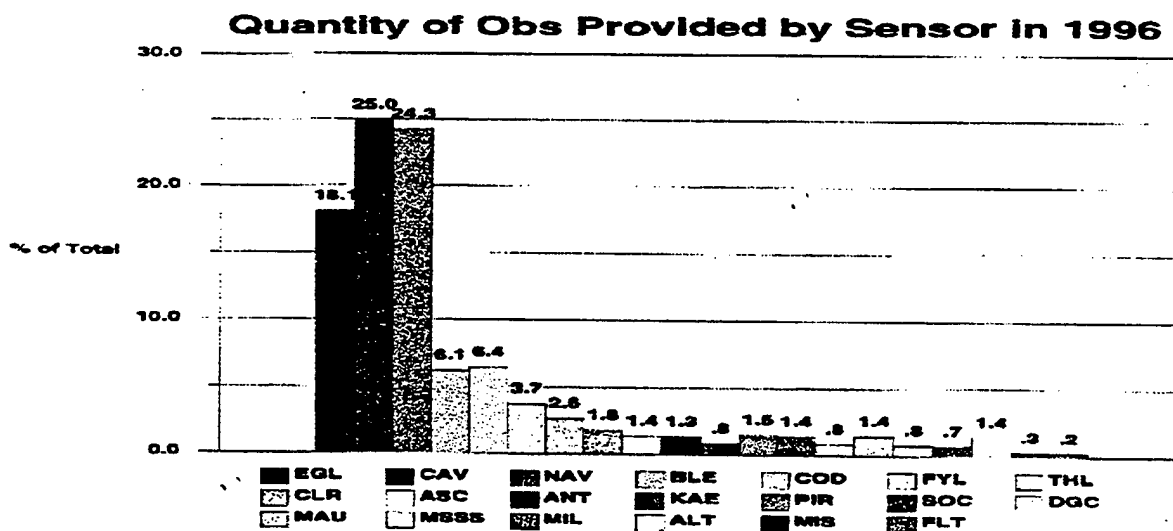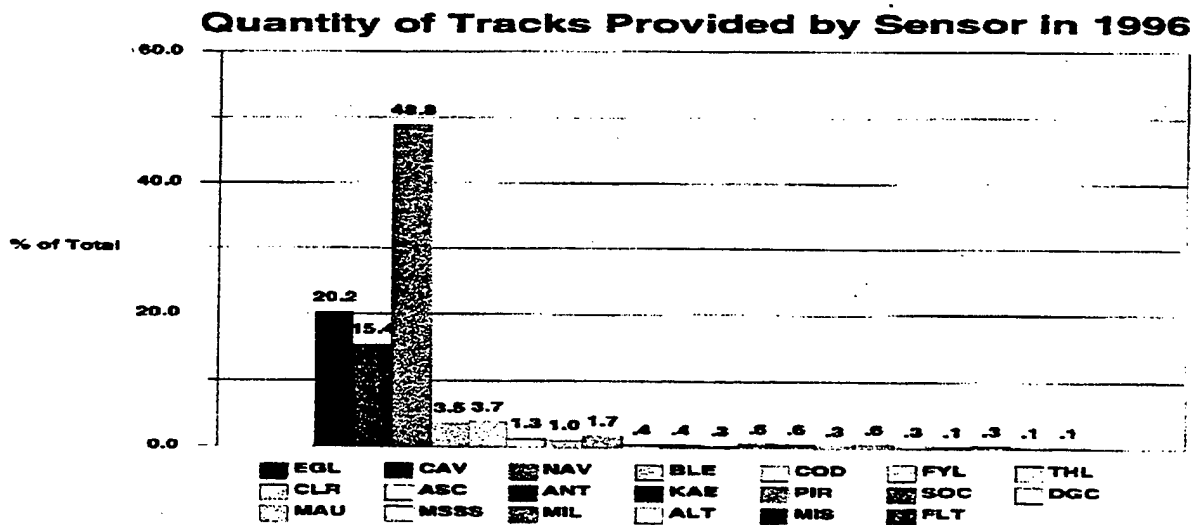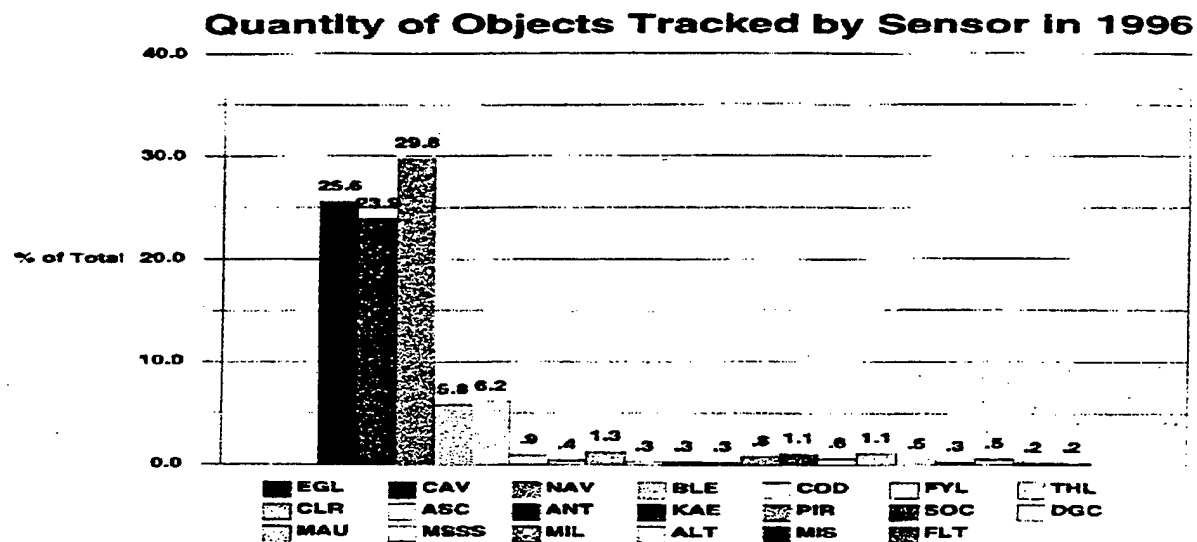


Figure 1. Different Measures of Quantity Contributions

## Quantity of Near Earth Objects by Sensor in 1996
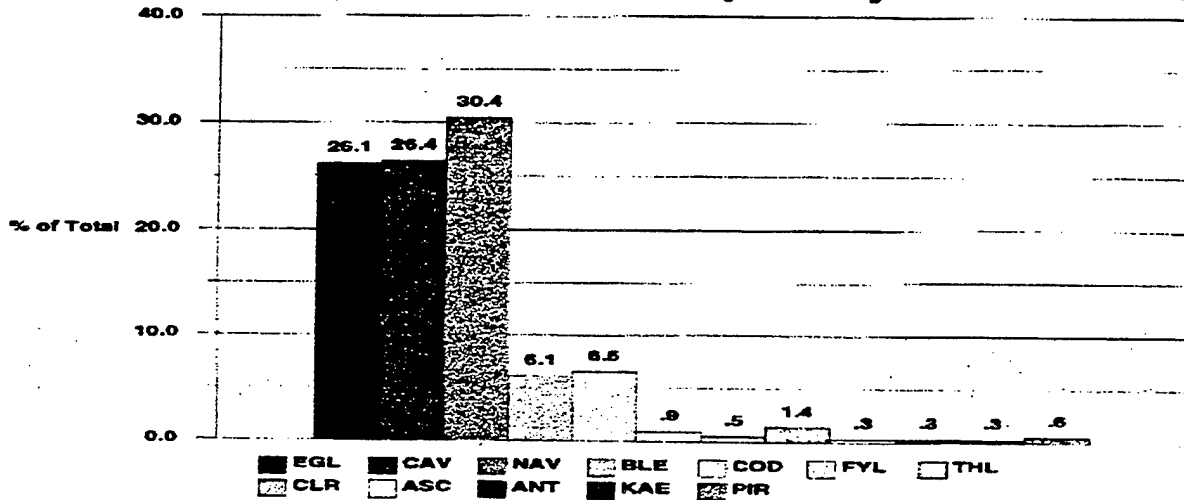


## Quantity of Near Earth Tracks by Sensor in 1996
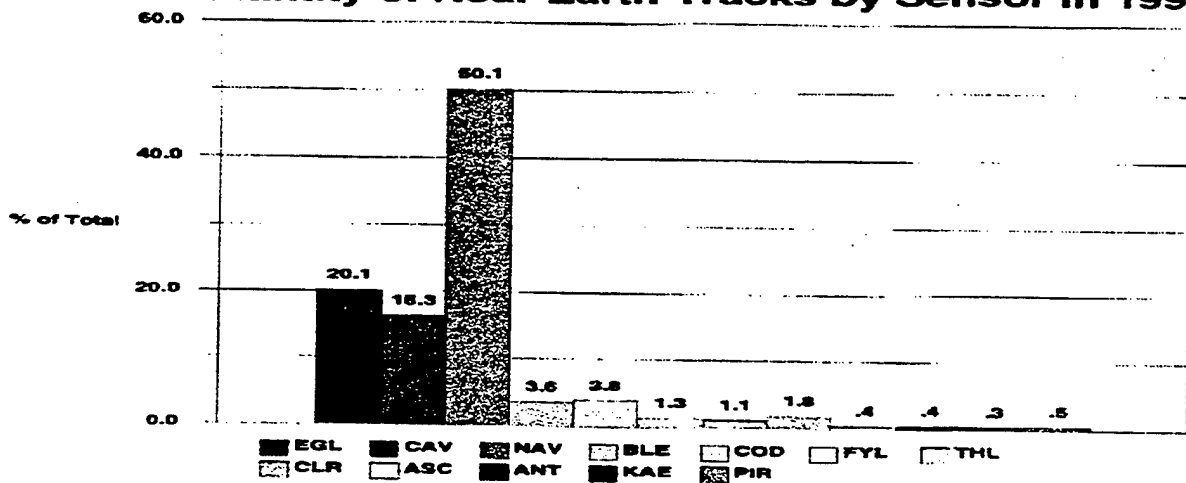


## Quantity of Near Earth Obs by Sensor in 1996
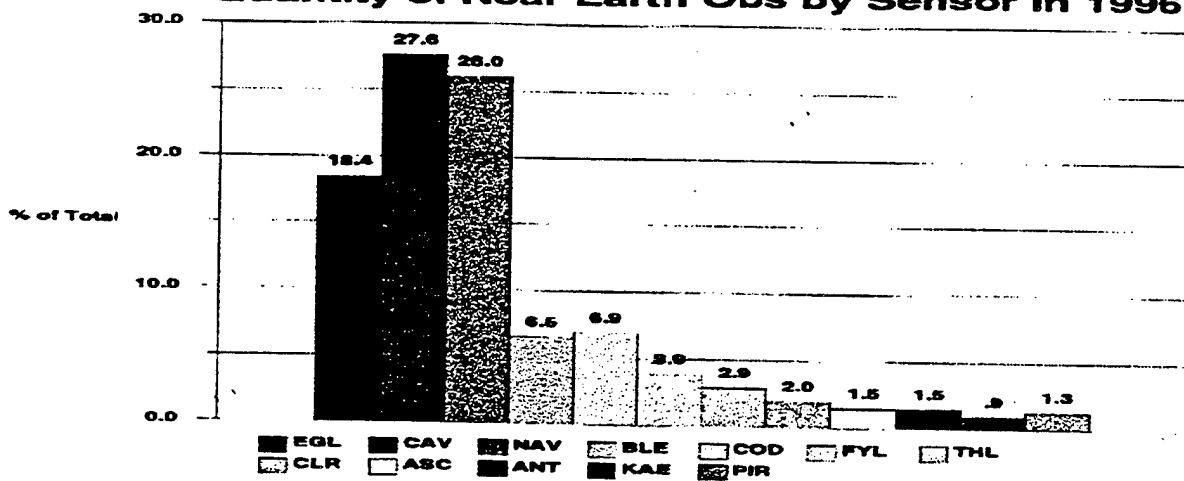


**Figure 2. Quantity Contributions to Near Earth**

## Quantity of Deep Space Objects by Sensor in 1996
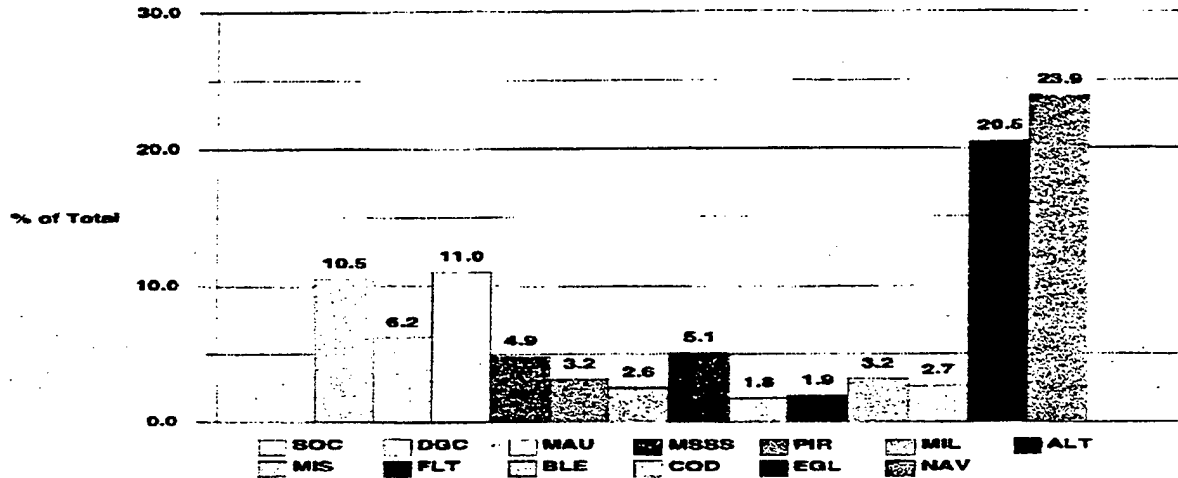


## Quantity of Deep Space Tracks by Sensor in 1996
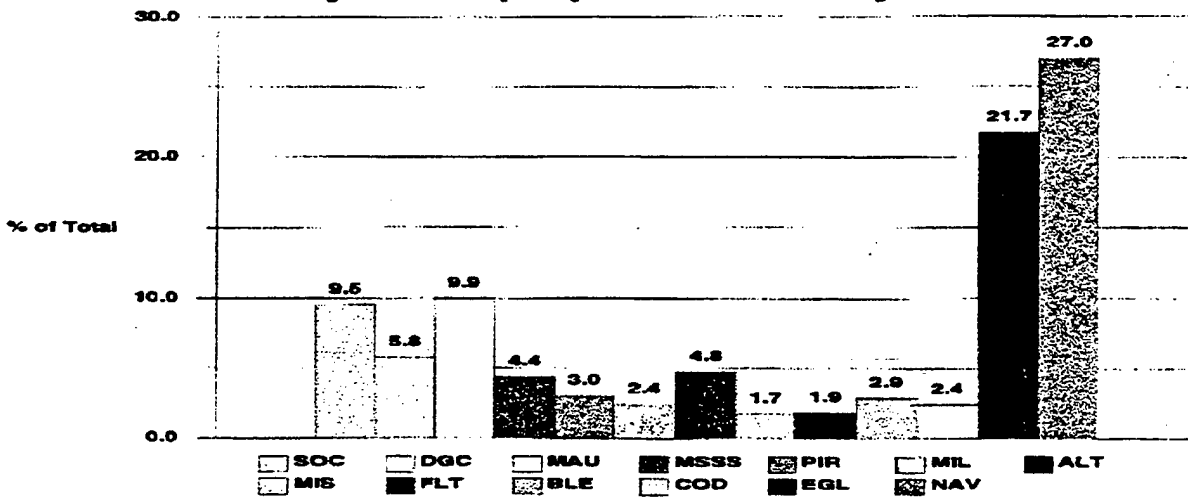


## Quantity of Deep Space Obs by Sensor in 1996
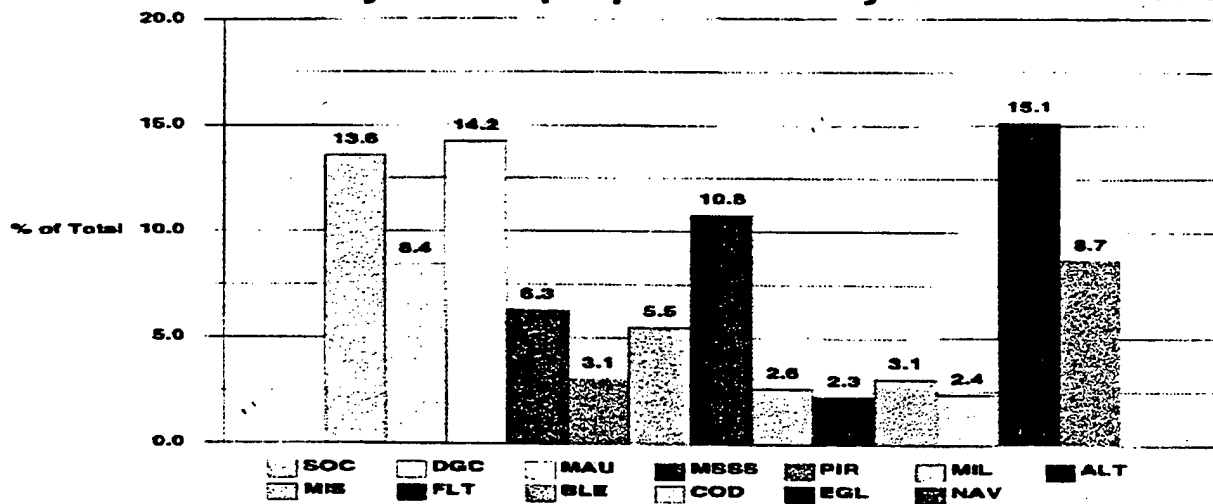


Figure 3.  Quantity Contributions to Deep Space

# Catalog Accuracy

Finding ways to express the overall accuracy of the space catalog
has always been difficult. When asked, "What is the accuracy of
the catalog?", the response is usually, "Well, it depends. What
objects are you interested in?" Then, an analyst could examine a
small number of such objects and after some time return a
reasonable answer that applies only to those objects. The only
general response that could be offered relied on statistics
derived from the vector magnitude (vmag) difference between the
position of the last observation and the predicted position from
the element set propagated to the same time. Old element sets
were automatically discarded (as were those where the vmag was
considered too big) when computing the percent of objects good to
2 or 12 or 150 Km (the common accuracy thresholds used). Often,
these element sets had just been corrected with those latest
observations. While that accuracy measurement might be OK at the
time of the observation, it does nothing to account for the age
of the element sets in the catalog. Nor does it account for cases
where other observations would prove the latest observation to be
poor or perhaps erroneously filed up to that object.

As part of the SSPAT project we have developed a better method of
estimating the accuracy of each and every element set which takes
the age and error growth rate into account. These numbers are
then averaged by orbit class, by near earth or deep space and
overall to give numbers that represent the average accuracy of
the catalog on a given day.

The latest element set and hundreds of observations are used to
measure the accuracy of each element set in the space catalog
every day. The vmags from all the observations in the fit span
(and predict span if obs newer than the element set exist) of an
element set are averaged while rejecting outliers to obtain the
current accuracy. If the element set is not current, its
accuracy is then adjusted by adding the error accumulated for its
age. These numbers then represent the accuracy of the latest
element set and can be compared to the standard accuracy for that
object computed in a separate process using many historical but
recent element sets.

Numbers for standard accuracies, error tolerances, error growth
rates and observation fit and predict spans (days) are computed
using tens of element sets and hundreds of obs to get good
average standards for each element set. These data are stored
both in flat files and in an Oracle database. These standard or
average values for individual objects can then be counted or
averaged in a variety of ways using SQL to give summary results
for the entire catalog or by orbit class or by period ranges
including near earth or deep space categories.

The charts in figure 4 illustrate deep space is a growing mission area that should consider more sensor resources. The top chart shows the number of deep space objects has steadily risen for the past 10 years. The middle chart shows the average age of the element sets by orbit class. The popular growing orbit class 63 has an average age of 3.6 days for 100 element sets. With less tracking resources, this number will rise. The bottom chart shows the past 10 years of deep space attention and lost list numbers. The past 5 years have seen the number of attention list objects rise as deep space tracking resources have been gradually lost. The number of lost objects has changed little. Only the average element set age increases as sensors track objects less frequently. Older element sets may mean less accuracy and/or less timely information about satellite orbit changes.
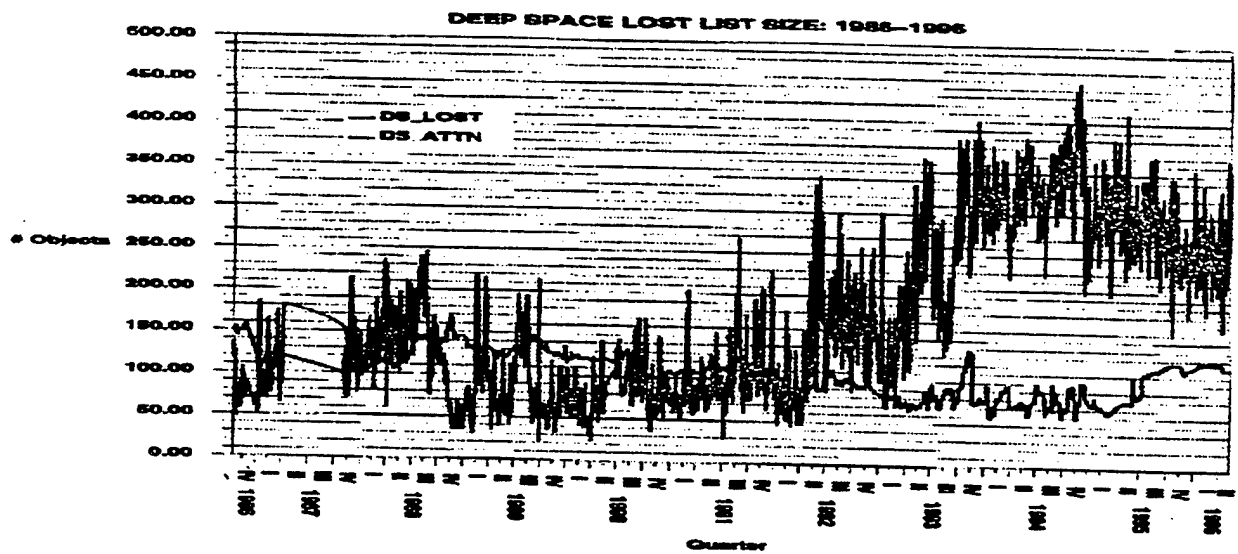
## Growth of Deep Space Catalog



## Deep Space Elset Age



## DEEP SPACE LOST LIST SIZE: 1986-1996
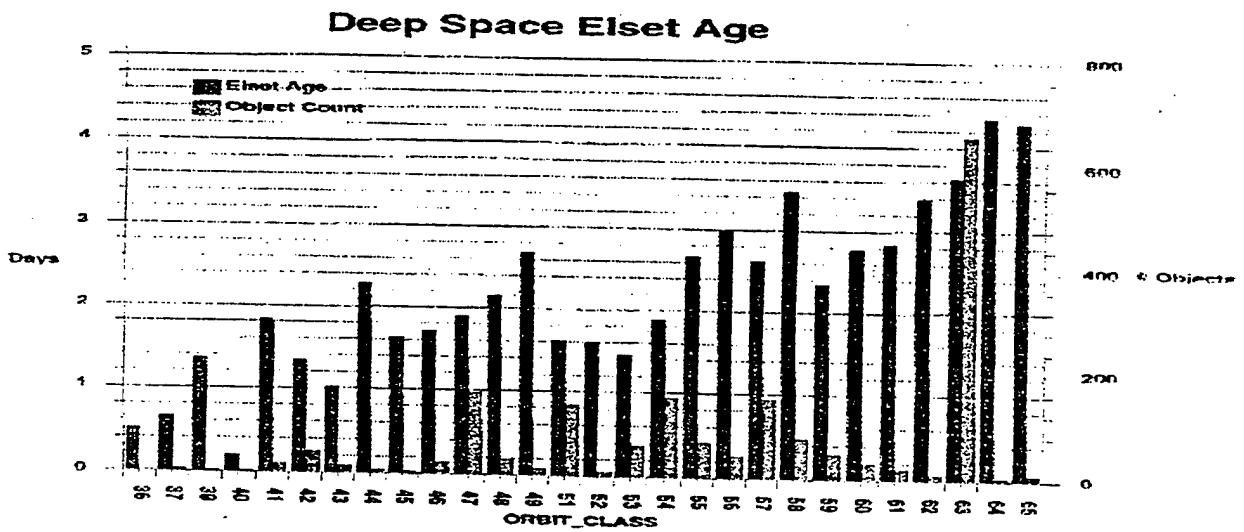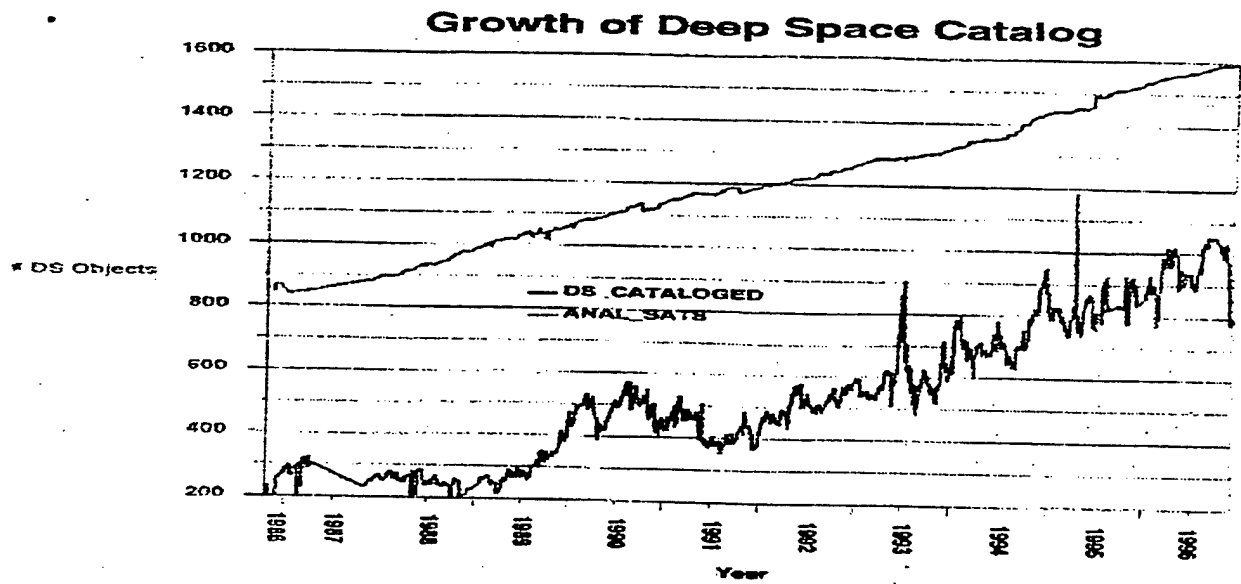


Figure 4.   Deep Space Trends

10

# Sensor Tasking Database Design

A relational database design for SSPAT was created for the sensor tasking data using an entity-relationship (ER) data model. Other data related to sensor tasking and used by the SPADOC sensor tasking function (e.g., period, orbit class, tasking group, and epoch age and error growth rate (EGR) of element sets) are also included in the design. Data may be aggregated by period for near-earth and deep-space satellites, by orbit class, and by tasking group. SPADOC attempts to maintain the satellite catalog based on thresholds contained in the tasking groups for epoch age and EGR. Historical trends of epoch age and EGR of element sets can be analyzed using SSPAT.

The top-level sensor tasking ER logical model is shown in Figure 5 based an IFEF1X data model. Boxes are entities and lines are relationships. Each of the entities are defined in Table 1. An entity has attributes that represent distinct characteristics of the entity. A set of attributes that uniquely identifies the instances of an entity is called a primary key. Attributes that are not part of the primary key are called non-key attributes. A fully-attributed ER diagram for some of the entities in the model is shown in Figure 6. The primary key attributes are in the top part of the box, and the non-key attributes are in the bottom part of the box.

A parent/child relationship is indicated by a solid dot next to the child entity. The cardinality of the relationship is by default zero, one or more unless the symbol "P", "Z", or a number appears next to the solid dot. As shown in Figure 5, a satellite may be tasked to zero, one or more sites. "P" indicates each parent instance is related to one or more child instances. For example, a site rank list comprises one or more site ranks. (Empty lists are not allowed.) "Z" indicates each parent instance is related to zero or one child instance. A number "N" indicates each parent instance is related to exactly N child instances. For example, a tasking group possesses exactly 45 tasking table cells. A tasking group has a 5 x 9 tasking table or matrix (not to be confused with database table) where the rows of the matrix represent the tasking categories 1 through 5 and the columns represent levels of tasking. Tasking table cell is the entity (database table) and is indexed by the row and column (primary key attributes) of the tasking table.

A rectangular box indicates an entity that depends on no other entity for its identification. A rounded box indicates an entity that depends on one or more other entities for its identification. A solid line indicates an identifying relationship between the parent and dependent child, and the primary key of the parent becomes part of the primary key of the

child.    A dotted line indicates a non-identifying mandatory
relationship between a parent and independent child, and the
primary key of the parent becomes a non-key attribute of the
child.    A dotted line with a diamond (optionality indicator) next
to the parent entity indicates a non-identifying non-mandatory
relationship.    In this kind of relationship a child instance may
have no parent instance.    Two such examples are shown in Figure
5.    In SPADOC, the tasking group's site rank list may be NULL.
In that case, SPADOC defaults the site rank list to every site in
the Space Surveillance Network (SSN) with default site ranks.
The orbit class of a tasked satellite may also be NULL.  This may
occur when a satellite is decaying and the perigee of the element
set is inside the earth.    Orbit class is not defined for such
orbits.



**Figure 5.    Entity-Relationship Logical Model**

12

**Table 1. Entity Definitions**

| Entity Name | Entity Definition |
|---|---|
| EXTRA METRIC | Daily extra track and object metric summary by site |
| OBJECT METRIC | Daily object metric summary by site |
| ORBIT CLASS | Class of satellite orbits bounded by apogee and perigee minimum and maximum limits |
| SITE | Collection of space surveillance sensors at a site that constitute a taskable entity in the Space Surveillance Network, referred to as a primary sensor in SPADOC |
| SITE RANK | Site ranking priority for the allocation of sites to satellites in the tasking assignment algorithm |
| SITE RANK LIST | List of candidate sites to which satellites in the tasking group may be tasked |
| SITE RESPONSE | Daily track response to tasking by site |
| TASKED SATELLITE | Satellite tasked to the space surveillance network |
| TASKED SITE | Daily satellite tasking by site |
| TASKING GROUP | Tasking control parameters for a group of satellites with similar characteristics |
| TASKING GROUP METRIC | Daily tasking group metric summary by site |
| TASKING TABLE CELL | Desired number of tracks and number of sites for a tasked satellite |
| TRACK METRIC | Daily track metric summary by site |

**SITE RESPONSE**

task date (FK)
satellite number (FK)
site number (FK)
track id

number of obs received
number of obs expected

provides

**SITE**

site number

site name
site short name

becomes

**TASKED SITE**

task date (FK)
satellite number (FK)
site number (FK)

category
suffix
number of tasked tracks
number of tasked obs

receives          is tasked to

**TASKED SATELLITE**

task date
satellite number

tasking group id (FK)
orbit class id (FK)
manual flag
tasking table category
tasking table number of tracks
tasking table number of sites
elset classification
period
epoch age
element quality prediction classification
error growth rate

**Figure 6. Full-Attributed Entity-Relationship Diagram**

In the physical design entities become database tables and their attributes become columns in the tables, and the relationships between entities are represented as foreign keys in the child entities. A foreign key is a primary key of a parent that is an attribute of the child and is indicated by (FK) after the attribute name in Figure 6.

## Tasking Philosophy and Sample Analyses

Orbit classes are used by catalog maintenance and sensor tasking functions in SPADOC and provide a convenient way to characterize the types of satellite orbits. Orbit classes are defined by dividing the possible satellite orbits into 65 apogee/perigee bins. Orbit classes 1 through 33 cover near-earth satellite

orbits (periods less than or equal to 225 minutes), orbit classes 41 through 65 cover deep-space satellite orbits (periods greater than 225 minutes), and orbit classes 34 through 41 are transitional and cover both near-earth and deep-space satellite orbits.

SSPAT was used to compute the average epoch age of cataloged satellites (not including analyst satellites) by orbit class for 1996. The average epoch age for the near-earth and transitional orbit classes is less than one day for most of these orbit classes. The average epoch age for the deep-space orbit classes generally increases with orbit-class number with the orbit class for geosynchronous satellites (orbit class 63) having an average epoch age of 4.4 days. However, a group of geosynchronous satellites are maintained with epoch ages much less than this average.

There are several tasking groups for satellites in geosynchronous orbit depending on their observation needs. For example, high-interest active payloads in geosynchronous orbit are assigned to tasking group 640 and are always tasked at category 2 to several sites. On average, three sensors per satellite are tasked each day with a response from two sensors. USSPACECOM desires to keep the epoch age of these satellites less than 2 days old. In order to meet this requirement, the epoch age threshold for tasking group 640 is set to one day. The daily average epoch age of the satellites in tasking group 640 for 1996 has typically been less than one day, and over 90 percent of these satellites have been maintained with an epoch age less than 2 days. The Pirinclik radar and the GEODSS site at Diego Garcia are the two most utilized sites for this tasking group because most of the satellites in this group lie in these two sensors' coverage of the geosynchronous belt. For 1996, Pirinclik's response for tasking group 640 was 78% and Diego Garcia's was 54%. Diego Garcia's lower response rate is due to weather.

Low-interest active payloads, dead payloads, rocket bodies, and debris objects in geosynchronous orbit are assigned to other tasking groups and are tasked at categories 2 through 5 (lower category corresponding to higher priority) depending on the epoch age and EGR of the individual satellites. At the lower priority categories (e.g., 4 and 5), these satellites often do not get tasked to any site because of insufficient deep-space sensor resources. When the epoch age of these satellites becomes greater than the epoch age threshold in its tasking group, the category is decreased (priority increased) so that it will be tasked to one or more sites. When the satellite is tracked and the element set is updated in SPADOC, the category is increased (priority decreased) and the satellite is not tasked again until the epoch age threshold is exceeded. The epoch age threshold for these tasking groups is 7 days. By using several tasking groups with different epoch age thresholds, the sensor tasking process

in SPADOC is managing deep-space sensor resources and different observation requirements for geosynchronous satellites.

SSPAT was also used to compute the average EGR of cataloged satellites by orbit class for 1996. The average EGR has spikes for the orbit classes corresponding to highly eccentric orbits with perigee height below 250 km. Rapidly decaying satellites with large eccentricities are responsible for the large average EGR for these orbit classes. These type of satellites are typically very difficult to maintain.

A group of satellites that has been difficult to maintain is the pieces of the Pegasus rocket body breakup, which occurred in June 1996. The daily average EGR of the Pegasus breakup exhibits large spikes on certain days. Using the ability to perform database drill down in SSPAT, the daily average EGR of the Pegasus breakup was broken down by orbit class. The average EGR of Pegasus breakup pieces for orbit classes 3, 5 and 9 with perigee height less than 575 km (referred to as the dense atmosphere) has pronounced spikes on certain days, whereas the average EGR of Pegasus breakup pieces for orbit classes 6 and 10 with perigee height greater than 575 km is consistently small. Drilling down to individual breakup pieces, some satellite histories show dramatic spikes in EGR on certain days. These spikes in EGR have been correlated with large changes in BSTAR, which models the amount of drag (and unmodeled forces) needed in the differential correction of the element set. These ill-behaved breakup pieces have large area to mass ratios and experience large amounts of drag in the dense atmosphere.

## Conclusion

SSPAT can be used to manipulate and display a wide variety of data to provide insight into the workings and performance of the Space Surveillance Network. A resourceful analyst can use these data to discover, investigate and even solve problems that affect the space catalog. Only a few samples were given in this paper in order to demonstrate some of the possibilities. The limit of possibilities depends on the imagination and persistence of the analyst.

# SBV PROGRAM OVERVIEW

Grant H. Stokes
MIT Lincoln Laboratory

## ABSTRACT

The Space-Based Visible (SBV) sensor was launched on-board the Midcourse Space Experiment (MSX) satellite on 24 April 1996. One of the objectives of the SBV program is to provide the first demonstration of space-based space surveillance. This paper provides an overview of the SBV program and its objectives, the MSX satellite and the facilities that are used to conduct the space surveillance operations on the MSX/SBV. The papers that follow in the Space-Based Visible Section of the agenda provide the details of how the SBV is operated for surveillance data collection events and elucidate the performance of the SBV which has exceeded our most optimistic expectations.

## SBV PROGRAM OBJECTIVES

The SBV program has three overall objectives. First, the SBV is intended as a demonstration of advanced technology for space surveillance applications. These technologies include the following:

High off-axis rejection optics - which allow the SBV to detect relatively faint targets near the lit limb of the sunlit earth. This capability is necessary to provide timely detection of resident space objects (RSOs) in low altitude orbits. One of the requirements for achieving high off-axis rejection, in addition to a good optical design, is maintaining the cleanliness of the optics. Through very stringent cleanliness procedures, the SBV optics have made it to orbit as clean as when the telescope was delivered to Lincoln Laboratory by the vendor.

Advanced staring focal planes - which allow the SBV to search large areas of the sky while maintaining high sensitivity to faint RSOs and providing an accurate measurement of the position of the detected objects. The SBV focal plane is constructed of four 420X420 pixel CCD chips. The CCD chips are abutted to form an essentially gap free coverage of the 1.4X6.6 degree field of view of the SBV telescope. The CCDs have very low readout noise and have a frame transfer capability, which allows the overlay of the integration and readout times. The frame transfer design allows a sequence of frames to be acquired very quickly with no delays for readout.

17

On-board signal processing - which reduces the large quantities of data collected from the CCDs to reports which contain only the target data. For space surveillance, the CCD is typically operated in a step stare mode where a series of frames (2-16) are taken while tracking the stars. The stars stay in constant positions on the focal plane while the RSOs make streaks. This method of operation yields almost 3 million pixels of data for a single look, which is well beyond the capacity of the available 1Mbps communications link between the MSX and the ground. The signal processor takes the series of data frames and processes them to yield signatures of several of the bright stars in the field, used for determining the pointing of the SBV, and reports of the streaking targets detected. Thus, the signal processor provides data compression which allows the data to be stored in a RAM buffer for later downlink via the 1Mbit link with the MSX ground station.

The second of the overall objectives is the demonstration of space-based space surveillance. The space surveillance demonstration includes a number of incremental objectives as follows:

Technology demonstrations - which are intended to assess the technical capability of the instrument to support space surveillance. These include measurements of the SBV's detection sensitivity for RSO targets and the metric accuracy of the sensor.

Functional demonstration - which are intended to assess the ability of the SBV to conduct space surveillance operations typical of those executed routinely by the SSN. Examples of these operations include response to a standard tasking list or executing a search of some portion of the Geosynchronous belt.

Phenomenology - which entails collecting background data in support of future programs, such as SBIR Low.

Operations - which entails demonstrating the operational techniques and developing a CONOPS for the operations required to execute the space surveillance mission.

The third overall objective of the SBV is the support of ballistic missile defense by collecting target phenomenology and background data. These data support future systems such as SBIRS and the development/validation of background models in the visible wavelength. The current visible modeling capability is not nearly as advanced as similar capability for the IR bands. Thus, considerable data are required to allow the maturation of the visible wavelength models to the point where they may be used to aid the target discrimination process.

**THE MSX SPACECRAFT**

The SBV sensor was launched on the BMDO supported MSX spacecraft on 24 April 1996. The MSX is an observatory class spacecraft, shown in Figure 1, with a series of

instruments spanning the wavelength range from LWIR through UV. More detailed information on the MSX may be obtained from Ref. 1. The three primary instruments on the MSX are as follows:



Figure 1. Midcourse space experiment satellite (MSX).

The SPIRIT 3 - which consists of a radiometer and interferometer which cover a number of long and mid wave IR bands. The sensor focal plane is cooled using a solid Hydrogen cryogen which will be depleted by April 1997.

The SBV - which has been designed as a space surveillance sensor.

The UVISIs - which are a series of UV and visible imagers and spectrometers.

The MSX was launched on a Delta booster into a 888 km, 99 degree inclination orbit on 24 April 1996. Each of the primary sensors are co-aligned along a common boresight axis with the pointing achieved by changing the attitude of the entire 5700 lb. spacecraft.

The science objectives of the MSX are managed by a series of Principal Investigator (PI) teams shown schematically in Figure 2 There are PI teams which focus on targets, natural backgrounds, technology transfer, contamination and space surveillance. The Space Surveillance PI team is led by Dr. Mike Gaposchkin from Lincoln Laboratory. Mike and his PI team are responsible for demonstrating the conduct of space-based space surveillance, as discussed above in the SBV objectives section.
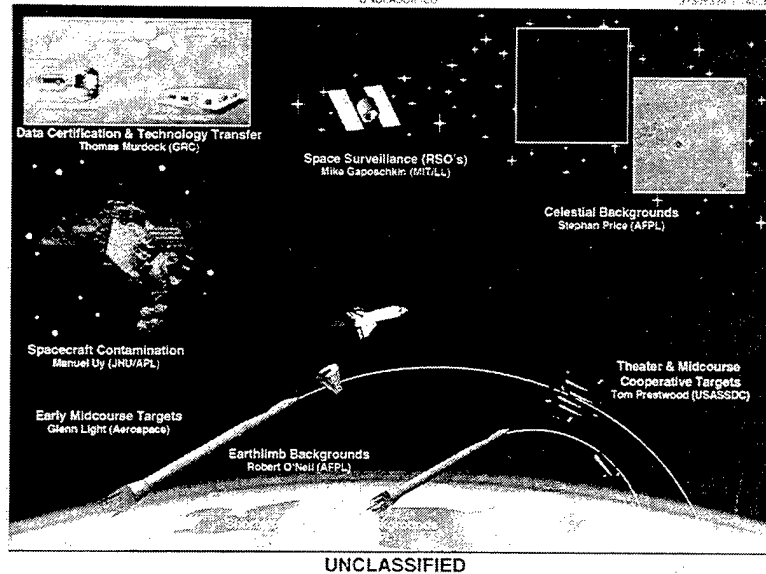
Figure 2. Midcourse space experiment principal investigator team structure.

The SBV hardware is shown in Figure 3. The SBV consists of a telescope assembly, shown on the left, and the electronics assembly, shown on the right, which supplies the data processing and sensor control capability. The 6 inch aperture telescope is constructed using an off-axis re-imaging design to provide the high out of field rejection (OFVR) needed to see targets near the sunlit earth limb. The telescope assembly also contains the CCD focal plane and the camera which converts the data to digital format. The telescope assembly, mounted on the front of the MSX, is connected to the electronics assembly, mounted on the rear portion of the MSX, via a long cable.

The MSX spacecraft is shown in Figure 4 during final preparation for booster integration at Vandenberg AFB. The SBV telescope assembly can be seen at the top left (rear) of the 17 foot long satellite. The other item of interest that can be seen in Figure 4 is the cryogen vent pipe that exits out the side of the satellite. This method of venting cryogen causes attitude and time dependent changes to the MSX orbit, which have presented a challenge when working to maintain the orbit knowledge of the MSX to the 10 meter level. The orbit of the MSX must be known to this level of accuracy to allow high accuracy metric observations to be derived from MSX data.
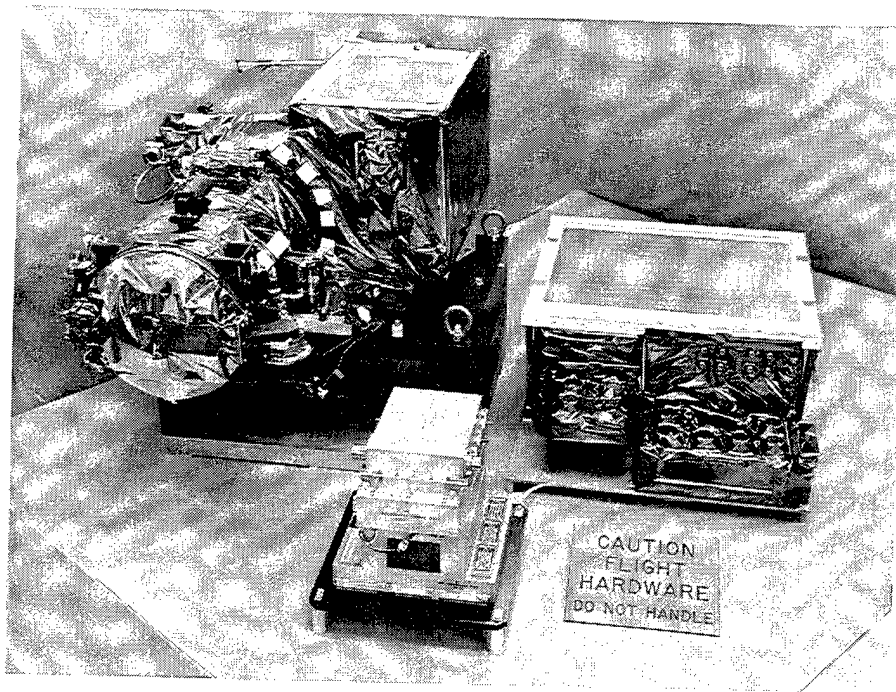
Figure 3. Space-based visible (SBV) flight hardware.



Figure 4. Midcourse space experiment satellite during fnal preparation for booster integration.
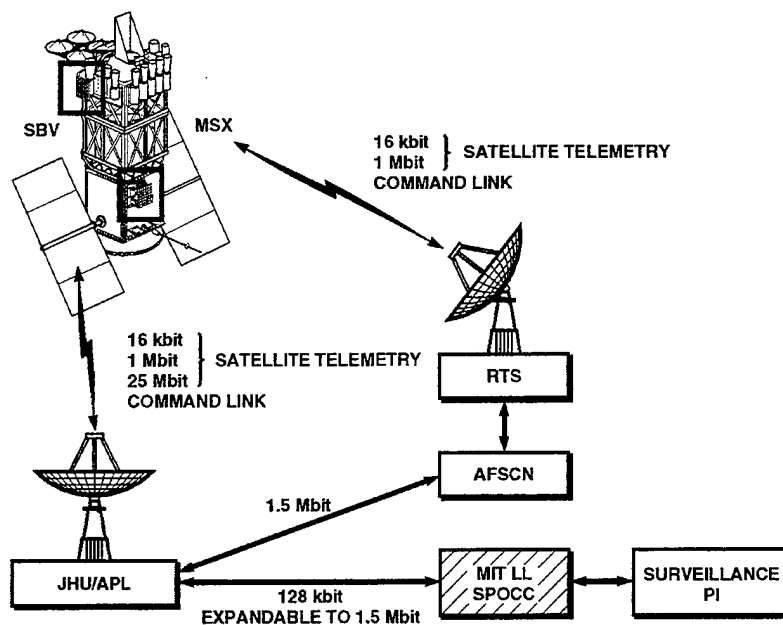
## SPACE SURVEILLANCE OPERATIONS

Conducting space surveillance observations using the MSX has presented several additional challenges. The most severe of these is the planning cycle for MSX experiments. The MSX is an experimental spacecraft and as such has a long planning cycle. Detailed planning for an event can start as long as 10 weeks before the execution of the event on the MSX. This timeline is inconsistent with demonstrations of operational space surveillance concepts, where Space Command tasks today - and expects observations back later today.

In order to address the planning and operations needs of the Space Surveillance PI team, a dedicated planning center was built at Lincoln Laboratory. The SBV Processing, Operations and Control Center (SPOCC) has the responsibility for generating all of the commanding required to execute space surveillance operations on the MSX satellite. This is done by interacting with the MSX Operations Planning Center (OPC) at APL to establish windows of time in the MSX schedule when space surveillance events can take place and to establish spacecraft resource budgets for each event. When the time for daily level planning comes, 24-36 hours before event execution, the SPOCC operators, with the aid of a highly automated planning system, generate the commands which will execute the events on the MSX. The commands will run an event which is compliant with all of the MSX operating constraints and will abide by the resource budgets established during the monthly and weekly planning cycles. A more detailed description of the SPOCC planning process and the interaction between the SPOCC and OPC planning systems may be found in Ref 2.

In addition to having mission planning responsibility for the space surveillance events, the SPOCC is also responsible for the long-term health and status maintenance of the SBV and for the processing of all of the SBV surveillance data to yield calibrated metric observations which are provided to the analysts in the collocated Space Surveillance Data Analysis Center (SDAC).

A view of the network control system for the MSX is shown in Figure 5. The SPOCC, located at Lincoln Laboratory, is connected to the APL facilities via a dedicated, fractional T-1 link. The commands are sent from the SPOCC to APL for upload at either the dedicated MSX ground station at APL or using the AFSCN SGLS stations. The 16 kbps health and status telemetry is received at either the APL station of the AFSCN stations and is forwarded to the SPOCC across the dedicated link. The processed SBV observations are stored aboard the SBV in a RAM buffer until they are down linked via the 1 Mbps communications link between the MSX and either the APL or SGLS stations. If large volumes of full frame SBV data are desired, they are stored on the MSX tape recorders, which are dumped via a 25 Mbps link to a dedicated facility at APL.

## MSX / SBV CONTROL NETWORK



296586-1

Figure 5. Control network for MSX space surveillance experiment.

## SUMMARY

In summary, the MSX/SBV have a wide range of objectives in the areas of technology demonstrations, space surveillance and ballistic missile defense measurements. In order to demonstrate operational timelines. The operations of the SBV for space surveillance operations are controlled by the specially constructed SPOCC facility at Lincoln Laboratory. As will be seen from the results to be described in the following papers, the SBV has been a productive sensor which has exceeded our most optimistic expectations with respect to performance and reliability.

## References

[1]Mill,J.D., O'Neil, R.R., Price, S., Romick, G.J., Uy, O.M., Gaposchkin, E.M., Light, G.C., Moore, W.W., Murdock, T.L., and Stair, A.T., "Midcourse Space Experiment: Introduction to the Spacecraft, Instruments, and Scientific Objectives," *Journal of Spacecraft and Rockets*, Vol. 31, No. 5, 1994, pp. 900-907.

[2]Stokes, G.H. and Good, A.C., "Joint Operations Planning for the Midcourse Space Experiment Satellite", *Journal of Spacecraft and Rockets*, Vol. 32, No. 5, 1995, pp. 812-816.

# SPOCC MISSION PLANNING SYSTEM PERFORMANCE

Herbert E. M. Viggh, Dave Blaufuss, Frederick Morton, Andy Wiseman,
and R. Sridharan
Lincoln Laboratory, Massachusetts Institute of Technology

## ABSTRACT

The SBV Processing Operations Command and Control (SPOCC) mission planning system was developed to facilitate space surveillance operations with the Midcourse Space Experiment (MSX) satellite. Designed to operate in a highly automated fashion with minimal operations personnel, the system has planned surveillance data collection events within the overall MSX schedule with consistent success. The mission planning system and it's operation are described. The effect of MSX constraints and Exclusion Zone avoidance on mission planning is discussed. Performance statistics of the mission planning system are presented.

## 1.0 Introduction

The Mid-Course Space Experiment (MSX) consists of a set of payloads on a satellite designed and built under the sponsorship of Ballistic Missile Defense Office (BMDO - formerly, the Strategic Defense Initiative Office) of the Department of Defense. The major instruments are a set of long-wave infra red sensors built by Utah State University and named SPIRIT III, a set of sensors operating in the visible wavelength and ultraviolet wavelengths called UVISI built by Johns Hopkins University's Applied Physics Laboratory (JHU/APL), and a space based visible (SBV) wavelength sensor designed and built by Lincoln Laboratory, Massachusetts Institute of Technology. The satellite bus was built by JHU/APL who also acted as the integrator for all the payloads and associated systems. The MSX satellite, shown in Figure 1, was launched on April 24, 1996 from the Vandenberg launch complex into a near-sun-synchronous orbit.
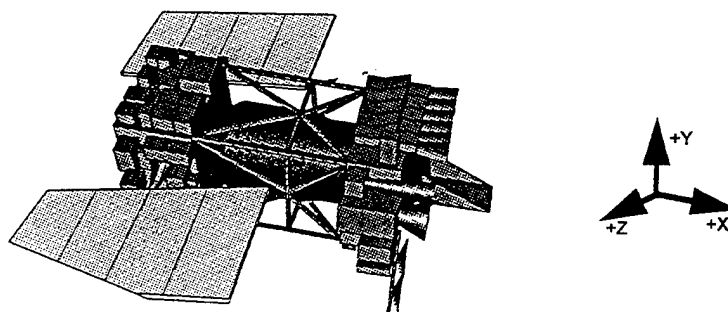


Figure 1. MSX Spacecraft

## 1.1. MSX Missions and Operations

Since its launch, the MSX satellite has been used to conduct a series of measurements on phenomenology of backgrounds, missile targets, plumes and resident space objects (RSOs), and engaged in functional demonstrations of detection, acquisition and tracking for ballistic missile defense and space-based space (satellite) surveillance missions. JHU/APL is the prime operator of the MSX and is responsible for scheduling all experiment data collection events (DCE) to be run on the spacecraft.

Eight Principal Investigators (PIs) are associated with the MSX project. The PIs developed experiment plans that were prioritized by the BMDO's Mission Planning Team (MPT). The MPT provides a prioritized list of DCEs on a monthly basis to JHU/APL's Mission Planning Center (MPC). The MPC schedules the DCEs and generates the MSX commands to carry out the experiments and collect science. The data are returned to the PIs for analysis and for refining the experiments.

## 1.2. SBV Hardware and Software

The SBV consists of an off-axis-imaging telescope with an aperture of 15 cm and a CCD camera at the focal plane. The design improves the off-axis light rejection capability of the telescope over conventional on-axis designs and thus enables the SBV to point within 100Km tangent altitude of a solar illuminate earth without saturation of the focal plane. The camera consists of four CCD arrays, each 420x420 pixels, laid out along the Z-axis of the spacecraft. The instantaneous field-of-view at each focal plane is 1.4 x 1.4 deg. Distortion due to the off-axis design causes the total instantaneous FOV to be ~6.6 x 1.4 deg.

The SBV carries a redundant pair of Signal Processors whose function is to detect moving targets in a stationary background. The Signal Processor (SP) (Ref. 3) collects a set of raw camera frame data (4 - 16 frames) and applies a space-time-filtering algorithm on these data. If the telescope is pointed in an inertially fixed direction, the stars will be stationary and the SP will detect streaks corresponding to any resident space object in the field-of-view of a CCD array. If, on the other hand, a RSO is being tracked, its image will appear stationary and the stars will generate streaks. Data from only one CCD focal plane array can be processed at a time. Typically, the SP takes a total time of 50 seconds from the initiation of the frame integration on the camera focal plane to writing out the results of star and streak detection. The algorithm can be controlled to produce a small number of stars for positional reference and a limited number of RSO streaks. The SP in routine operation, depending on the mode typically achieves a data compression factor of 500-50,000.

The entire operation of the SBV is internally controlled by an Experiment Controller. Timed commands are stored in the EC and sent to the various components. Another major function of the EC is to store the results from the Signal Processor in its memory until they are downlinked during a ground station contact.

The SBV has been designed for space-based surveillance of RSOs. The large field-of-view enables rapid search. The off-axis design enables low and high altitude RSOs to be detected and tracked near the earth limb, near the moon, and within 25 degrees of the sun without saturation of the focal planes. The Signal Processor design optimizes the detection of RSO streaks against a stationary background. The data compression, and the collection of positional data on stars and streaks, permits positional accuracy on the order of a third of a pixel (4") which is adequate to support the current requirements of space surveillance. Use of internal memory to store the results and downlinking of the data on demand to a ground station enables the SBV to avoid using the on-board power-hungry tape recorder for storage of data. Further, as in most low altitude experimental satellites, real-time communication is not available and the on-board storage of processed results enables the effective use of limited downlink opportunities.

More detailed descriptions of the SBV hardware and software can be found in References 2-4.

## 1.3. MSX Spacecraft

The capabilities and limitations of the MSX spacecraft (Ref. 5) greatly affected the design of the SPOCC mission planning system. The MSX (Figure 1) is a large satellite with all major sensors co-aligned rigidly along the X-axis. Thus re-pointing any sensor is equivalent to reorienting the entire spacecraft. The instruments of concern to the Surveillance PI are the SBV, the SPIRIT 3 radiometer, and the UVISI imagers and spectrometers.

The MSX is severely resource limited (Ref. 6). Power is generated by two solar panels. If all the instruments are on and the MSX is tracking a target, the power demand is greater than what can be generated by the solar panels even at full illumination. The excess demand is serviced from rechargeable Nickel-Hydride batteries. Further, the MSX is in a near-sun-synchronous orbit, and as a result, there are extended shadow periods (up to 20 minutes long in an orbital period of 103 minutes) during which the spacecraft relies completely on battery power.

The data storage capability of the MSX is limited. Only one tape recorder can be used at a time, and the total data that can be stored is ~36 minutes of data at 25 Mb/s and 180 minutes of data at 5 Mb/s. These data can be relayed down only at the APL ground station. It takes 2-3 passes over the APL ground station to read out all the data on a full tape recorder. The SBV onboard memory can be downloaded at either the APL ground station or at any Air Force Satellite Control Network ground station.

The MSX has severe geometrical constraints (Ref. 6) affecting pointing and attitude. The most significant of these is levied by SPIRIT 3 sensor, which is cryogenically cooled by solid hydrogen. Thermal input into the sensor from the earth and the sun must be minimized to conserve the depletion of the cryogen and prolong the life of the sensor. This necessitates

27

pointing constraints on the +X-axis and the −Y-axis of the spacecraft. The other sensors have other pointing restrictions along the +X-axis as well (Ref. 6).

## 1.4. SBV Processing, Operations and Control Center

The JHU/APL mission planning system begins scheduling and planning DCEs 6-10 weeks before the events actually run on the MSX. While most MSX experiments can be planned that far out, most Surveillance PI experiments cannot. This is due to changes in the element sets of target satellites and the MSX itself, and because many surveillance DCEs involve response to tasking lists which can change up to a few days before a DCE is to run. Therefore, a special mission planning system had to be developed to support Surveillance PI experiments on the MSX. The SBV Processing, Operations and Control Center (SPOCC) was developed for this purpose.

SPOCC is located at Lincoln Laboratory, MIT and is a component of the APL's Mission Planning Center. In this role, SPOCC (Ref. 1) generates the necessary commanding for the MSX and its sensors for all space-based space surveillance experiments, and converts and calibrates the returned science data before turning them over to the Surveillance PI's Surveillance Data Analysis Center. Further, SPOCC maintains the health and status of the SBV sensor on board the MSX. Figure 2 depicts the system architecture of SPOCC, which is broken down into a DCE planning side, and a data processing side.

The Surveillance PI Team provides requirements on what data is to be collected for each experiment via the MPT. These requirements serve as inputs to the surveillance data collection event-planning pipeline. Some DCEs require tasking response scheduling or searches; others go directly to the event planning and simulation stage. The simulated event timeline is then converted into MSX and SBV commanding. The commands are then sent to APL, uploaded to spacecraft, and run. The SPOCC databases are updated with information on the events planned and the files exchanged with APL. The mission planning interaction with APL is an iterative one, with monthly, weekly, and daily levels of planning.

The downloaded telemetry is decoded into two streams: SBV science data and SBV health and status data. The health and status data are monitored for short term anomalies, and processed for long term trending. The science data are then calibrated and reduced, the results being passed back to the surveillance PI team. The data processing side of SPOCC is nearly completely automated, requiring little operator involvement. The rest of this paper will concentrate on mission planning in the SPOCC.

The mission planning system in SPOCC was originally conceived and designed to support the detailed commanding of the SBV sensor on the MSX. However, because of changing requirements, it expanded to also encompass the commanding of the SPIRIT 3 and UVISI sensors in support of surveillance experiments.

changing requirements, it expanded to also encompass the commanding of the SPIRIT 3 and UVISI sensors in support of surveillance experiments.
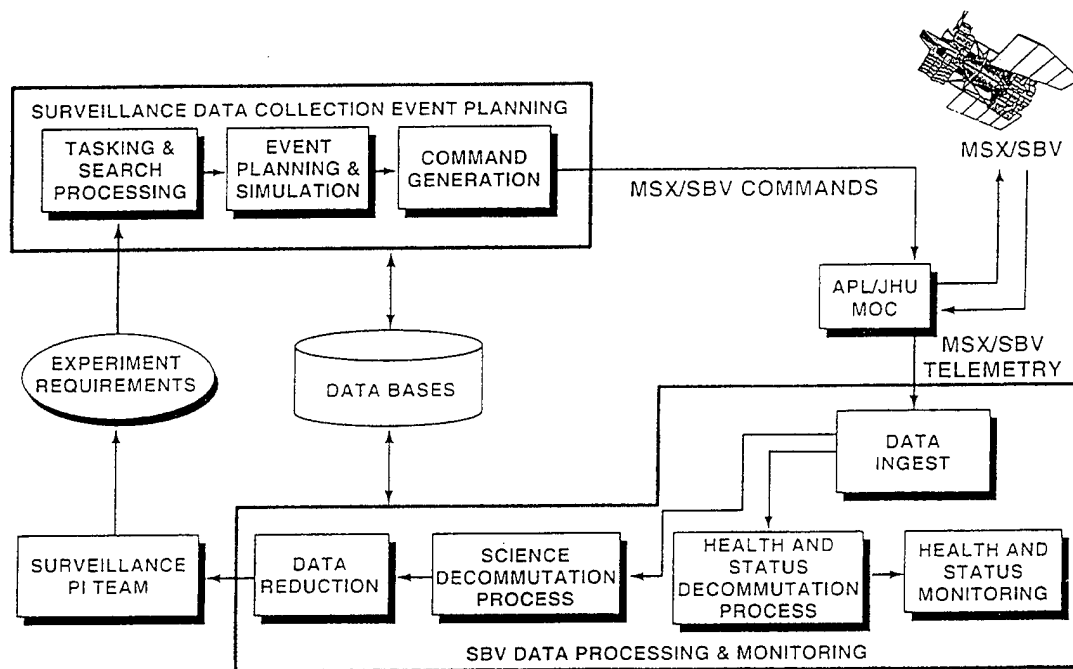


Figure 2. SPOCC System Architecture

## 2.0 SPOCC Mission Planning System

The mission planning system (Ref. 7-8) has the following requirements:

1) Command the MSX spacecraft for all surveillance experiments.
2) Command the SBV in all its operational modes.
3) Command SPIRIT 3 and UVISI in a restricted set of operational modes in support of Surveillance experiments.
4) Monitor constraints and resource usage.
5) Provide a high level language interface to the experimenter.
6) Ensure that modes of operation that are incompatible with the health, safety or operational philosophy of the instruments or the spacecraft are precluded.
7) Provide a pipelined operational capability in support of rapid and automated generation of commanding for experiments.

The components of the mission planning system are shown in Figure 3 in a more detailed breakdown than in Figure 1.

The tasking and search processing is carried out by the SSIP block, which takes a tasking (TAS) file as input. Event planning and simulation are performed by the Simulator (SIM), which takes a number of inputs. These include a file which describes the high level goals of the data collection event (SLED), orbital geometry information regarding the MSX (OG), and the current catalog of resident space objects (MOF).
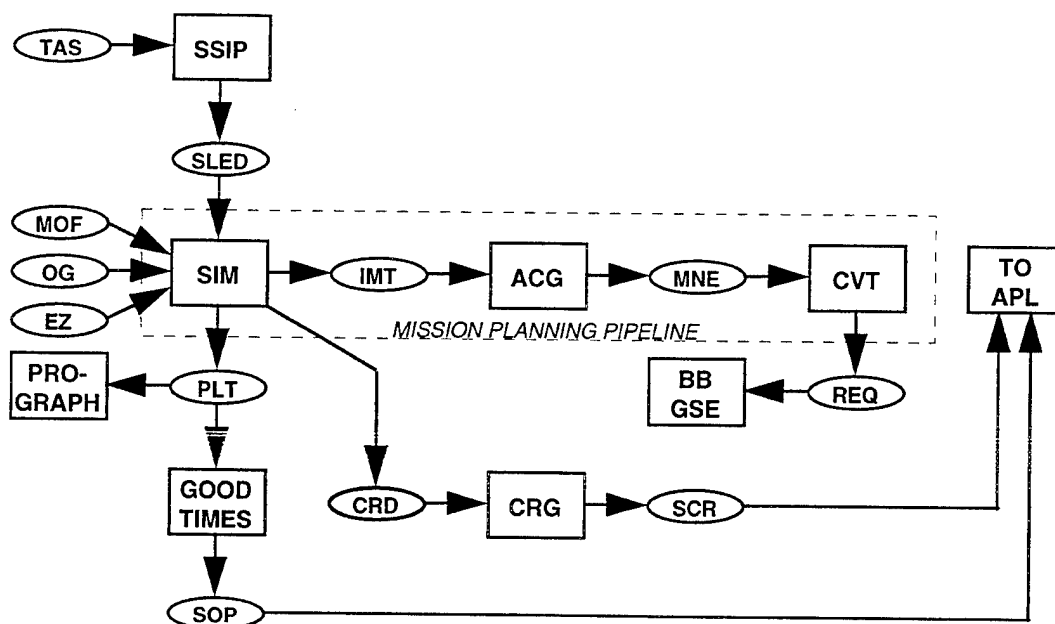
Figure 3: SPOCC Mission Planning System

The Simulator generates several types of output data. One of the more important is the performance data (PLT) file which is used by the PROGRAPH software to verify that all constraints are met by the event, and by the GOOD_TIMES software to verify that the event is a valid opportunity during monthly planning. The file of surveillance DCE opportunities for the month (SOP) is sent to APL as part of monthly planning (see Section 3.0 below for a more detailed description of monthly planning). A Cost Report Data (CRD) file is also output, and is used by the Cost Report Generator (CRG) to compile a detailed Spacecraft Cost Report (SCR) which is sent to APL for every DCE planned during weekly and daily planning. The last output of the simulator is the Instantiated Mission Timeline (IMT) which contains a timeline of high level spacecraft events that are needed to carryout the DCE.

The IMT file is input to the Automatic Command Generator (ACG) which is the first step in the command generation process. The ACG expands each IMT spacecraft and sensor event into a sequence of SBV command mnemonics and MSX spacecraft command packet mnemonics and outputs them to the Mnemonics (MNE) file. The Command Vettor Translator (CVT) takes the MNE as input, converts all the SBV mnemonics into 16 bit hex commands, and expands the MSX spacecraft command packet mnemonics into individual MSX command identifiers.

The first output of the CVT is a file of SBV commands (REQ) which can be run on a brassboard ground version of the SBV sensor (BB GSE). The second output of the CVT is the Event Definition File (EDF), which contains the commanding necessary to execute the data collection event. The EDF commanding is sent to APL for a final command safety check and upload to the MSX.

## 2.1 Joint APL/JHU and SPOCC Mission Planning Operations

There are two major factors that challenge the performance of the SPOCC mission planning system. The first factor is the set of interactions with the APL Mission Planning Center (MPC) and is described in this section. The second factor is the set of constraints that each planned data collection event must meet, which is described in Section 4.

SPOCC operations are done in coordination with the APL MSX mission planning system in the MPC. The MSX planning system operates at three different levels: monthly, weekly, and daily. The interactions between SPOCC and APL during theses three levels are summarized in Figure 4.
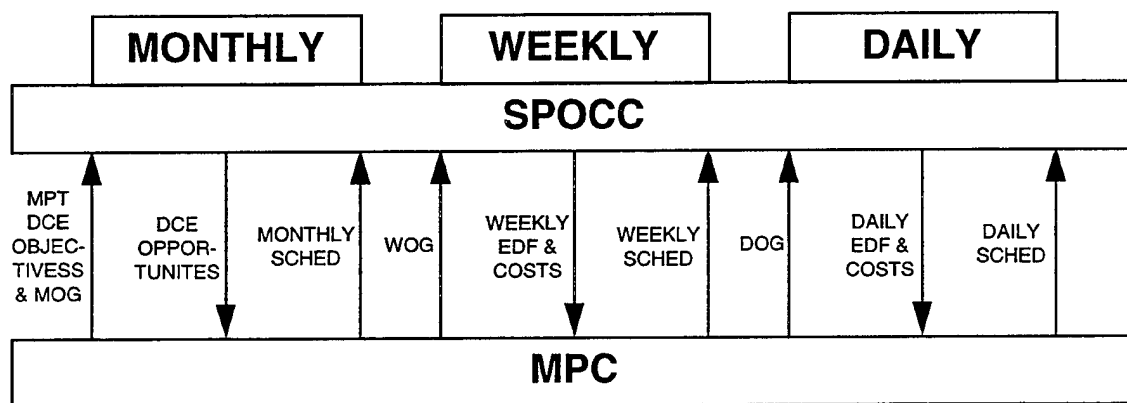


Figure 4. SPOCC Mission Planning Interactions with APL MPC

Monthly planning is done for each four week MSX mission month and is initiated 6 weeks before the start of the mission month. Therefore, monthly planning for a DCE begins 6-10 weeks before it will actually run. At the monthly level, SPOCC receives the Mission Planning Team objectives defining the surveillance DCEs they would like to have run on the MSX, along with the Monthly Orbital Geometry (MOG) file for the MSX. The SPOCC mission planning team then runs the mission planning pipeline in a special monthly planning mode, which identifies all of the opportunities during the month when each type of DCE can be conducted. This set of opportunities must be generated and transmitted to APL within two days of receipt of the MOG.

APL picks and chooses from the opportunities to achieve the MPT goals for surveillance and other PI teams. Example not-to-exceed costs for each type of surveillance event are on file at APL and used by the MPC in their scheduling process. The result is a monthly schedule of event start times for all DCEs scheduled that month. This schedule is then sent back to SPOCC.

Weekly planning is done for each week of the MSX mission and is initiated two weeks before the start of the week when the DCEs will run. At the weekly level of mission planning, SPOCC receives the Weekly Orbital Geometry (WOG) file. Using this updated orbital information; SPOCC generates the commanding for each surveillance event scheduled

31

for that week. Each of these DCEs are planned and checked to not exceed the example costs APL used during the monthly scheduling. Within two days of receipt of the WOG, the weekly commanding EDF files and associated costs are then sent to APL where they are run through software that performs an independent check that the DCEs do not violate constraints or exceed costs. APL then builds a weekly schedule, which is sent back to SPOCC.

Daily planning is done for each mission day that a Surveillance DCE is scheduled, and begins 36 hours before the start of the mission day with the receipt of the Daily Orbital Geometry (DOG) file. At the daily level of planning, SPOCC generates the actual to be run EDF commanding file for each DCE. The EDF commanding file and cost data are then sent to APL within two hours of receipt of the DOG. APL performs final constraint and cost checks and then uploads the commanding to the MSX spacecraft. A daily schedule is produced after receiving the daily EDF and sent back to SPOCC.

All three levels of mission planning can occur at the same time, since planning for the next month, the next week, and the next day can all fall on the same day. Therefore, every four weeks, monthly, weekly, and daily planning are performed simultaneously. The timelines involved can be challenging, especially the two hour daily planning period, which must still be met even if weekly and daily planning activities are in progress.

## 3.0 Constraints on SPOCC Mission Planning

All on-orbit operations, including the planning and implementation of mission operations must adhere to all constraints and restrictions required for safe and efficient operation of the spacecraft. The MSX Operational Constraints and Requirements Handbook (MOCARH) specifies these requirements (Ref. 6).

Constraints are separated into two categories: "hard" and "soft", both of which encompass a total of five subcategories. Hard constraints are those which are damage related, or involve physical design limitations. An example of a damage related hard constraint is the UVISI Sun Keep-Out Zone constraint. This constraint requires that the Sun be kept outside the UV sensor FOV at all times and that the Sun be kept outside of all nine sensor FOVs at all times when the filters or slits are not closed. This constraint translates into maintaining the S/C X-Axis to Sun angle to always be greater than 20 degrees during a DCE.

Soft constraints are those considered costly in terms of spacecraft resources, including constraints that involve the use of expendables, affect lifetime, or degrade spacecraft performance. An example of a soft constraint is the SPIRIT III Aperture and Radiator Sun Restrictions constraint. To avoid baffle heating and consequent excessive cryogen depletion, this constraint requires that the Sun remain outside a 70 degree half-angle cone centered on an axis +20 degrees from the +X axis in the X-Y plane when the Sun is visible.

32

## 4.0 Mission Planning Automation

In order to achieve acceptable performance under the challenges of interactions with APL and planning events with the previously described spacecraft constraints, much of the mission planning process has been automated (Figure 5).
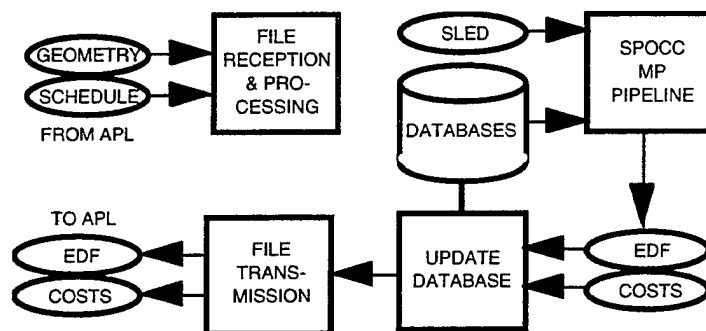


Figure 5. Automation of SPOCC Mission Planning

The health and status of all communication links, software processes, and computer systems required for mission planning are monitored with an automated system that flags problems and pages the appropriate SPOCC personnel. The schedule and orbital geometry files sent by APL are automatically processed upon receipt, archived, and the appropriate data entered into the SPOCC databases.

The SPOCC mission planning system performs design, analysis, and command generation for all surveillance DCEs while complying to all MOCARH requirements. During mission planning, the Simulator checks constraint compliance and monitors resource usage during its simulation of a DCE by using high fidelity models for the spacecraft, sensors, orbital mechanics, attitude control system, power, and thermal systems. With the ability to accurately predict all aspects of a DCE, various optimizers have been developed and are employed automatically to prevent constraint violation. This optimization capability, coupled with constraint filtering during the opportunity analysis phase of mission planning, greatly facilitates the successful planning of Surveillance DCEs.

During monthly level planning, the GOOD_TIMES software tool automates the large task of identifying all opportunities for each type of DCE to run. During weekly and daily planning, the PROGRAPH software tool automates the entire process of doing a final check that all constraints are met and that there are no violations. Prograph uses a graphical user interface that allows the operator to view either a summary display of all major constraint checks, or zoom in on a particular one. The confidence gained during operations to date allow the SPOCC mission planners to quickly verify that each event meets all constraints.

The Simulator, ACG, and CVT constitute the core of the mission planning pipeline that is run end to end for each data collection event at the weekly and daily levels. The mission planning system incorporates several types of automation to minimize human operator workload during mission planning. The pieces of the pipeline can be run either

33

individually, or the whole pipeline can be run with one call to a script. A script is also available to assist the mission planners in properly naming SLED files, as well as a weekly level script which automatically archives the pipeline output files, transmits the EDF and cost report files to APL, and updates a database as to what files were sent.

## 5.0 Performance Statistics

For the purposes of this paper, performance is measured by SPOCC's ability to plan DCEs that meet all MOCARH constraints under the APL mission planning timelines. Table 1 summarizes the performance of the SPOCC mission planning system as of the end of Month 9, Week 2 of the MSX mission. The left most column under "On Monthly Objectives" shows the total number of events requested by the MPT for inclusion in the monthly schedule. Of these, the right column shows with a * the number of priority 5 DCEs. Priority 5 DCEs have a very low priority and typically do not get scheduled. Therefore, the expected number of "Scheduled" DCEs, which make it onto the monthly schedule, will approximate the total number of requested DCEs minus the priority 5 DCEs.

**TABLE 1**
**Number of Events Planned BY SPOCC As of the end of Month 9, Week 2**

| | Number of Data Collection Events | | | |
|---|---|---|---|---|
| Month | On Monthly Objectives | | Scheduled | Run on SBV |
| 2 | 14 | 4* | 10 | 9 |
| 3 | 10 | 3* | 8 | 7 |
| 4 | 12 | 5* | 10 | 7 |
| 5 | 18 | 9* | 8 | 7 |
| 6 | 17 | 8* | 8 | 8 |
| 7 | 20 | 10* | 10 | 10 |
| 8 | 26 | 11* | 14 | 14 |
| 9 | 30 | 15* | 14 | 5** |
| 10 | 25 | 9* | 14 | N/A |
| 11 | 23 | 10* | N/A | N/A |
| Total | 195 | 84 | 96 | 67 |

* Number of Priority 5 DCEs
** As of week 2

Note that not all of the surveillance DCEs scheduled at the monthly level were run on the MSX. The bulk of the DCEs removed from the schedule or canceled were due to factors unrelated to SPOCC mission planning performance. These reason include schedule conflicts due to spacecraft anomalies whose resolution ran into the scheduled time of an event, over subscription of spacecraft resources (such as tape recorder) by other preceding events, or schedule changes in high priority events involving target missions for other PIs. Only one surveillance DCE was canceled by APL at the daily level due to a constraint violation. However, this cancellation turned out to be unnecessary, since subsequent analysis by APL

found that the constraint was not properly defined and is no longer in effect. Therefore, SPOCC has successfully planned 67 of 68 events at the daily level, or a success rate of 99%.

During the planning of the 67 DCEs run on the spacecraft thus far, the SPOCC mission planning system planned the collection of 802 frame sets of SBV data. This includes both raw frames sent to the tape recorder as well as frame sets processed onboard. In the 802 framesets, 479 detected objects were successfully correlated against the catalog of resident space objects.

## 6.0 Summary

The SPOCC mission planning system has been developed to operate as part of the APL mission planning system for the MSX spacecraft. Despite many constraints and challenging planning timelines, SPOCC has achieved a very high performance with a success rate of nearly 99% in planning events run on the MSX spacecraft. To date, SPOCC has successfully generated monthly level opportunities for 195 events, weekly EDF for 96 events place on the schedule, and daily EDF for 67 events that have run on the MSX.

## 7.0 References

1. The SPOCC team : "SPOCC Design Document, revision 6.0", Doc. no. 91PM-SPC-0024, MIT Lincoln laboratory, 28 Feb. 1992.
2. D.C.Harrison : "Space-Based visible (SBV) Program : System definition document", Project Report SBV-10, MIT/Lincoln Laboratory, 6 Feb. 1991.
3. P. Chu : " Efficient Detection of Small Moving Objects", Technical report TR-846, MIT/Lincoln Laboratory, 21 July 1989.
4. T.P.Opar : "Space-Based Visible Band Sensor Detection performance Analysis", Project Report SBS-9, MIT Lincoln Laboratory, 16 Aug. 1988.
5. Mission Research Corporation : " MidCourse Space Experiment (MSX) Preliminary Data Management Plan, DoD SDIO Report, 15 July 1991.
6. Anon : "Mission Operations, Constraints and Requirements Handbook (MOCARH)", MSX report, MSX Mission Operations Center, Johns Hopkins University / Applied Physics Laboratory, 1994.
7. SPOCC Mission Planning Team : "The Simulator Reference manual, Version 3.0", MIT Lincoln Laboratory, 1994.
8. R.Sridharan et al : "Opportunity Analysis for Space - Based Surveillance Experiments" MIT Lincoln Laboratory Technical Report No. 1011, 1994.

# SBV Data Reduction

J. Sharma[1], C. von Braun[1], and E.M.Gaposchkin[2]

## Abstract

The Midcourse Space Experiment (MSX) satellite, launched 24 April 1996, carries the Space Based Visible (SBV) sensor package designed for conducting Space Surveillance from a space platform. The SBV consists of a visible imaging CCD sensor that generates sets of images of resident space objects (RSOs) against a star background. These images are either directly sent to a tape recorder for later transmission to the ground for processing, or more commonly they are processed onboard the sensor package and only the data associated with the stars and potential RSO's are downlinked for processing. This paper will describe the SBV data reduction process of generating metric observations from SBV data. This process consists of first determining an accurate pointing of the SBV sensor using the star background. The refined pointing is then used to generate right ascension and declination observations for the RSO. Finally, the RSO is identified by correlating the observations with a complete RSO catalogue. This paper will discuss the algorithms used and present a summary of data processed.

## Introduction

The goal of SBV is to demonstrate the ability to make observations of resident space objects (RSOs) from a space based platform. This paper describes how these data are reduced to generate metric observations of RSOs. The SBV sensor is a 15 cm aperture off-axis, re-imaging, all-reflective telescope with a thermo-electrically cooled, bare CCD focal plane. Also contained aboard the MSX spacecraft is a signal processor and supporting electronics. The SBV focal plane consists of four three sided abuttable frame transfer CCDs, each composed of 420x420, 27 $\mu$m pixels. Additional characteristics of the SBV are presented in Table 1.[Ref 1]

---

[1] Technical Staff Member, Massachusetts Institute of Technology Lincoln Laboratory, Lexington

[2] Senior Staff Member and MSX Surveillance Principal Investigator, Massachusetts Institute of Technology Lincoln Laboratory, Lexington

Table 1. SBV Characteristics

| | |
|---|---|
| Spectral Range | 0.3 - 0.9 μm |
| Spatial Resolution | 12.1 arcsec/pixel |
| Field of View | 1.4 x 6.6 deg |
| Aperture, f/no | 15 cm, f/3 |
| Frame Integration Times | 0.4, 0.5, 0.625, 1.0, 1.6, 3.125 sec |
| Frame Sizes | 420x420, 357x420, 178x420 pixels |
| Dynamic Range | 12 bit |
| Quantum Efficiency | 28 % |

The principal task for SBV is to perform space surveillance. There are two tracking modes that are employed to observe RSOs. The most commonly used method is to track the background stars so they appear as point like sources on the focal plane. All RSOs will have a relative motion with respect to stars and will appear as streaks on the focal plane. This first method is known as sidereal tracking. The second method is to track the RSO such that it appears as a point source on the focal plane, and the stars appear as streaks on the focal plane. The method is called ephemeris track mode. Any additional RSOs that are in the SBV's field of view and are not being tracked will also appear as streaks on the focal plane in the ephemeris track mode.

**Data Processing**

The data flow for SBV is shown in Figure 1. A typical observation of an RSO by SBV consists of 6-16 420x420 pixel frames. These frames can be downlinked as raw images via an onboard tape recorder. A second option is to process all the frames through the onboard signal processor. The SBV signal processor extracts the pertinent information from the raw frames, which are then downlinked as a signal processor report. The report contains data on focal plane detections in the frame set that appear as point sources and those that appear as streaks. The most significant advantage of using the signal processor is the reduction in the amount of information that has to downlinked by two orders of magnitude. For 16 420x420 frames, 5000 KBytes of raw image data are reduced by more than two orders of magnitude to 3 KBytes. The onboard processing allows more data to be returned from the spacecraft in a timely fashion. The signal processor is primarily used to process observations using the sidereal tracking mode, which constitutes the primary method of observing RSOs.
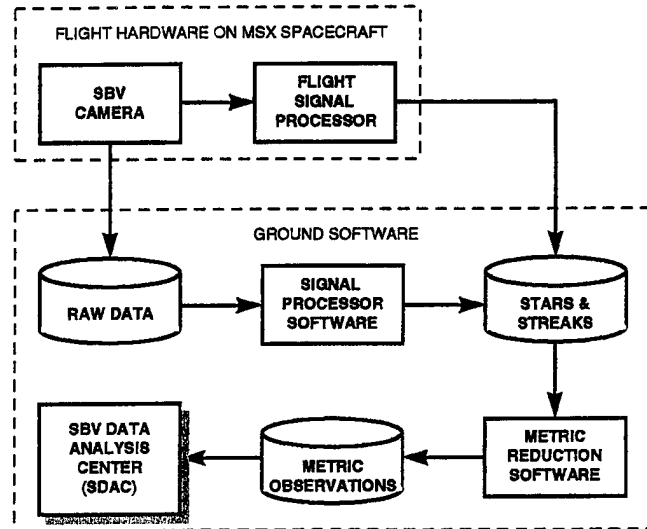
38

Figure 1. SBV Data Flow Diagram

Figure 2 shows examples of the different data types and the two different data modes. A description of the examples is summarized in Table 2. Figures 2a and 2b represent a special data-take mode where both the raw frames and signal processed frames are sent to the ground. Figure 2b is an reconstructed image of the signal processor report file. This image shows the square blocks (7x7 pixels), representing detections that the signal processor labels as star candidates. The number of star candidates desired must be specified to the signal processor, and was set to 20 for this observation. The streak detection is also plotted and consists of a 5 pixel wide region that the signal processor labels as a streak candidate. Figure 2c represents data taken using the ephemeris track mode in which two satellites were identified, one that was being tracked and another that appeared coincidentally.
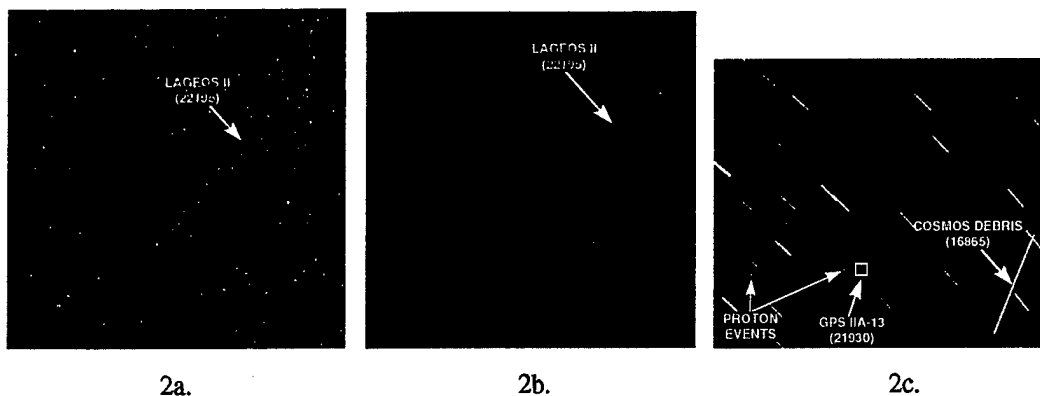


2a.                              2b.                              2c.

Figure 2. Examples of SBV Data

39

Table 2. Description Summary

|  | Figure 2a | Figure 2b | Figure 2c |
|---|---|---|---|
| Image Type | Raw | Signal Processed Report | Raw |
| Tracking Mode | Sidereal | Sidereal | Ephemeris |
| Number of Frames | 16 | 16 | 16 |
| Frame Integration Time | 0.625 sec | 0.625 sec | 1 sec |
| Correlated Object | Lageos II | Lageos II | GPS IIA-13, Cosmos Debris |
| Image Size (pixels) | 420x420 | 420x420 | 357x420 |

Once the image has been processed through either the on board or ground processor and the star and streak-ike detections have been identified, the next step is to perform metric reduction on the data. A flow diagram of the processing is presented in Figure 3.
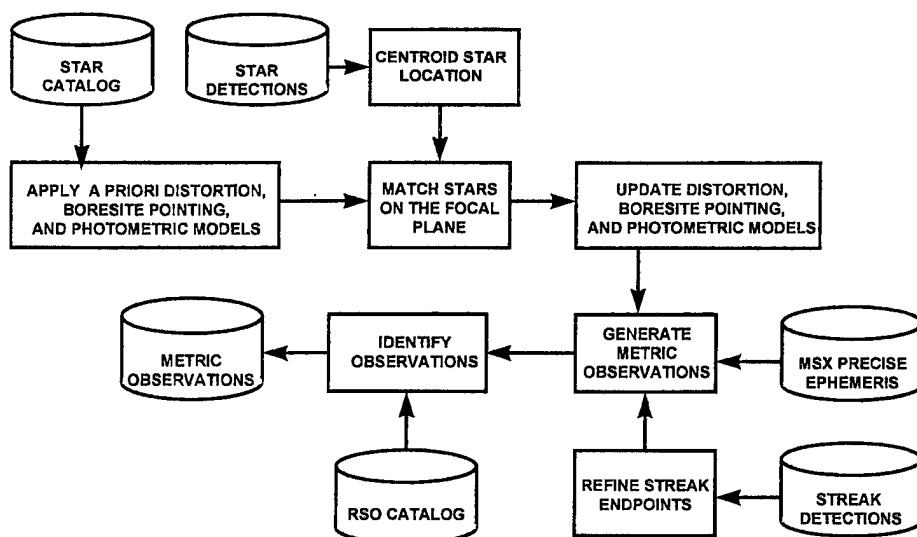


Figure 3. SBV Metric Data Reduction

The SBV is a self-alibrating sensor, in that it determines the borsight pointing from the data it collects. This is accomplished by matching the detected stars to catalog star positions. This matching is performed on the focal plane, and requires the mapping of catalog stars onto the focal plane. The SBV has highly distorted optics (not defraction limited) due to its design which maximizes the rejection of stray light from the focal plane. This distortion must be accurately modeled for the start matching procedure to work. The mapping of catalog stars to the

focal plane is a two step process. The convention for the focal plane adopted here is the mapping of the MSX spacecraft body-fixed axis on to the focal plane, and is shown in Figures 4 and 5 respectively.
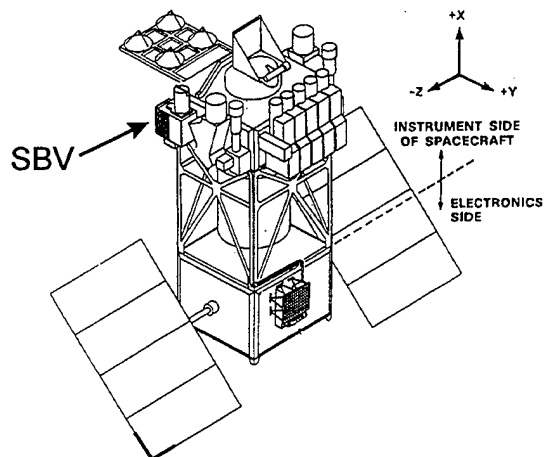


Figure 4.  MSX Spacecraft Body Fixed Axes
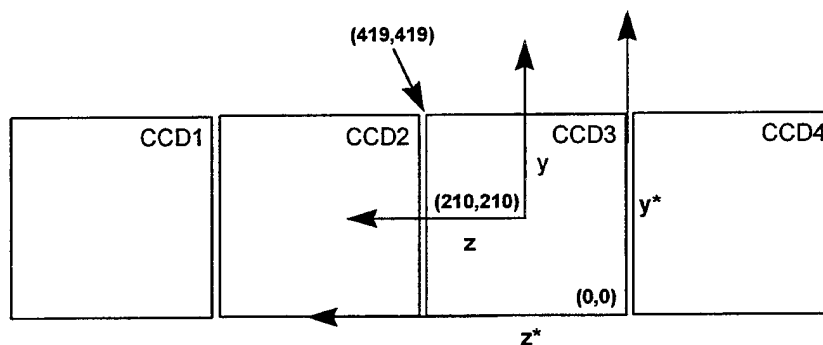


Figure 5.  Focal Plane Coordinates

(The x axis is directed out of the paper)

The first step involves the mapping the catalog stars to an undistorted focal plane position (z, y):

$$
\begin{bmatrix} 1 \\ y / P_{scale} \\ z / P_{scale} \end{bmatrix} = \mathbf{R}_1\!\left(\psi_o\right)\mathbf{R}_2\!\left(-\delta_o\right)\mathbf{R}_3\!\left(\alpha_o\right) \begin{bmatrix} \cos\alpha^* \cos\delta^* \\ \sin\alpha^* \cos\delta^* \\ \sin\delta^* \end{bmatrix}
$$

$\left(\alpha^*,\delta^*\right)$ = Star catalog position (Right Ascension - RA, Declination - DEC)

$\left(\alpha_o,\delta_o,\psi_o\right)$ = A priori RA, DEC, and Roll Angle of SBV borsight

41

$\mathbf{R}_1, \mathbf{R}_2, \mathbf{R}_3$ = Rotation matrices about (x, y, z) MSX body fixed axes respectively

Assuming 12.5 arcsec /pixel, the plate scale is

$$P_{scale} = \frac{1}{\sin\left(\dfrac{12.5}{3600}\right)} = 16501.185.$$

The next step in transforming the undistorted focal plane coordinates into distorted focal plane coordinates is to account for offsets in the borsight $(z_o, y_o)$, and an error in roll angle $(\theta)$:

$$\begin{bmatrix} \zeta \\ \eta \end{bmatrix} = \begin{bmatrix} \cos\theta & \sin\theta \\ -\sin\theta & \cos\theta \end{bmatrix} \begin{bmatrix} z - z_o \\ y - y_o \end{bmatrix}$$

The final transformation is the application of the distortion model to generate distorted focal plane coordinates $(\tilde{z}, \tilde{y})$.

$$\begin{bmatrix} \tilde{z} \\ \tilde{y} \end{bmatrix} = \mathbf{A} \begin{bmatrix} \zeta \\ \eta \end{bmatrix}$$

$$\mathbf{A} = \begin{bmatrix} a_{11} & a_{12} \\ a_{21} & a_{22} \end{bmatrix},$$

$$a_{11} = a_{11}^{00} + a_{11}^{10}\zeta + a_{11}^{01}\eta + a_{11}^{10}\zeta + a_{11}^{20}\zeta^2 + a_{11}^{11}\zeta\eta + a_{11}^{02}\eta^2$$

$$a_{21} = a_{21}^{00} + a_{21}^{10}\zeta + a_{21}^{01}\eta + a_{21}^{10}\zeta + a_{21}^{20}\zeta^2 + a_{21}^{11}\zeta\eta + a_{21}^{02}\eta^2$$

$$a_{12} = a_{21}$$

$$a_{22} = a_{22}^{00} + a_{22}^{10}\zeta + a_{22}^{01}\eta + a_{22}^{10}\zeta + a_{22}^{20}\zeta^2 + a_{22}^{11}\zeta\eta + a_{22}^{02}\eta^2$$

An illustration of the distortion that is present is illustrated by Figure 6. This figure shows the star detections from actual SBV observations. The distortion model coefficients $\left(a_{ij}^{nm}\right)$ have been determined from analysis of on orbit data taken in dense star fields. The plot shows the position of distorted and undistorted detection locations for CCD3 and CCD1. The distortion is on the order of tens of pixels for CCD3 and increases to more than 100 pixels on CCD1.
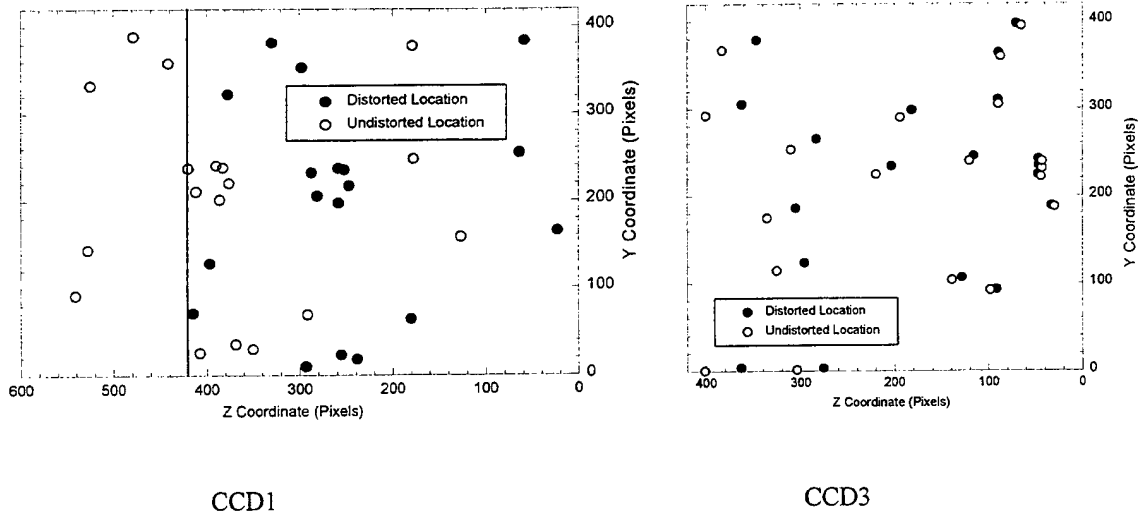
CCD1                                            CCD3

Figure 6. Illustration of SBV Distortion

The star matching consists of matching the coordinates $\left(\widetilde{z},\widetilde{y}\right)$ to the centroid locations of the star detections

$\left(z,y\right)$. The centroid location is calculated by fitting a point spread function to each detection to minimize errors from the detection of apparent and partial double stars. The matching process involves two steps. The first step consists of a coarse star match that involves matching a pattern of lines and vertices connecting a few selected stars, and is intended to account for initial pointing errors. Once the first step has succeeded, the next step is a more precise star matching procedure that involves comparing the (z,y) pixel locations of detected and catalog stars. The difference of the two star positions is used to drive a least squares operation that updates the SBV attitude by adjusting the parameters $\left(z_o,x_o,\theta,a_{11}^{00},a_{22}^{00}\right)$. The remaining terms in the distortion model are not estimated for each data set. The final matching process is iterated until the number of matched stars does not increase. The matched stars are also used to update the magnitude offset term $\left(V_o\right)$. This offset used to convert the detected intensity to a SBV magnitude:

$$\text{SBV Magnitude} = -2.5 Log\left(\frac{Total\ Intensity}{Total\ Integration\ Time}\right) + V_o.$$

The final step in updating the SBV attitude requires converting $\left(z_o,x_o,\theta\right)$ to an updated attitude $\left(\alpha,\delta,\psi\right)$. The right ascension and declination are calculated using the following relationship:

43

$$\begin{bmatrix} \cos\alpha\cos\delta \\ \sin\alpha\cos\delta \\ \sin\delta \end{bmatrix} = \mathbf{R}_3(-\alpha_o)\mathbf{R}_2(\delta_o)\mathbf{R}_1(-\psi_o)\begin{bmatrix} \sqrt{1-(y_o/P_{scale})^2-(z_o/P_{scale})^2} \\ y_o/P_{scale} \\ z_o/P_{scale} \end{bmatrix}.$$

$$= \hat{l}_1$$

Updating the roll angle is slightly more complex and is described below:

$$\tan\psi = \frac{\hat{l}\cdot\hat{l}_3}{\hat{l}\cdot\hat{l}_2}$$

where

$$\hat{l} = \mathbf{R}_3(-\alpha_o)\mathbf{R}_2(\delta_o)\begin{bmatrix} 0 \\ \cos(\psi+\theta) \\ \sin(\psi+\theta) \end{bmatrix}$$

and

$$\hat{l}_2 = \begin{bmatrix} 0 \\ 0 \\ 1 \end{bmatrix}\times\hat{l}_1 \quad,\quad \hat{l}_3 = \hat{l}_1\times\hat{l}_2.$$

Once the attitude has been updated the next step is to refine the streak end points using the signature information that is sent down with the streak. The signature data, generated by the signal processor, is a 5-pixel-wide swath that encompasses the streak, and consists of the maximum minus the mean intensity of streak pixels, and the frame in which it occurs. The signature allows the data reduction process to overcome two limitations of the signal processor: integer arithmetic limits the accuracy of endpoint calculations to one pixel and the signal processor is unable to screen out bad pixels. The refinement process consists of throwing out bad pixels not belonging to the time continuum of the streak and of fitting a line through the signature data. The endpoints of the line are taken as the refined endpoints. Once the endpoints have been determined, they must be transformed from focal plane coordinates to object space coordinates (RA, DEC). The streak endpoints must first be transformed from distorted to undistorted focal plane coordinates. This step requires the inversion of the distortion model, and is a iterative process due to its nonlinearity. The following expression is iterated to calculate the undistorted focal plane location $(\zeta,\eta)$ of the detection.

$$\begin{bmatrix} \zeta_{n+1} \\ \eta_{n+1} \end{bmatrix} = \mathbf{A}^{-1}(\zeta_n,\eta_n)\begin{bmatrix} \tilde{z} \\ \tilde{y} \end{bmatrix},$$

using the following initial condition

$$\begin{bmatrix} \zeta_o \\ \eta_o \end{bmatrix} = \begin{bmatrix} \tilde{z} \\ \tilde{y} \end{bmatrix}.$$

$$\begin{bmatrix} z \\ y \end{bmatrix} = \begin{bmatrix} \cos(-\theta) & \sin(-\theta) \\ -\sin(-\theta) & \cos(-\theta) \end{bmatrix} \begin{bmatrix} \zeta \\ \eta \end{bmatrix} + \begin{bmatrix} z_o \\ y_o \end{bmatrix}$$

$$\begin{bmatrix} \cos\overline{\alpha}\cos\overline{\delta} \\ \sin\overline{\alpha}\cos\overline{\delta} \\ \sin\overline{\delta} \end{bmatrix} = \mathbf{R}_3(-\alpha_o)\mathbf{R}_2(\delta_o)\mathbf{R}_1(-\psi_o) \begin{bmatrix} \sqrt{1-\left(y/P_{scale}\right)^2-\left(z/P_{scale}\right)^2} \\ y/P_{scale} \\ z/P_{scale} \end{bmatrix}$$

$(\overline{\alpha}, \overline{\delta})$ = Streak endpoint position (Right Ascension - RA, Declination - DEC)

After the (RA, DEC) locations of the streak endpoints are calculated, two observations are formed by attaching the precise location of MSX in WGS84 earth fixed coordinates to each observation. [Ref 2]

Once the observations have been formed it is necessary to identify the observations. This is accomplished by taking a complete catalog of RSOs and propagating each of the orbital element sets to the observation's time and by comparing the predicted RSO position to the observation. In practice the performance of the correlation process is increased by first performing a coarse correlation by propagating all of the RSOs using a simple propagation model (2-Body+J2 terms). Only RSO's that pass through the first filter are
then propagated again using a more precise ANODE model (2-Body, J2, J3, J4, Sun, & Moon). [Ref 3]  To minimize propagation errors, RSO catalogs no older than 48 hours from the observation time are used. Once identified , the observations are available for orbit processing and further assessment.

**Processing Results**

As of January 17, 1997 over 1300 data sets of surveillance data have been taken, of which over 95% consists of on orbit signal processed data. This section describes the processing results of 1148 onboard signal processed data sets that have more than 3 star matches. Nearly all the data have been collected with CCD3, although no degradation of performance has been observed with data taken with the other CCDs. The data spans 240 days from May 22, 1996 to January 17, 1997. The distortion model coefficients were calculated with onboard data collected during the first several weeks of SBV operation.[Ref 4] The goal of this section is describe the current performance of the SBV surveillance data processing. The results for the star matching process are based on the use of the Astrographic Catalog which has the lowest systematic errors of currently available catalogs at 0.2 arcsec for the majority of stars

in the catalog. [Ref 5] The star positions used are in J2000 inertial frame. It contains approximately 320,000 stars down to a visual magnitude of 10.5. The distribution of the number of stars matched for each data set is shown in Figure 7, and shows that on average 13 stars are matched.
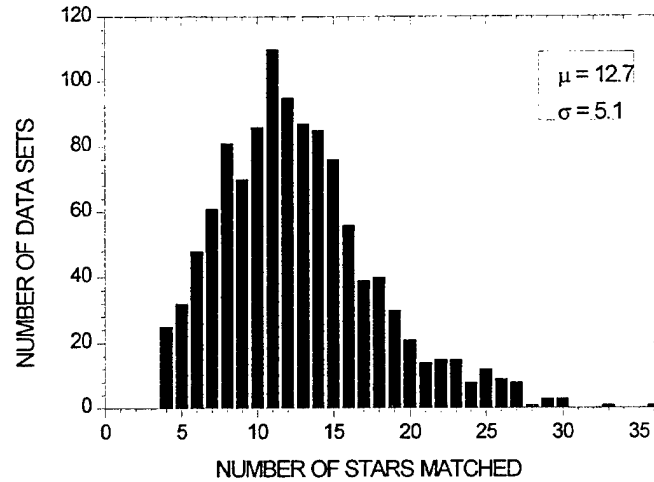


Figure 7. Number of Star Matches per Frameset

The quality of the star matches currently is being achieved is shown in Figure 8. This plot shows the distribution of the RMS star fit residuals over all the data sets and indicates the quality of the average star match. The tightness of the results indicates that there are no significant variations in the distortion model coefficients and that it is sufficient to estimate only the linear terms in the distortion model $\left( a_{11}^{00}, a_{22}^{00} \right)$.



Figure 8. RMS Star Fit Residual per Frameset

The above two graphs can also be used to approximate the uncertainty of the estimated borsight for each data set. Since the borsight is estimated using a least squares process, an estimate of uncertainty in the borsight can be

46

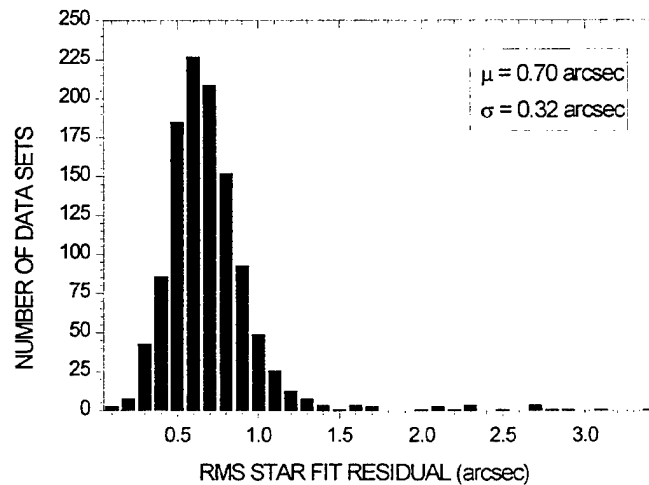approximated by scaling the RMS star fit residuals by the square root of the number of matched stars used in the fitting process. This approximation implies a borsight point uncertainty of a few tenths of an arcsec, which approaches the accuracy of current star catalogs.

Over 722 signatures have been correlated. The distribution of SBV-RSO ranges is shown in Figure 9. SBV primarily observes deep space objects, and the two broad categories that were observed are indicated on the figure. Objects in geotransfer orbits may appear in both semisynchronous and geosychronous categories.
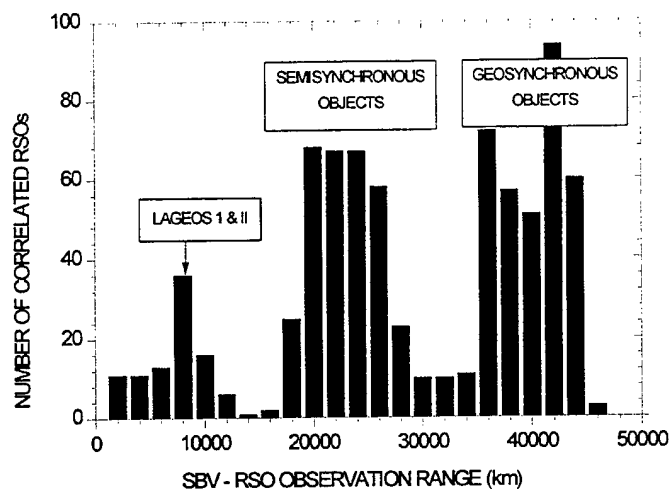


Figure 9. Categories of Objects Observed

The estimated magnitude of these observations is plotted in the Figure 10. This plot shows that detections down to 14th magnitude are routinely correlated.
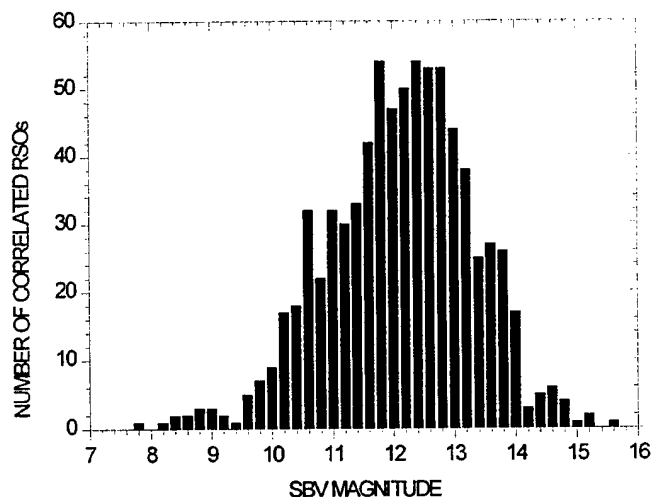


Figure 10. SBV Magnitude of Correlated Objects

47

**Summary**

The SBV instrument on MSX has successfully collected over 1000 frame sets of space surveillance data. These data have been successfully processed through the metric data reduction software. The distortion model has been accurately modeled and has produced sub-arcsecond star matches over the first eight months of the mission. Observations have been correlated on over 700 resident space objects as dim as 14$^{th}$ SBV magnitude.

**References**

1. Mill, J.D., et. al., *Midcourse Space Experiment: Introduction to the Spacecraft, Instruments, and Scientific Objectives*, J. Spacecraft and Rockets, Vol. 31, No. 5, 1994, pp. 900-907.

2. Abbot, R. I. et. al., *MSX Precise Ephemeris*, Submitted to the Space Control Conference, 1997.

3. Lane, M. T., *Increased Accuracy for ANODE High Altitude Orbit Calculations*, Presented at Space Surveillance Workshop, MIT Lincoln Laboratory, 1989.

4. von Braun, C., et. al., *SBV Metric Accuracy*, Submitted to the Space Control Conference, 1997.

5. Corbin, T.E, et. al., *Astrographic Catalogue Reference Stars (Documentation for the Computer-Readable Version)*, Doc. No. NSSDC/WDC-A-R&S 91-10, 1991.

# SBV METRIC ACCURACY

## C. von Braun[†], J. Sharma[†], E.M. Gaposchkin[††]

In April 1996 the Midcourse Space Experiment (MSX) satellite, sponsored by the Ballistic Missile Defense Organization (BMDO), was launched into an 898-km altitude, near sun-synchronous orbit. One of the principal sensors on-board the spacecraft is the Space-Based Visible (SBV), a visible-band opto-electronic camera used for space surveillance. The instrument is equipped with four adjacent 420x420 pixel CCDs and was designed with high off-axis stray light rejection characteristics for observing near the earthlimb. As the first space-based space surveillance sensor, SBV's principal role is to gather metric and photometric information on a wide variety of resident space objects (RSO). In order to assess the metric performance of the sensor, routine on-orbit metric calibration is performed. In addition, a complete error assessment was made using actual flight data. The goal of producing 4-arcsec (1-sigma) observations of RSOs was set during design, and early results show that this goal is being reached. This paper will present the analysis of each of the error sources within the SBV error budget and will show results from both calibration and routine surveillance data collection events. Error sources such as those associated with the sensor boresight pointing, including star catalog errors, spacecraft jitter, star centroiding and optical distortion, along with the MSX ephemeris and the streak endpoint determination will be discussed.

## INTRODUCTION

The Midcourse Space Experiment (MSX) is funded and managed by the Ballistic Missile Defense Organization (BMDO) with the goal of addressing fundamental phenomenological and functional issues associated with ballistic missile defense and space-based space surveillance. With its host of state-of-the-art visible-band, long-wavelength infrared and ultraviolet sensors, the spacecraft has successfully gathered high-quality data on strategic ballistic missile targets, resident space objects (RSO), and earth, earthlimb and celestial backgrounds over a wide range of the spectrum. In addition to supporting the fundamental objectives of the BMDO, MSX has also acquired data on a variety of civilian science objectives in the areas of remote sensing, atmospheric sciences and astronomy.

---

† Technical Staff Member, Massachusetts Institute of Technology Lincoln Laboratory, Lexington
†† Senior Staff Member and MSX Surveillance Principal Investigator, Massachusetts Institute of Technology Lincoln Laboratory, Lexington

One of the principal sensors on-board MSX is the Space-Based Visible (SBV), a visible-band opto-electronic camera designed to conduct technological and functional demonstrations in support of space-based space surveillance. The instrument was designed at the Massachusetts Institute of Technology Lincoln Laboratory through funding from the Space and Missile Center (SMC). As a possible flight technology demonstration for the Space-Based Infrared System - Low (SBIRS-Low), the SBV represents the first space-based staring sensor for use in space surveillance. The instrument is equipped with four adjacent 420x420 pixel CCDs and was designed with high off-axis stray light rejection characteristics for observing near the earthlimb.

As the first space-based space surveillance sensor, SBV's principal role is to gather metric and photometric information on a wide variety of resident space objects (RSO). In order to assess the metric performance of the sensor, routine on-orbit metric calibration is conducted. This is accomplished by observing satellites for which the positions are very well established and comparing these known positions with SBV-observed positions. During the design phase of the SBV program, the goal of producing 4-arcsec (1-sigma) metric observations of RSOs was set. This 4-arcsec error budget is comprised of a wide variety of error sources ranging from the estimated position of the sensor on-orbit to systematic uncertainties within the established star catalogs. While on-orbit metric calibration is the only true method of determining the metric performance of the SBV, an independent error assessment was made using actual flight data. This was performed by isolating each error source within the error budget and quantifying its effect on the SBV observation.

This paper will present the analysis of each of the error sources within the SBV error budget and will compare the results with those established from routine calibration. Error sources such as those associated with the sensor boresight pointing, including star catalog errors, spacecraft periodic motion, star centroiding and optical distortion, along with the MSX ephemeris and the streak endpoint determination will be discussed in detail. Finally, some conclusions will be drawn regarding the overall metric performance of the SBV and its impact on space surveillance.

## SBV DATA PROCESSING

The SBV performs data collection in, most commonly, a staring mode. In this mode, light from stellar sources, the cosmic background and any diffuse or specular reflection of an RSO within the field of view (FOV) will be detected on the focal plane. The light is gathered on the detector for integration periods of 0.4, 0.625, 1.0, and 1.6 seconds, depending on the operating type of data collection. An image gathered over one integration period is referred to as a frame. One raw or unprocessed frame of SBV data appears as a star field on a dark background, and, if an RSO is in the FOV, a short streak of illuminated pixels. Typically, a streak taken over one frame is not long enough to distinguish it from a stellar point source. As a consequence, it is necessary to superimpose multiple frames to produce an image which can be effectively processed.

A collection of frames, or frameset, typically consists of between eight and 16 frames. Figure 1 shows an SBV image of the Laser Geodynamics Satellite (LAGEOS) with a 16-frame frameset with an integration period of 1.0 seconds.

The process of establishing an observation (right ascension and declination) of an RSO entails, first, determining the precise pointing of the boresight of the sensor in absolute space, then determining the position of the beginning and end points of that streak on the focal plane. Once these focal plane positions are known, they can then be transformed into absolute space. Finally, the absolute position of the observing platform must be established to support the angular measurements.
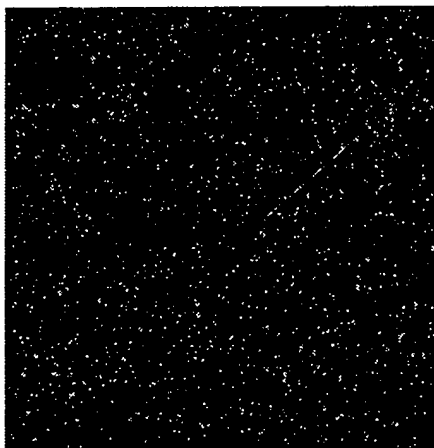
*Figure 1. SBV Image of LAGEOS*

For a detailed discussion of the processing of SBV image data, the reader is referred to Sharma *et al.*, (1997).

Once the observations of an RSO are established, they must be qualified through calibration. This is conducted routinely in operations, and the data are compiled and compared with the independently determined error budget. Metric calibration is performed by observing satellites for which the positions are known to a very high accuracy. These satellites, herein referred to as calibration objects, are tracked using high precision laser ranging observations. These laser data, along with ground radar measurements, are used to establish the satellites' positions to better than about 10cm. By tracking these objects using SBV, it is then possible to calibrate the metric observations using the known positions and to isolate those errors caused by the SBV sensor. Now a detailed discussion of each of the known error sources will be presented.

## SBV ERROR BUDGET

### MSX Ephemeris and Timing

As mentioned above, observations of an RSO from a moving space platform would be incomplete if they were not accompanied by information regarding the location of the sensor in space during the data collection. This is precisely the case for the SBV. As a consequence, it is necessary to supplement the reduced right ascension and declination observations of a target with the ephemeris of the MSX.

As part of the Surveillance Data Analysis Center (SDAC) at Lincoln Laboratory, the orbital position of MSX has been produced every day since launch. This is performed using the S-band Ground Link System (SGLS), a global network of tracking stations used by the Air Force for tracking a large number of its satellites. While the principles underlying the modeling and routine processing of the tracking data of MSX are beyond the scope of this paper, detailed explanations can be found in Abbot *et al.* (1997) and von Braun (1996).

The contribution of the error of the position of MSX to the SBV error budget is a function of the range to the RSO. For example, a target at a range of 3,000km produces a 1-arcsec error in the SBV observation, if the uncertainty in the position of MSX is limited to 15m. In contrast, an RSO in geosynchronous orbit at a range of 42,000km produces an error in the SBV observation of

51

just 0.07 arcsecs. Given that ranges of only 3000km are uncommon during operations and that 1-arcsec is limited to 25% of the total SBV error budget, the goal of routinely producing a 15-meter orbit for MSX was set during design. This goal has, in fact, been exceeded, with orbit position uncertainties routinely reaching the 10m level, as reported in Abbot *et al.* (1997). As a consequence, the contribution of the error in the MSX position to an SBV observation is typically less than 0.5 arcsecs and, for geosynchronous objects, is essentially negligible. It should be noted that for near real-time (less than 24 hours) ground processing of SBV data within the Space Surveillance Network (SSN), post-fit orbits of MSX are not possible and errors in the predicted MSX position may be as large as 30-50 meters. This is not a concern for deep space objects but could be an issue for RSOs at close range.

Uncertainties in the on-board system clocks used to tag SBV observations also contribute to the SBV error budget. The MSX system requirements, established independently from those of SBV, placed the specification of 1 millisecond on the system clocks. Since timing errors are a function of range to the RSO and the relative motion of the RSO across the SBV focal plane, it is possible to set reasonable bounds on the errors. In a worst-case scenario, such as observing a target at 2,500km when the relative velocity is at its maximum of 15km/s, a 1-millisecond timing error produces a 1.3-arcsec error in the SBV observation. In contrast, a best-case scenario entails observing a geo-belt satellite while MSX crossed over one of the poles, giving a relative velocity of 3.1km/s (absolute velocity of the target only). This situation produces an error of about 0.02 arcsecs. Conseqently, timing errors are typically less than 1 arcsec and are frequently completely negligible.

**Boresight Pointing**

In order to determine the boresight pointing of the SBV, it is necessary to match the collection of star detections on the focal plane with cataloged star positions. In matching these positions in a least-squares sense, a correction to the *a priori* boresight pointing is determined. The product of this process will be a set of star-match residuals which, as an ensemble, quantify the ability to match an "average" star. The formal uncertainty of the boresight pointing can then be determined based on this information, in addition to the number of stars matched in a given field of view. It is this stage of SBV data reduction which introduces some of the most subtle and important errors in the process. Errors associated with the star catalogs, the algorithms used for centroiding the star detections on the focal plane, the distortion of the CCD image introduced by the optics, and the actual spacecraft drift and periodic motion all contribute to the boresight pointing error. A discussion will now be made of each of these error sources.

### *Star Catalogs*

During routine processing of SBV data, the Astrographic Catalog of Reference Stars (ACRS) is most commonly used. This catalog, compiled at the U.S. Naval Observatory, contains some 320,000 stars with visual magnitudes of 10.5 and brighter. In addition to this catalog, the SDAC uses the Hubble Guide Star Catalog (GSC) which was constructed to support the Hubble Space Telescope during operations. The GSC contains more than 15 million stars with visual magnitudes of 16 and brighter. Table 1 shows the various characteristics of each catalog.

With regard to the discussion of the SBV error budget, the random and systematic errors are of critical importance. While the GSC offers a far denser array of stars per square degree than does the ACRS, the systematic errors are larger. In fact, as will be illustrated in the section which follows, it is the systematic errors in the ACRS which are limiting the boresight pointing for SBV.

Table 1
Star Catalogs Used With SBV

| Star Catalog | Affiliation | No. of Stars | Limiting Magnitude | Avg # of Stars Per Sq. Degree | Systematic Errors | Random Errors |
|---|---|---|---|---|---|---|
| ACRS | U. S. Naval Observatory | 320,000 | 10.5 | 7.9 | 0".1 - 0".2 | 0".25 - 1".0 |
| GSC | Hubble Space Telescope Institute | 15 Million | 16 | 365 | 0".4 - 1".6 | 0".3 - 0".8 |

## *Star Centroiding*

A study of the errors due to the centroiding of the group of illuminated pixels comprising a star detection was conducted prior to launch. These results found that the performance of the centroiding algorithm decreased as the signal-to-noise of the star detection on the focal plane decreased. From a Monte Carlo simulation of the errors as a function of detected magnitude, it was found that for a star of $10^{th}$ magnitude, the centroiding errors were limited to 0.1 arcsec. Similarly, for stars as dim as $14^{th}$ magnitude, centroiding errors rose to as large as 6.6 arcsec. As a consequence of this study, the star matching process is typically limited to stars of $12^{th}$ or $13^{th}$ magnitude or brighter.

In the sections which follow, it will be discussed how centroiding error is affected by spacecraft drift and periodic motion and the influence they have on the overall boresight pointing error.

## *Spacecraft Drift and Periodic Motion*

Although spacecraft drift and periodic motion do not factor directly into the SBV error budget, they do influence the ability to perform centroiding on the star detection. While the sensor is gathering light during one integration period, or "exposure", the spacecraft attitude is experiencing some degree of secular and periodic motion. The secular behavior causes the grouping of illuminated pixels from a detection to elongate in the direction of the drift motion. This effect, if substantial, shifts the location of the centroid, when compared to one determined when drift is not present. Similarly, the periodic motion tends to create an enlargement or "blurring" of the group, which affects the centroid location. While neither of these effects is large, they both degrade the quality of the star-fit residuals.

During a pointing alignment event on the MSX, the SBV produces an image every 1.0 seconds. As mentioned earlier, these frames are routinely processed in batches of between eight and 16. However, if each frame, individually, is matched to the star catalog, the corrected pointing can be determined every 1.0 seconds. This, effectively, produces a time series of the attitude of the spacecraft, identifying both the drift and the 1-Hz periodic motion. It should be noted that periodic motion at frequencies both higher and lower than 1-Hz do exist, but these can not be identified using SBV.

This process was carried out using 10 framesets from five different MSX pointing alignment events conducted over the first six months of the mission. From these, an average value for the drift and 1-Hz periodic motion was determined. Figure 1 (left) shows a typical time series of the difference of the right ascension, declination and roll (RA, DEC, ROLL) from the boresight pointing of the initial frame for a 16-frame frameset. The accompanying plot effectively removes the drift
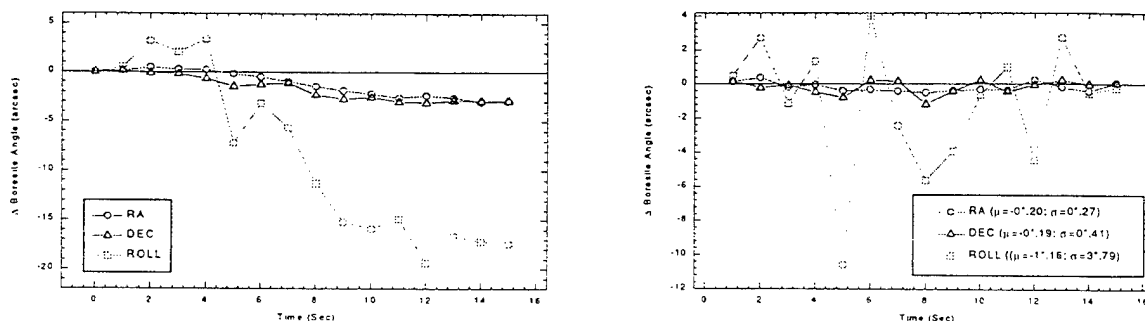
53

*Figure 2. Spacecraft Drift and 1-Hz Periodic Motion*

effect by differencing the pointing results for a given frame with those of the previous frame. This allows for the assessment of the 1-Hz periodic motion.

For the pointing alignment data analyzed, the drift varied between zero and 0.3 arcsec/sec, in absolute value, and the average standard deviation of the 1-Hz periodic motion in RA and DEC was 0.4 arcsec. Given that these quantities only indirectly contribute to the error budget by degrading the centroiding, these values will not adversely affect the boresight pointing. It should be noted that, while the roll angle appears to vary to a much larger degree than do the RA and DEC, this is only an artifact of the poor sensitivity of SBV to this direction of motion and should not be concluded as the actual roll behavior.

### *Optical Distortion*

In order to produce boresight pointing results to the level of 1 arcsec, it is necessary to model the optical distortion of the camera. Predominantly for the purposes of reducing stray-light from the earthlimb, the SBV has a number of hyperbolic and elliptic mirrors which project the incoming light onto the focal plane. These mirrors produce an image which is distorted and this distortion must be accounted for during the star matching process. It is interesting to note that this distortion is severe enough, particularly at the outer edges of the CCD, to shift the position of a star or RSO detection by as much as 100 pixels.

During the first few months of the mission, a rigorous determination of the distortion model was conducted using actual flight data. The primary requirements of this mathematical distortion map are that it be valid over the entire CCD, that it be stable over time, and that the remaining unmodeled distortion errors not be so large as to produce boresight pointing results poorer than 1 arcsec. As a consequence, the MSX pointing alignment events, which are staring events at fields rich in stars, were used for this purpose. To achieve a model which is valid over the entire array, it was necessary to have a large number of stars detected everywhere on the focal plane. This allowed for the accurate determination of the map.

The process of matching the distorted detected star positions to the actual catalog star positions is performed in focal plane coordinates. As a consequence, the star positions are mapped onto the array by first translating and rotating the cataloged star field and "aligning" it with the detected field. Then the distortion map is used to project these translated/rotated cataloged positions onto the distorted focal plane image. Once this is complete, the star matching is performed in a least-squares sense and the residuals are determined.

The mathematical structure of the distortion map consists of the translation, referred to as the boresight offset, $(z_o, y_o)$, followed by a rotation about the roll axis by the error in the roll angle, $\theta$, such that

where

$$\begin{bmatrix} \xi \\ \eta \end{bmatrix} = R(\theta) \begin{bmatrix} z - z_o \\ \\ y - y_o \end{bmatrix}$$

where

$$R = \begin{bmatrix} \cos(\theta) & \sin(\theta) \\ -\sin(\theta) & \cos(\theta) \end{bmatrix}$$

This produces the coordinate pair $(\xi, \eta)$, which represents the undistorted cataloged star positions on the focal plane. These coordinates are then transformed into distorted coordinates, $(z', y')$, such that

$$\begin{bmatrix} z' \\ y' \end{bmatrix} = A \begin{bmatrix} \xi \\ \eta \end{bmatrix}$$

where

$$A = \begin{bmatrix} a_{11} & a_{12} \\ a_{21} & a_{22} \end{bmatrix}$$

and

$$a_{11} = a_{11}{}^{00} + a_{11}{}^{10}\xi + a_{11}{}^{01}\eta + a_{11}{}^{20}\xi^2 + a_{11}{}^{11}\xi\eta + a_{11}{}^{02}\eta^2$$
$$a_{21} = a_{21}{}^{00} + a_{21}{}^{10}\xi + a_{21}{}^{01}\eta + a_{21}{}^{20}\xi^2 + a_{21}{}^{11}\xi\eta + a_{21}{}^{02}\eta^2$$
$$a_{12} = a_{21}$$
$$a_{22} = a_{22}{}^{00} + a_{22}{}^{10}\xi + a_{22}{}^{01}\eta + a_{22}{}^{20}\xi^2 + a_{22}{}^{11}\xi\eta + a_{22}{}^{02}\eta^2$$

For the determination of the distortion map, it was necessary to simultaneously estimate the boresight offset, the error in roll and each of the 18 distortion coefficients during the star matching procedure. This was performed for each of the four CCDs using 36 framesets from five pointing alignment events (DC-29) and one SBV calibration event (SU-03). Due to the large number of stars needed for the determination of the map, the GSC was used. Figure 3 shows a typical pointing alignment star field and the stars which were matched in the least squares process. In this particular case, over 290 stars were correlated to the catalog. Table 2 shows the quality of the residuals of the least squares star
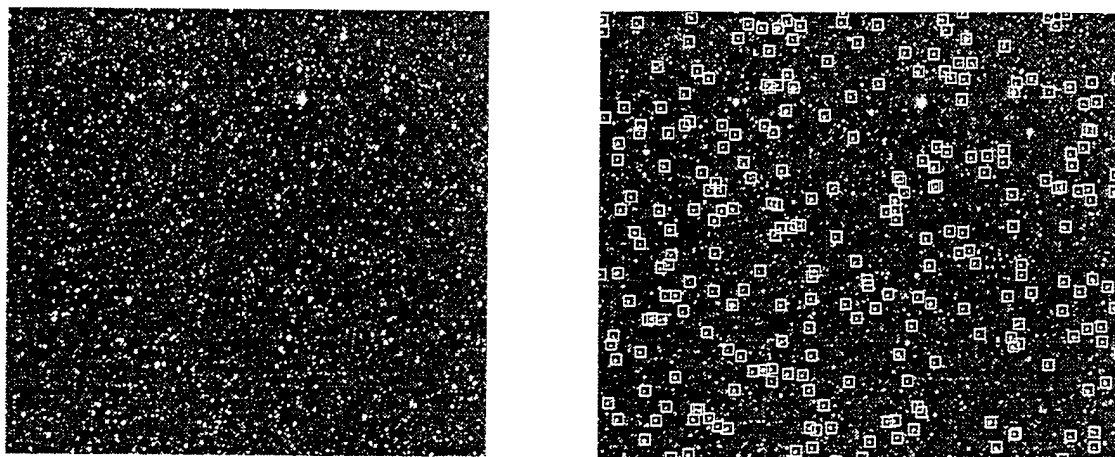
*Figure 3. MSX Pointing Alignment Event*

matching procedure, and Table 3 shows the estimated values for the offset, the error in roll and their formal estimated uncertainties. It was found that, while it was clearly necessary to estimate all 18 coefficients in the distortion map during its development, it is sufficient to estimate the boresight offset, the error in roll and only the two most important terms in the distortion map, $a_{11}^{00}$ and $a_{22}^{00}$. These coefficients represent the zeroth order distortion or "stretching" along the $z$ and $y$ coordinates.

Table 2
Star Match Quality in Distortion Map Study

| CCD | # of Framesets | RMS Star Fit (arcsec) |
|---|---|---|
| 1 | 6 | 0.8 |
| 2 | 9 | 1.0 |
| 3 | 13 | 0.9 |
| 3 | 9 | 0.9 |

Table 3
Determination of Offsets and Roll Error

| | | $<z_0>$ Pixels | $\sigma_{zc}$ Pixels | $<y_0>$ Pixels | $\sigma_{yo}$ Pixels | $<\theta>$ deg | $\sigma_{\theta}$ deg |
|---|---|---|---|---|---|---|---|
| DC-29 | CCD-1 | 974.50 | 0.66 | 2.85 | 0.21 | -0.610 | 0.005 |
| DC-29 | CCD-2 | 500.80 | 0.76 | -11.88 | 0.18 | -0.493 | 0.006 |
| DC-29 | CCD-3 | 17.66 | 0.66 | -7.87 | 0.16 | -0.383 | 0.009 |
| SU-03 | CCD-3 | 18.74 | 0.47 | -9.05 | 0.12 | -0.378 | 0.009 |
| DC-29 | CCD-4 | -455.54 | 0.77 | 14.87 | 0.24 | -0.277 | 0.007 |

## Boresight Pointing Results

Having identified the various error sources involved in determining the boresight pointing, it is now possible to get an estimate of the total contribution which pointing makes to the 4-arcsec performance goal for SBV. As discussed, the pointing error budget is made up of star catalog error, spacecraft drift and jitter, centroiding error, and optical distortion. These errors, however, do not simply superpose to yield the total pointing error; they merely act to produce the residual error when star detections are matched to a catalog.

The formal uncertainty in pointing is, essentially, based on the "average" star fit quality, an example of which is shown in Table 2, and the total number of stars matched in a given frameset. If there were no systematic errors present in the star catalog and the errors in pointing and roll were not correlated with each other, the formal error covariance would be a diagonal matrix. In such a case, the error in each of the two pointing variables (RA and DEC) would be simply the star fit residual reduced by $\sqrt{n}$, where $n$ is the number of matched stars. With star matches of between 10 and 500 stars, depending on the star field and star catalog used, this would produce a boresight pointing uncertainty of between 0.3 and 0.05 arcsecs, respectively. It, however, is not possible to determine pointing to these lowest levels, since the ACRS star catalog has systematic errors of 0.1-0.2 arcsec and the GSC has errors between 0.4 and 1.6 arcsec.

This limitation in boresight pointing due to systematic error in the star catalogs is evident from all the SBV data gathered since launch. Routine processing of SBV data uses the ACRS and matches, on average, 13 stars per frameset, with an average RMS residual of 0.7 arcsec (Sharma *et al.* 1997). As a consequence, the pointing uncertainty of SBV is limited by the current star catalog systematic errors. It should be noted that the small average number of star matches, given the dense field of stars often available, is due to a deliberate thresholding of the dimmest stars and to the use of the ACRS, which offers only about 8 stars per square degree.

### Streak Endpoint Determination

The last and, currently, the largest error source in the SBV observation budget is that created during the determination of the beginning and end points of an RSO streak passing through the focal plane (Figure 1). Streak endpoint determination is performed either on-board or during ground processed using a least squares technique. The algorithm gathers a 5-pixel-wide swath of data comprising the streak and performs a best-fit of a line to the data. The linear assumption of the streak is well supported for the integration periods of the sensor and the rate of motion of RSOs across the CCD. For a more detailed explanation of the process of determining the endpoints in focal plane coordinates and how these are then transformed to RA and DEC, the reader is referred to Sharma *et al.* (1997).

The assessment of the quality of streak endpoint determination was performed by evaluating the ability to match stars to the catalog in a mode of tracking referred to as ephemeris tracking. As previously mentioned, the normal mode of data collection with SBV is a staring mode, which produces an image as shown in Figure 1. However, SBV is also able to track a target, such that the object stays fixed in the center of the focal plane. In this way, the object will appear as a centralized grouping of illuminated pixels, while the stars will streak across the focal plane. Figure 4 shows a typical image from an ephemeris track data collection event. It can be seen that the stars appear as uniform lines of comparable lengths. By using the ephemeris track mode of data collection, it is possible to match the beginning and end of each of the streaks on the focal plane to stars in the catalog. Through the determination of this RMS fit over the entire CCD and over a number of data sets, an overall assessment of the performance of the algorithm can be made.
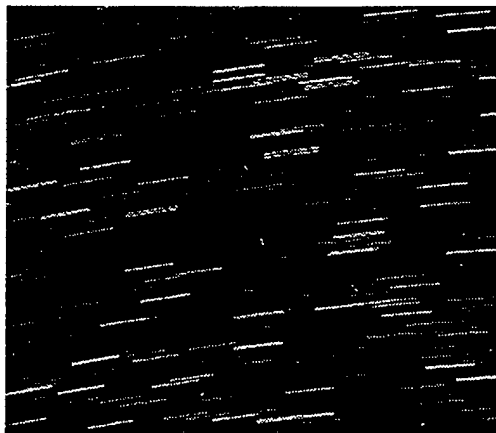
*Figure 4. Ephemeris Track Data Collection*

A study was made using five framesets of ephemeris track data of the Lincoln Experimental Satellite - 8 (LES-8) within the first few months of the MSX mission. For the dataset shown in Figure 4, with star detections dimmer than $14^{th}$ visual magnitude thresholded out, 28 detected streaks were matched to 27 cataloged stars to an RMS fit quality of 0.9 arcsec. Table 4 shows the results from the four other framesets, giving an average RMS fit of 1.2 arcsec. It was expected that the process of matching stars during an ephemeris track data collection would not perform as well as during a staring mode. This is because it is, fundamentally, more challenging to perform accurate metric detection and processing while the vehicle is slewing than while the vehicle is stable. By comparing the results from Table 2 with those of Table 4, it can be seen that there was a 20-30% degradation in the quality of the matches.

One important characteristic that the streak endpoint determination algorithm have is that it be robust across a wide range of visual magnitudes. This would allow for the observation of RSOs ranging from as bright as $6^{th}$ magnitude, possible during high specular periods, to as dim as $14^{th}$ magnitude, for highly emissive objects. This was assessed by investigating the quality of the endpoint determinations as a function of magnitude. Figure 5 shows both the individual endpoint

Table 4
Star Match Quality for
Streak Endpoint Determination

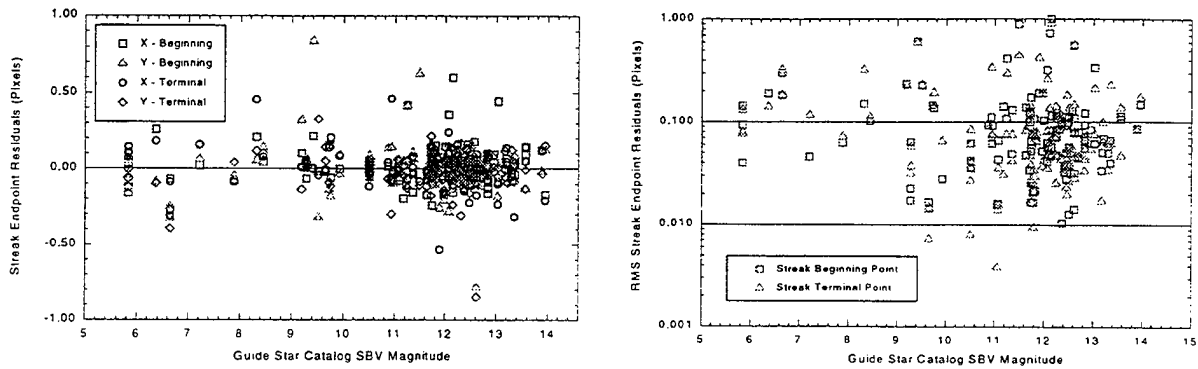| Frameset # | Matches/Streaks | RMS Star Fit (arcsec) |
|---|---|---|
| 11163 | 29/30 | 1.2 |
| 11167 | 22/23 | 1.3 |
| 11169 | 29/30 | 1.5 |
| 11170 | 20/21 | 1.0 |
| 11173 | 27/28 | 0.9 |
| | | Avg: 1.2 |

*Figure 5. Streak Magnitude Dependence*

focal plane coordinate star-fit residuals and the overall RMS of the fit to the endpoints as a function of SBV magnitude. It is clear from these results that the algorithm performance is quite robust over the desired range.

Given these early results, it seems that both the quality of the streak endpoint determination algorithm and the robustness of its performance across visual/SBV magnitude is sufficient to meet the total 4-arcsec goal for SBV observations.

**Pre-Launch Budget Assessment**

Prior to the launch of SBV, a complete error determination was made based on observations taken by an SBV-grade CCD located at the Lincoln Laboratory Experimental Test Site (ETS) in Soccorro New Mexico in 1991. Observations of a variety of RSOs were gathered for the purposes of hardware and software testing and error assessment. From these data, a rigorous study, using the techniques described earlier, was performed. The overall results of this work are shown in Table 5.

A few comments should be made on the determination of this error budget. It is clear that, prior to launch, it was not possible to assess the actual MSX ephemeris error. However, simulations had shown that it would be possible to meet the 15-meter position goal (von Braun, 1996). As a consequence, a contribution of 15 meters in ephemeris error was used in the error budget. A similar approach was taken for the satellite clock timing errors: the spacecraft spec of 1 msec was used. Finally, during the ETS observations using the SBV-quality CCD, no optical distortion was present.

Table 5
SBV Pre-Launch Error Budget

| ERROR SOURCE | NOMINAL | | |
|---|---|---|---|
| EPHEMERIS (15 METER) | 1".0 | STAR CATALOG (ACRS) | |
| TIMING (1 MILLISEC) | 0".6 | (RANDOM) | 0".5 |
| BORESIGHT POINTING* | 1".0 | (SYSTEMATIC) | 0".2 |
| DISTORTION** | 1".5 | STAR CENTROIDING | 0".2 |
| STREAK ENDPOINTS (SEP)* | 1".8 | PERIODIC MOTION | 1".0 |
| TOTAL RSS ERROR | 2".8 | | |

* BASED ON ACTUAL ETS CCD OBS
** NO DISTORTION PRESENT IN ETS DATA

59

As mentioned earlier, the distortion exists due to the presence of the elliptic and hyperbolic mirrors in the housing of the SBV. Since only the CCD and not the entire telescope was taken to ETS, distortion was absent from the data. An independent simulation of the distortion placed the error at 1.5 arcsec, but this would be incorporated in the boresight error.

The total SBV error budget is determined by assuming that the error sources due to the MSX ephemeris, the satellite clock used for tagging the observations, the determination of the sensor boresight and the determination of the streak endpoints are independent. As elaborated upon earlier, errors due to the star catalogs, centroiding, spacecraft drift and periodic motion and optical distortion all exist but as part of the boresight pointing error. With the assumption of independence, the total error can be expressed by

$$\sigma^2 = \sigma^2_{ephemeris} + \sigma^2_{timing} + \sigma^2_{boresight} + \sigma^2_{SEP} + \sigma^2_{unknown}$$

where the errors due to unknowns have yet to be established.

### On-Orbit Budget Assessment

In much the same way as described above, the actual error budget for SBV was determined. It can be seen in Table 6 that there are a number of improvements from the budget shown in Table 5. The first improvement is with respect to the MSX ephemeris. For the on-orbit assessment, actual MSX positions are known (Abbot *et al.*, 1997). Estimation of the position of MSX is routinely at the 10-meter level, thus giving a 30% reduction from pre-launch levels in the errors due to this source. The other significant difference in the pre-launch and on-orbit error assessments is in the boresight pointing. Prior to launch it was expected that distortion would be a limiting error in the determination of the boresight. However, due primarily to a redesign of the distortion model in the early part of the mission and to a number of software enhancements since launch, the boresight pointing is now limited by the quality of the star catalogs and contributes only modestly to the overall error budget.

It seems from these results that RSO observations using SBV are available at the 2-arcsec level, a reduction of 50% over the 4-arcsec goal set during design. However, it is only possible to verify this finding through on-orbit metric calibration.

Table 6
SBV Post-Launch Error Budget

| ERROR SOURCE | NOMINAL | | |
|---|---|---|---|
| EPHEMERIS (15 METER) | 1".0 | | |
| TIMING (1 MILLISEC)* | 0".6 | STAR CATALOG (ACRS) (RANDOM) | 0".5 |
| BORESIGHT POINTING** | 0".2 | (SYSTEMATIC) | 0".2 |
| STREAK ENDPOINTS (SEP)** | 1".2 | STAR CENTROIDING | 0".2 |
| TOTAL RSS ERROR | 1".7 | PERIODIC MOTION | 0".4 |

\* ASSUME SPEC ACHIEVED
\*\* DISTORTION INCLUDED

## SBV METRIC CALIBRATION

While an independent assessment of the SBV errors is of tremendous value to our understanding of sensor performance, the only true test of the quality of the observations is through routine calibration using known references. This is performed routinely on-orbit using calibration objects. Typically, SBV operations uses LAGEOS II as its calibration object, although other objects such as LAGEOS I, AJASI and Starlette have been tracked. In addition, it has been found that the constellation of GLONASS satellites has proven to be an extremely reliable calibration target, due, primarily, to the rich supply of ground observations from the SSN network which are needed to produce a reference position. Through the use of LAGEOS II and a variety of GLONASS satellites, it has been possible to establish the current performance of SBV. Figure 6 shows the current metric performance of SBV with GLONASS (#23511) data gathered currently. It is clear that the quality of the residuals is at the 4-arcsec level but is not at the level of the independent error assessment. There
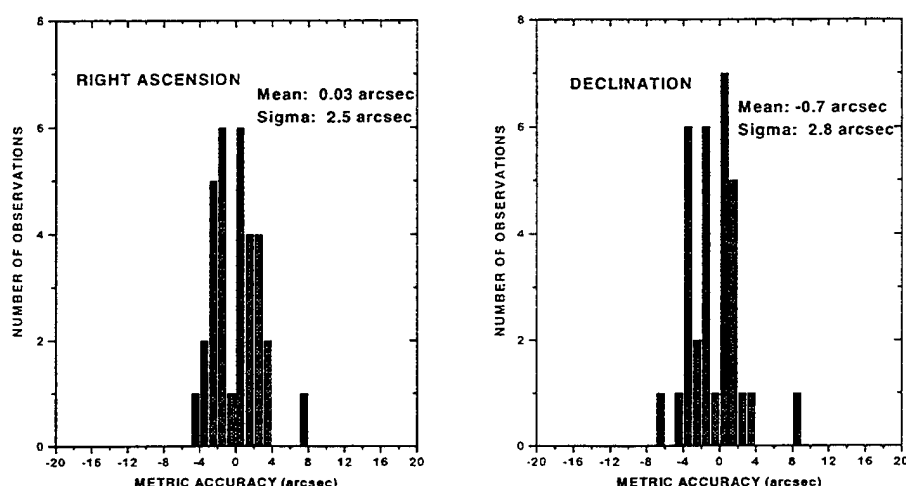


*Figure 6. GLONASS (# 23511) Residuals from SBV*

are several possible explanations for this discrepancy. Firstly, at the time these data were analyzed, the precise ephemeris of MSX was not available. All of these data were processed using predicted positions of the satellite and are likely to have errors at the 30-50 meter level. This could degrade the quality of the observation by as much as 1 arcsec. In addition, corrections to the clock -- updates to the telemetry stream correcting for biases and drifts in the satellite clock -- were also not applied to these data. These corrections, while different from the timing errors discussed earlier, could lead to errors at least as large in magnitude to those already in the error budget.

In a similar way, Figure 7 shows residuals of observations of LAGEOS II with known positions on orbit. These results show, to a larger degree than with GLONASS, the issues of using a predicted ephemeris instead of a precise position estimate, and the effect of the clock corrections. the fact that that the clock corrections have not been applied. Both of these errors are larger for LAGEOS II than for GLONASS because of the range to these satellites. GLONASS (SSN #23511) is in a semi-synchronous orbit at 19,070km in altitude and LAGEOS II is in 5,780km orbit. Both the ephemeris error and the clock correction problem are reduced as the range to the target increases. As a consequence, for objects at close range, both of these error sources can become substantial. It is felt that, when these data are reprocessed using updated ephemeris and clock correction information, the results of the LAGEOS II observations will be reduced by as much as 20%, while the GLONASS residuals will likely reduce by somewhat less.
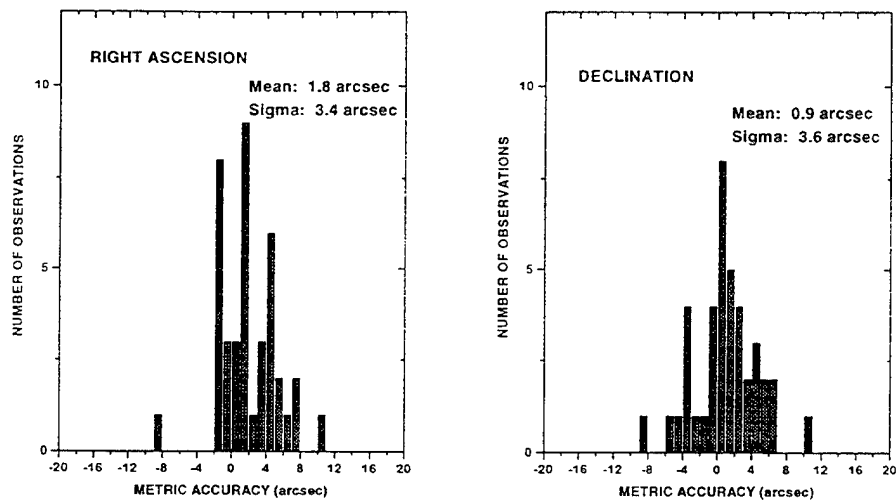
*Figure 7. LAGEOS II (# 22195) Residuals from SBV*

## CONCLUSIONS

Given some of the caveats discussed above, it is clear that the goal of producing 4-arcsec observations of RSOs using a space-based sensor has been reached and will, likely, be surpassed. The independent error assessment presented in this paper indicates that observations to the 2-arcsec level are possible, when the tuning of the process is complete.

This paper has focused on the assessment of errors for the SBV. For a discussion on the impact of SBV to space surveillance, including discussions on satellite catalog maintenance, the reader is referred to Gaposchkin, (1995) and Gaposchkin *et al.* (1997).

## REFERENCES

1.  Abbot, R.I., E.M. Gaposckin, C. von Braun (1997). *MSX Precision Ephemeris,* submitted to the AAS/AIAA Astrodynamics Conference, Sun Valley Idaho, August 4-7.

2.  Gaposchkin, E.M., (1995). *Space-Based Space Surveillance with MSX,* Advances in the Astronautical Sciences: Spaceflight Mechanics, vol. 89. Ed. Proulx, Liu, Seidelman, Alfano, pp. 1681-1690.

3.  Gaposchkin, E.M., C. von Braun, J. Sharma, (1997). *Space-Based Space Surveillance with SBV,* submitted to the AAS/AIAA Astrodynamics Conference, Sun Valley Idaho, August 4-7.

4.  Sharma, J., C. von Braun, E.M. Gaposchkin (1997). *SBV Metric Data Reduction,* submitted to the AAS/AIAA Astrodynamics Conference, Sun Valley Idaho, August 4-7.

5.  von Braun, C. (1996). *Cryogen Thrust Modeling For MSX Ephemeris Generation,* AAS/AIAA Spaceflight Mechanics Meeting, Austin Texas, February 12-15.

# MSX PRECISION EPHEMERIS

R. I. Abbot, E. M. Gaposchkin, C. von Braun
MIT Lincoln Laboratory, Lexington, MA

## ABSTRACT

The Midcourse Space Experiment (MSX) satellite, hosting a suite of state-of-the-art sensors, was launched into an 898 km altitude sun-synchronous orbit in April 1996. One of the primary tasks of the Space Surveillance Principal Investigation team is to evaluate the utility of the MSX sensors in performing space surveillance tasks. One of the critical issues in assessing the sensors' performance is to determine the metric accuracy of the satellite observations. The ability to do this depends on the MSX ephemeris accuracy. In particular, to support the accuracy requirements of the Space-based Visible (SBV) sensor observations, the ephemeris accuracy requirement for the MSX satellite is 15 meters (1 sigma). There are two issues that have to be addressed in meeting the ephemeris accuracy requirement: 1) the quantity and quality of the tracking data and 2) the dynamic modeling of the satellite motion. The tracking is performed by the Air Force S-band Ground Link Stations (SGLS) network while the Space Surveillance Network (SSN) Millstone Radar in Westford, MA, is providing tracking data which is used to assess orbit accuracy. The quantity of the SGLS tracking data has met our requirements. In addition, we have improved the calibration of the SGLS tracking data. In the area of dynamic models, most attention has been given to handling the affect of the anomalous accelerations due to cryogen gas venting. Results are presented with results that show that the 15-meter ephemeris accuracy requirement is being met. In addition, this paper addresses relevant aspects of our procedure for generating both a quick-look and a definitive ephemeris for MSX.

## 1. INTRODUCTION

The Midcourse Space Experiment (MSX) satellite, hosting a suite of state-of-the-art sensors was launched into an 898-km altitude, sun-synchronous orbit in the Spring of 1996. MSX represents the first space-based platform for surveillance. The MSX is funded and managed by the Ballistic Missile Defense Organization (BMDO) to address critical phenomenological and functional issues related to ballistic missile defense. The functions of a midcourse surveillance system include: 1) detecting, acquiring, and tracking potential targets; and 2) discriminating between lethal and benign targets.

Space surveillance is an integral part of the midcourse surveillance mission because of, among other things, the need to discriminate between lethal Re-entry Vehicles (RVs) and benign Resident Space Objects (RSOs). Therefore, part of the MSX mission is to demonstrate space-based space surveillance. The object of space surveillance is to create and maintain current information on all man-made objects in earth orbit. The suite of MSX sensors will acquire both metric and photometric/radiometric observations of RSOs. These RSOs include active and inactive payloads, rocket bodies, upper stages, and orbital debris. The present ground-based Space Surveillance Network (SSN) has limitations of coverage, capacity, sensitivity, available optical wavelengths, and accuracy.

A primary requirement on all sensors used for space surveillance is metric accuracy adequate to support the various missions of the Space Surveillance Network. These missions include routine tracking of Resident Space Objects (RSOs) for catalogue maintenance, tracking of new satellite launches, status monitoring of satellite activity, and signature analysis. An array of radar and optical ground-based sensors exist that have been designed and characterized for space surveillance tasks. They comprise the Space Surveillance Network (SSN). Both the Space-Based Visible (SBV) and Space Infrared Imaging Telescope III (SPIRIT III) sensors on the MSX satellite will be capable of collecting precise metric observations on targets which are detectable in their respective fields of view/regard. Therefore, experiments are being performed to characterize and calibrate the metric accuracy of the SBV and SPIRIT III sensors observing in stressing (high backgrounds, such as near the Earth-limb) and non-stressing (looking away from the Earth, Moon, and Sun) environments.

These experiments will determine the metric accuracy and precision of the SBV and SPIRIT III sensors, determine biases for metric data products, and characterize the metric error as a function of the target, target velocity, focal plane orientation and background, MSX jitter and drift, and data collection and reduction parameters. The SBV satellite observations should be accurate to 4 arc-seconds (1 sigma). Since the accuracy of the MSX ephemeris could limit the quality of the sensor performance assessment, it was desired that the contribution to the four arc-second budget due to ephemeris error be no larger than 1.3 arc-seconds. By considering the more stressful scenarios for MSX (e.g., viewing an object 2500 km away in a 90 minute parking orbit), it was decided that the ephemeris accuracy goal for the MSX satellite should be 15 meters (three-dimensional RMS) in order to support the assessment of the sensors' metric performance. Therefore, an effort has been undertaken to compute MSX ephemerides at the 15-meter level and meet the metric calibration requirement.

This task is formidable because of the limited tracking data available and the cryogen thrusting on the spacecraft. In order to reduce the instrumentation noise of the SPIRIT III sensor to an acceptable level, it is necessary to maintain the device at a temperature of about $8°K$. This is accomplished through the use of a hydrogen cryostat system which is designed to absorb much of the radiant energy encountered by the sensor. In doing so, a block of solid hydrogen sublimates, and the gas is vented to the rear of the spacecraft. This venting creates a thrust which must be modeled if high precision position estimates of the satellite are to be obtained. In principle, if the thrust were entirely in the along-track direction, it could produce an along-track perturbation of 30 km per day. To model this anomalous thrusting rigorously, a model requiring the continual mass flow rate of hydrogen would be needed to establish the exhaust velocity and pressure of the vented gas, while attitude quaternions are needed to determine the direction of the thrust. As will be discussed, the need for such a completely rigorous flow model has, however, been circumvented.

In this paper, we discuss the relevant aspects of the tracking scenario of the MSX mission: the procedures used to routinely generate and assess the quality of the MSX ephemeris, and the modeling of the forces acting on the satellite.

## 2.    EPHEMERIS GENERATION OVERVIEW

Two primary requirements have been levied on the MSX ephemeris generation.  The first is that a preliminary ephemeris is generated for a cursory view of the SBV and SPIRIT III experiment data as it is collected (Ref. 1).  This is performed for both a fitted and predicted ephemeris.  The second is that, as all required input data types are finalized and modeling reviewed, a final MSX ephemeris, which meets the 15-meter accuracy specification, is generated.

To meet the first requirement, the following data types must be automatically collected on a daily basis onto a single orbit computation platform.

- Tracking data

- Predicted attitude data

- Transponder information

- Geophysical data for the drag model

- Earth orientation data from USNO

The first three of these will be discussed in the sections which follow.  Once these data have been acquired, a procedure automatically performs an orbit-fit, generates the satellite ephemeris, and performs an evaluation of the orbit quality.  When the process is complete, the generated preliminary ephemeris is sent, in the Defense Mapping Agency (DMA) format, to users at the MSX Surveillance Data Analysis Center (SDAC) at MIT Lincoln Laboratory and made available to other users in the MSX community.

The quick-look, preliminary ephemeris may meet the 15-meter accuracy requirement specified for the final or definitive ephemeris, but arrival of the final sets of data and additional inspection and analysis in the following areas may be necessary to meet the specification:

- Review of SGLS sensor calibration

- Raw Attitude data

The delay in generating the definitive ephemeris is one week, at which time the definitive ephemeris is generated in the DMA format.  This is sent to the SDAC users, made available to the MSX community, and deposited in the Background Data Center (BDC).

# 3. DATA

## 3.1 Tracking Data

The primary tracking data for orbit determination comes from the Air Force S-band Ground-Link Stations (SGLS) network. Tracking data is also obtained from the SSN's Millstone radar. The radar data is used primarily to evaluate the SGLS tracking data and the orbits derived from these data.

The SGLS network is primarily used for S-band satellite communications, but metric tracking data is also obtained for maintenance of the satellite orbits. With the coherent S-band transponders on MSX, measurements of range and range-rate are obtained. Measurements of azimuth and elevation are made but not used nor needed. The precision of the SGLS data is 6 meters in range and 3 cm/s in range-rate. The measurement biases can be determined to a few meters in range; the range rate should be unbiased.

The SGLS network provides, on average, eight to twelve metric tracks of data per day. This data is collected at the Test Support Complex (TSC) in Sunnyvale, California, and transmitted to the Applied Physics Laboratory (APL) at The Johns Hopkins University, and then, finally, to Lincoln Laboratory.

The SGLS range data has a nominal sensor and transponder bias correction applied by TSC. For MSX, ongoing analysis of range residuals is performed to ensure the best possible calibration of the SGLS data. This will be discussed in more detail below. With regard to refraction corrections, the measurements have tropospheric corrections applied to them, but none are applied for the ionosphere. MSX initially is flying during a period of very low solar activity.

## 3.2 Attitude Data

Attitude data is required for the modeling of the forces of drag, solar radiation pressure, and cryogen thrusting. MSX is kept in a park-mode except when it is maneuvered for Data Collection Events (DCEs). Park-mode is defined in such a way as to minimize the amount of direct, radiant energy that would enter the SPIRIT III sensor. This is accomplished by first pointing the satellite in a radial direction, then rotating it about its boresight axis until the sun shade blocks the sun. Finally, the solar panels are rotated about their support axis so as to maximize their power gain.

Two different sets of attitude information are used in our orbit determination. The attitude history buffer on MSX holds quaternions and time tags at 100-second intervals for roughly five orbits at which time it is down-loaded. This attitude information is decommutated from the telemetry. This raw on-board attitude data for a given day is not usually completely collected until after it is needed for the preliminary orbit computation, and so it is only used for the definitive orbits. To compute a preliminary and predicted orbit for MSX, the predicted attitude quaternions for the planned surveillance events are obtained from APL and combined with the predicted park-mode quaternions. The predicted attitude seems very reliable for this purpose.

## 3.3 Transponder Data

MSX has two S-band transponders on-board. Each is used according to the orientation of the satellite. A SGLS contact schedule provides information with regard to which is being used. At the present and as best as has been determined, the transponder biases are close enough that it is not absolutely necessary to have the transponder switch information, but this could change in the future.

## 3.4 Calibration Data

An important aspect of achieving the required orbit accuracy is to have well-calibrated data from the SGLS network. Historically, the range biases of the sensors within the SGLS network have been determined from the data themselves. This will remain a primary means of monitoring the sensor range biases for the MSX orbit computation. For the range bias, the assumption is that a common mode bias seen at all stations is due to the transponder. With this bias eliminated from the measurements, one can begin to disentangle the sensor range bias from the uncorrected ionosphere mean range error by using night-time, high elevation, and range-rate data only and then analyzing the residuals of the range measurements with the resulting orbit. After enough MSX orbits had been computed using the SGLS tracking data, a study was made of the calibration of the SGLS station biases in range measurement. Nominal corrections were determined and suggested to TSC who then independently determined and adopted similar biases. Continued monitoring has shown some of these biases to drift or otherwise change with time.

Other means of determining the sensor biases are also being used. The use of the radar data for providing an independent reference orbit is useful in providing an independent measure of the SGLS sensor biases. The SGLS sensor biases are also studied at TSC using data from other satellites which are tracked by the network.

## 4. SUMMARY OF DYNAMICAL MODELS FOR MSX

The MSX ephemerides is computed with a high-precision orbit computation program known as DYNAMO. Table 1 summarizes the force models that are used in the process of generating orbits for the MSX-user community.

Simulation studies (Ref. 2) prior to launch indicated that the cryogen venting could be simply modeled as a continuous thrust in the direction determined by the satellite attitude and that a simultaneous estimate of a thrust scale factor and a drag factor on a daily basis could absorb the thrust effect to well below 10 meters, with little correlation between the two. This methodology was adopted and, based on the orbit accuracy achieved and discussed in the next section, seems to be an effective way of treating this anomalous thrusting.

Besides being able to use the attitude quaternions, DYNAMO can also compute the park-mode attitude of MSX if, for example, some of the raw on-board attitude data is missing.

67

**TABLE 1**

**Force Models Used For MSX Orbit Computation**

| EFFECT | MODEL/PARAMETERS |
|---|---|
| GRAVITY | JOINT GRAVITY MODEL (JGM-3) (40 X 40) |
| ATMOSPHERIC DRAG | MSIS (CIRA '86) |
| CRYOGEN FLOW | MODELED WITH SATELLITE ATTITUDE AND AS A SCALEABLE CONTINUOUS THRUST |
| SOLAR RADIATION | TOTAL MASS & 8 SURFACES WITH AREAS AND REFLECTIVITIES |
| BODY TIDES | K2 = 0.3, PHASE LAG = 0.0 |
| OCEAN TIDES | GEM-T2 |
| EARTH ALBEDO | |
| THIRD BODY | SUN/MOON, USNO LUNAR EPHEMERIS, JPL DE200 PLANETARY EPHEMERIDES |

## 5.    MEASURE OF ORBIT ACCURACY

A number of measures are used to evaluate the day-to-day ephemeris quality. The conventional technique of overlapping subsequent daily orbits provides a measure of consistency and a fairly good indication of accuracy. Post-fit residuals of the SGLS data are examined for systematic errors, biases, the precision of the data, and an acceptance level of data from each SGLS site. To provide an external measure, the Millstone radar data is not used in combination with the SGLS data in the orbit fit, but is used to monitor the SGLS data and the orbits derived from them. The Millstone radar range is accurate to 1 meter. These radar range measurements can be compared with the SGLS derived orbits and the residuals should provide a direct measure of the orbit accuracy over part of the orbit. Orbits can also be computed exclusively from the radar data, and the orbits derived from the SGLS data can be compared with these orbits to check for timing or other errors. Finally, both the cryogen thrust and the drag solve-for parameters are checked for realism and consistency. The cryogen thrust scale factor is expected to adjust the nominal average hydrogen mass flow rate and should depend on the surveillance activity, especially that of the SPIRIT III sensor. In addition to absorbing errors associated with the mismodeling or the atmosphere, the drag scale factor seems to have a more important role in absorbing some of the modeling error of the cryogen thrust in the along-track direction.

To provide an estimate of orbit accuracy from the overlap analysis, the MSX orbit fits are designed so that they span 2.25 days. The ending 0.25 day of one orbit fit will just overlap the first 0.25 day of an orbit fit that starts two days later. All orbit fits are therefore compared with those orbit fits starting two days before and two days after. From the 2.25 day orbit fits, state vector ephemerides are generated in an inertial reference frame at 900 second intervals over the common period for both overlapping orbits. The method then differences the state vectors at each epoch in common. An often more physically intuitive way of characterizing these differences is to convert the differences in x, y, z to differences in what are known as the along track, radial, and cross track directions with respect to the orbit. The along track is along the velocity vector, the radial is along a vector from the center of the earth to the satellite position, and the cross track is perpendicular to these two and measures the orbit differences in terms of the out of plane component. These differences are computed and then summarized statistically by their RMS. As a measure of accuracy for each orbit, this RMS difference is divided by two, the assumption being that the

68

orbit differences are contributed equally from errors in each orbit. Figure 1 shows a histogram of this measure of orbit accuracy expressed in radial, cross track, and along track directions. The along track error is the largest and as a measure of accuracy indicates that the orbits are within the 15-meter requirement (1 sigma RMS). Figure 2 shows the other orbit accuracy assessment based on the residuals of the Millstone Hill radar range measurements as compared with the SGLS determined orbit. The residuals are generally better than 15 meter.
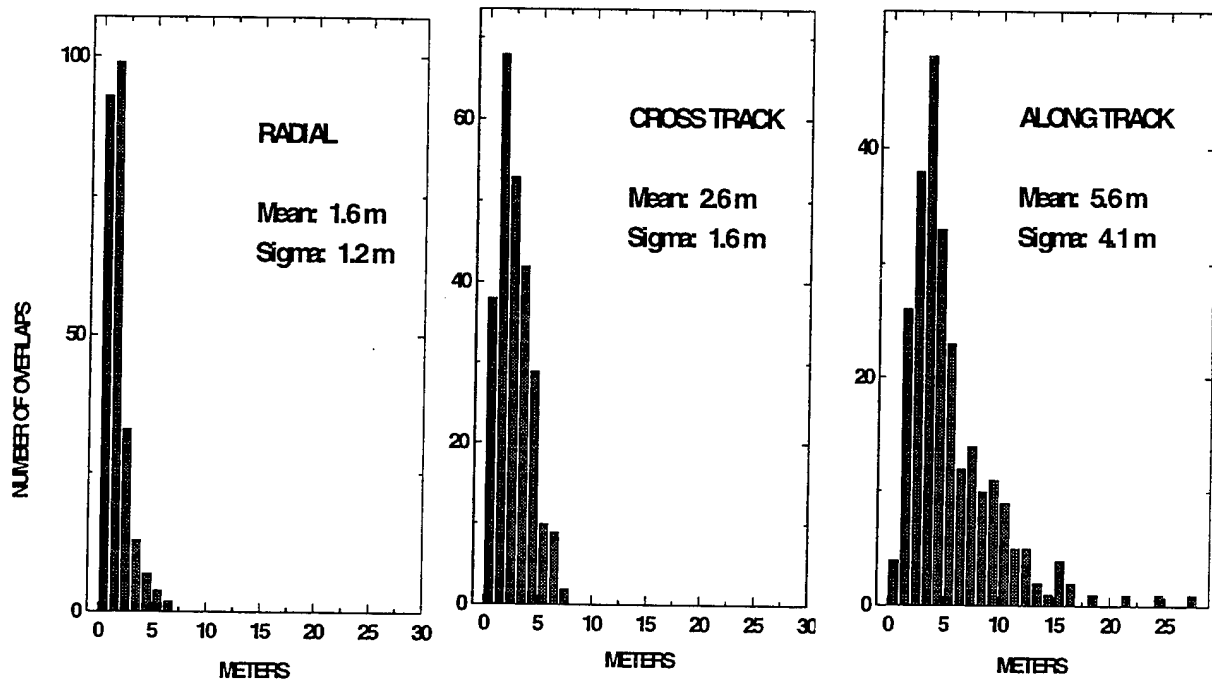


Figure 1. RMS Difference divided by two of 0.25 day overlap for
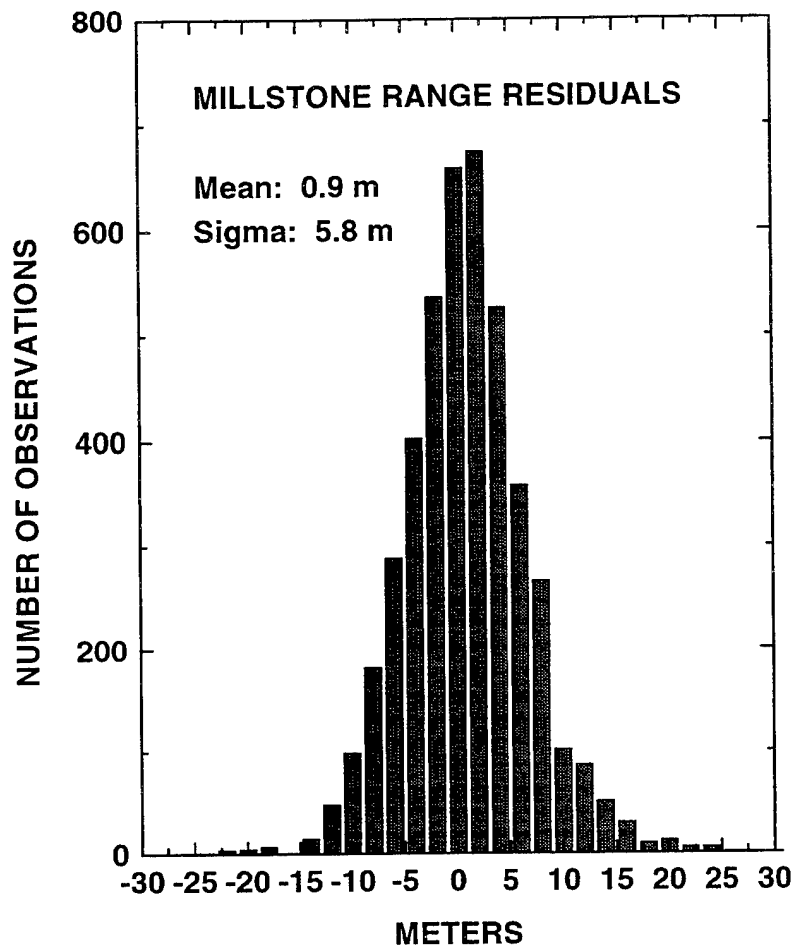orbits fit from Day 28 of 1996 to Day 56 of 1997.

*Figure 2. Millstone range measurement residuals computed with orbits determined from SGLS tracking data.*

## 6. CONCLUSIONS

In order to provide a quick-look capability for SBV and SPIRIT III surveillance data, a preliminary MSX ephemerides is generated on a daily basis. This is performed by a complex but timely and automatic flow of data to an orbit determination computer, which fits an orbit, generates an ephemeris, performs quality analyses, and transmits the ephemeris to users. On a less stringent schedule, and as all the data and force models are finalized, a definitive daily ephemeris is generated which has been shown to meet and generally supersede the 15-meter accuracy specifications for the mission. This procedure will be carried out for the lifetime of MSX.

One of the more difficult problems encountered in modeling the various forces acting on the satellite is that of the low thrust created by the continuous venting of hydrogen gas from the SPIRIT III

cryostat. By having 1) continuous information about the attitude of the MSX satellite, 2) a representation of the venting as a constant but scaleable thrust, and 3) an along track acceleration parameter that absorbs any residual effect of the venting, we have had impressive success in treating this force.


**REFERENCES**

1. Gaposchkin, E. M., Lane, M., and R. I. Abbot. *Reduction and Analysis of MSX Surveillance Data.* AAS/AIAA Spaceflight Mechanics Meeting, Albuquerque, New Mexico, February 13-16, 1994.

2. Abbot, R. I., von Bruan, C., and G. E. Powell. *MSX Precision Ephemeris Generation.* AAS/AIAA Spaceflight Mechanics Meeting, Albuquerque, New Mexico, February 13-16, 1994.

Space Based Space Surveillance with SBV

E.M.Gaposchkin[1], C. von_Braun[2], J. Sharma[2]

Contents:
Abstract

---

[1] Senior Staff Member and MSX Surveillance Principal Investigator, Massachusetts Institute of Technology Lincoln Laboratory, Lexington

[2] Technical Staff Member, Massachusetts Institute of Technology Lincoln Laboratory, Lexington

Abstract

Space Surveillance is the activity of keeping a current catalogue of information on man made earth bound resident space objects (RSOs). Some necessary functions to perform this task are search and detection, acquisition and tracking, tasking and scheduling, and data reduction and processing. The MSX satellite, launched 24 April 1996, carries the Space Based Visible (SBV) sensor package designed for conducting Space Surveillance from a Space Platform. Other presentations in this workshop discuss SBV operations, data reduction and accuracy. SBV provides high accuracy angle measurements (RA and Dec). Based on these data, we can demonstrate space based space surveillance catalogue maintenance. To this end, orbits are calculated based on ground based data, space based data, and various combinations of these data. From these results a number of surveillance elements can be demonstrated. For example, compatibility and fusion of space based and ground based metric data. Where a high accuracy independent orbit is available, an assessment of the orbit accuracy is made. In other cases differences between the orbits are computed. In addition, access to the complete Geosynchronous belt and catalogue maintenance for Geosynchronous satellites will be demonstrated. Effectiveness of space based space surveillance data, is assessed.

## I. Introduction

Space Surveillance from the ground started with the launch of Sputnik I in 1957 (40 years ago). Lincoln Laboratory has been involved from the very beginning. It is a mature discipline. Both optical and radar tracking techniques have developed, and an elaborate data analysis system, with conventions, procedures, communications and practices , has evolved over the years. The system has expanded from low altitude to deep space , tracking objects far beyond the Geosynchronous belt, and maintaining a satellite catalogue with more than 23000 entries, and an active subset approaching 10000. The capability exists to maintain orbits on low earth orbit (LEO) objects with a size to a few centimeters, and Geosynchronous objects with a size of 1.0 $m^2$. The GEODSS cameras -- a fair weather fly by night system -- has impressive capability for deep space search. The deep space radars (Millstone and Altair), using coherent integration techniques borrowed from radio astronomy, can track Geosynchronous satellites with an accuracy of a few meters. We have come far in 40 years. We are on the verge of the next major technological change in space surveillance, ***Space Based Space Surveillance.***

In 1987, the MidCourse Space Experiment (MSX) was begun. The MSX has a number of objectives supported by a suite of optical sensors (Mill et al., 1994). The breadth of the program is illustrated by the eight Principal Investigator Teams representing different phenomenologies, objectives, and disciplines. Space Surveillance is one of these disciplines. The intervening 10 years has been devoted to building, launching, and operating the MSX satellite. This talk is intended to discuss the Space Surveillance results available to date. Overall MSX program objectives and results are discussed elsewhere in this conference (Smith & Mansberger, 1997). Although, the space surveillance experiments make use of the full complement of MSX sensors, the primary sensor for space surveillance is the Space Based Visible (SBV) built at Lincoln Laboratory, and this will be the focus of this discussion.

At this point in the program, we are fully into experiment data collection and analysis. It is important to note that we are riding on a train built with much excellent work by the designers and integrators of the spacecraft at the Applied Physics Laboratory (Peterson, 1996) and the Space Based Visible Payload at Lincoln Laboratory (Chow and Harrison, 1994). They in turn built on the outstanding vision that let to technology development of the focal plane arrays used (Bergemann, 1995), the on board signal processor, and many other subsystems that make you the instrument we are now using so successfully.

The 10 years between program inception and producing results is not unusual -- before the days of *better, faster, cheaper* — and at many times in these years we have described what we intended to accomplish. It is a great pleasure, now, to be able to present results, and describe what we have accomplished. These results, truly usher in the next phase of space surveillance. I believe that there are unique challenges, great opportunities, and exciting results in store in this new era of ***Space Based Space Surveillance.***

## II. Space Surveillance Issues

The space surveillance objectives are described in the SRD (anon, 1991), the SMRD (anon,1992) and in Gaposchkin (1995), and so we confine ourselves to a few remarks. We define space surveillance as (figure 1) :

**The task of keeping a current catalogue of information on man-made, earth-bound , resident space objects (RSOs), to support military and civilian needs.**

To accomplish this, we need to perform a number of missions:

| Missions |
| --- |
| New Launch Processing |
| Catalogue Maintenance |
| Catalogue Augmentation |
| ASAT Support |
| Satellite Attack Warning |
| Mission and Payload Assessment |
| Treaty Monitoring |

and a number of functions:

| Functions |
| --- |
| Search and Detection |
| Acquisition |
| Tracking |
| Data Processing |
| Tasking and Scheduling |
| Integration into the SSN |

We need to have the technology at hand to do these functions, and we will demonstrate the MSX/SBV capability.

Now the characteristics of Space Surveillance begin with short time lines (figure 3). This means that there is limited usefulness of old data. We need to know the space order of battle today, not last week. For reacquisition of uncorrelated targets (UCTs) rapid response is necessary because of the limited prediction accuracy based on "discovery" observations. In addition, rapid initiation of tracking is necessary to respond to launch and satellite manoeuvers. The wide range of target size, target geometry and relative velocity places requirements on the sensor, network, communications, and data processing system. Targets of interest range in size from centimeter debris to hectometer payloads. RSOs exist in low earth orbit (LEO), to deep space (DS) , geosynchronous (GEO), and beyond. The relative angular velocity of observing targets ranges from $\approx 0$ to more than 2400 arcsec/sec. Finally, the space surveillance network (SSN) is made up of many different sensors with different operational characteristics and capabilities. With the exception of 3 GEODSS camera sites and 3 PAVEPAWS radar sites, none of the surveillance sensors are the same. This leads to complex issues of tasking and scheduling. A new sensor system — in this case space based — should both supplement and complement the existing capability to make use of strengths and ameliorate weaknesses. *Only do things from space that are better done there!*

Our early objectives with the MSX/SBV to demonstrate space based space surveillance, of course, aim to show what can be done. However, this is done in the context of current realities. There are some current issues with the existing space surveillance network. Where appropriate , we are addressing these issues (figure 3) with the MSX/SBV experiments. For example, the gap time between tracks for the current SSN is significantly longer than present requirements. The MSX/SBV cannot address this due to the communications architecture. However, the present tracking resource shortfall can be mitigated with the MSX/SBV. The shortfall is especially acute in DS, which is where the MSX/SBV is particularly powerful. The MSX/SBV has access to all space. Its complete coverage of the geosynchronous belt coupled with the wide field of view will allow it to provide data on all GEO satellites with multiple observations in each "look". The current network has a coverage "hole" in the eastern hemisphere, which can be filled with the MSX/SBV. The detection sensitivity of MSX/SBV allows tracking of debris — for which there are two experiment plans — and small satellites. In addition the use of specular phenomena — due to the long specular season enjoyed by SBV — will allow tracking of satellites not now maintained as well as gathering of signature data on the physical properties of satellites. Finally, many of the current SSN sites are on foreign territory. This is expensive and possibly operationally complex. A space based asset provides complete geographical coverage while operated and controlled from the CONUS. We believe that the MSX/SBV will also alleviate these issues.

III. Technology Demonstrations

There has been a lot of planning for space based space surveillance with a visible band optical sensor. Based on these considerations, the SBV is based on technologies that were available in 1988 when the MSX/SBV project was initiated. It is fair to say that the system on orbit today has been a success, and a tribute to the vision of those planners.

The SBV characteristics are give in Figure 4. The SBV is a staring sensor. The principal mode of operation is to point in space — sidereal tracking — such that the background stars are point sources in the focal plane and the target RSO is streaking. Of course, the SBV can also be operated in ephemeris track where the pointing follows the target and the stars streak. Both types of data have been taken (von_Braun et al.). The SBV uses a wide band CCD array (4000 Å to 9000 Å) , with a quantum efficiency of about 30% compared with an S20 with about 7% quantum efficiency. The telescope has a 6 inch aperture, and an off axis reimaging design to maximize out of field of view rejection (OFVR), which allows tracking within 100 km of the earth limb. The camera consists of four (420x420 pixel) three side abutable CCD arrays. This results in a 1.4x6.4 deg total field of view (FOV), though only one CCD array can be used at a time. Each pixel is 60μrad on a side (12 arc sec). We have succeeded in dividing the pixel signature data by factors of 3 to 10. Nominal integration time is 0.4 or 1.6 seconds. There is also a 1.0 second integration time used when data is stored on the on board tape recorder. A critical technology for space based space surveillance is the on board signal processor (SP). The SP processes multiple frames of data to extract the target streak and star positions, rejecting background clutter and single proton events. For example a 16 frame set consists of $5.6 \times 10^6$ bytes. The SP will produce a report containing star and streak signatures of $3.2 \times 10^3$ bytes, a reduction in data downlink bandwidth needed by 2000. In addition there is a programmable computer, the experiment controller (EC), for running the SBV. The on orbit detection sensitivity of the SBV is somewhat better than expected, allowing tracking of a geosynchronous target (range = 36000 km) with $\rho A = 0.5 \ m^2$. This is equivalent to a 2 cm sphere are 1000 km range. Finally we have two modes of recording data. The first, shared with other sensors on MSX, is the 25Mbit/sec tape recorder. This is used for the prime science data for the MSX satellite. Data is stored on the tape, and down linked at a later time to the single ground station at the Applied Physics Laboratory equipped to receive the data.. This mode of data acquisition often results in several days delay in down linking the data to the ground, and further delays as the data is processed and distributed through the Backgrounds Data Center (BDC). Unique to the SBV among the MSX sensors, is a link to the 1Mbit SGLS down link. In this mode, the SBV data is taken, and signal processor results stored in the electronic ram of the SP or the EC. When a ground contact is available, the data is down linked, and directly transmitted to Lincoln Laboratory/SPOCC for analysis. This results in data availability within hours of the event, and time lines that are consistent with performing space surveillance functions.

Figure 5, illustrates how the observation process fits together. We have full frame data processed by the SP producing a streak signature and a number of stars. For each detected star a 7x7 pixel array is saved and down linked. On the ground, star centroids are calculated in pixel coordinates. These stars are then matched to a star catalogue, and the astrometric positions are used to obtain the sensor bore sight pointing. Usually approximately 30 stars are detected, of

which 10 to 20 are matched to the catalogue. For routine work, the Astrographic Catalogue is used. The Astrographic catalogue has approximately 300,000 stars, and when more stars are needed — for example, when studying optical distortion — the Guide Star Catalogue is used. The example given here is typical. The star centroids are matched to the star catalogue with an rms accuracy better than one arcsec — subdividing the pixel by a factor better than ten. The statistical estimate of the bore sight pointing is then a fraction of that, however limited by the accuracy of the star catalogue to about 0.2 arcsec rather than the intrinsic accuracy of the sensor. The second part of the process is to take the streak end points and determine the pixel coordinates of the satellite. For this purpose, a swath of pixels (5 pixels wide) centered on the streak is saved and down linked. The streak signature is processed on the ground. We see the residuals of a calibration satellite (Lageos II) plotted in the third panel. The accuracy of the Lageos II orbit, determined using laser ranging data, is decimeters and the orbit error is negligible in computing the residuals. We see the rms residuals of approximately 4 arcsec, our metric accuracy goal, again subdividing the pixel by a factor of 3. Note that the GEODSS A Spec was 10 arcsec. The last part of the process is knowledge of the MSX platform position, or ephemeris. To obtain this requires careful analysis of SGLS ranging data. This modeling was made more challenging by the cryogen venting, which provided a significant thrusting. We have achieved the goal of a 15 m orbit. These all provide the principal technology demonstrations with SBV, illustrated in figure 4. The Signal processor and data reduction (Sharma et al., 1997), metric calibration (von_Braun et al., 1997) and platform ephemeris (Abbot, et al., 1997) are described more thoroughly elsewhere in these proceedings.

## IV. Functional Demonstrations.

The MSX/SBV is an experimental observatory, with eight principal investigator teams. For the first year of operation, satellite resources were distributed among these teams, based on priorities established by the Program Office through the Mission Planning Team. The satellite operations were scheduled by Data Collection Event (DCE). The baseline mission had approximately four DCEs each day. Through January 1997 (Mission Month 9) the surveillance investigator team allocation is given in table 1.

| Table 1 Surveillance DCEs | | |
|---|---|---|
| Successful | 85 | 85% |
| Failed or Canceled | 16 | 15% |
| Total | 101 | 100% |

In an attempt to make best use of the allocated DCEs, the Surveillance PI team established a methodology of combining a number of experiment objectives in each DCE, so best use could be made of the existing opportunities. Nevertheless, this amounts to about 2 DCEs each week. The data collected thus far allow us to show how and what a space based sensor can provide. It is possible to give examples of all the functions mentioned above, and show some aspects of catalogue maintenance.

### I) Tasking

The tasking test experiment emphasized deep space (DS) satellites. A set of satellites were chosen as high priority — mostly geosynchronous and calibration satellites — , and the remaining opportunities were selected from the USAF First Command and Control Squadron (1CACS) who has responsibility for tasking the SSN. The optimizing scheduler (Burnham and Sridharan, 1997) attempts to make an observing schedule that respects the space craft operating constraints (e.g. do not point at the sun), taking into account the RSO observability. This is a static scheduler that preplans every DCE from beginning to end.

The first example of a tasking event is given in figure 6, which shows the data obtained for the active payload SSC #23621 (Cosmos 2317, Glonass). In this case the observation residuals are quite respectable (less than 4 arcsec). This frame set leads to another important point. In this wide field camera one often finds other satellites. Here we have the serendipitous observation of a low altitude rocket body. In this case, there was an elements set suitable for correlation, but we had no observations to compute a refined orbit and assess the data.

A second example, figure 7, is an observation of the geosynchronous belt. In this case we see a cluster of satellites in one frame set, and the SBV detected all objects at once. This is a valuable data set, in that it helps to keep track of clusters of satellites. Mistaken association, or correlation, of satellite observations satellites in clusters is a continuing problem in maintaining the deep space catalogue. In this case, the observations are properly correlated. The observation

residuals in this case represent the orbit accuracy based on the SSN data, and the accuracy of the SBV data, which is believed to be acceptable.

Catalogue maintenance, of course, results in updating orbital element sets for catalogue objects. Though, the data density is not as high as would be expected from an operational sensor we can give some preliminary results. Table 2 gives the results for a variety of satellites.

| Table 2 Catalogue Maintenance with SBV | | | | | | |
|---|---|---|---|---|---|---|
| Satellite | SSN +SBV | | SBV Only | | Orbit Difference (m) | #SBV Passes | Arc Length (days) |
| | rms (mdeg) | #obs | rms (mdeg) | #obs | | | |
| Lageos II | 3.48 | 32 | 1.87 | 31 | 6 | 3 | 28 |
| Glonass | 0.9 | 22 | 1.3 | 23 | 56 | 4 | 37 |
| Glonass | 0.8 | 28 | 0.8 | 28 | 11 | 4 | 25 |
| Molniya | 1.4 | 41 | 0.9 | 41 | 24 | 6 | 28 |
| Ekran | 1.2 | 20 | 0.7 | 20 | 30 | 4 | 97 |

We see that the SBV data is consistent with the SSN data, and can be used with SSN data to obtain optimal orbits. Radar data from Millstone and Altair are always combined successfully with SBV data, and we argue that space based data has been successfully fused with ground based data. We note that in some cases the GEODSS data does not fit, and we believe that the GEODSS data has significant biases. This is consistent with the calibration results obtained at Millstone Hill (Buchmann, 1997). Furthermore, we note that the difference between the SSN+SBV orbits and the SBV only orbits is of the order of 50 meters. This shows the power of high fidelity orbital mechanics models combined with high accuracy (unbiased) data. At geosynchronous ranges, one second of arc (5 µ radians) amounts to 180m. Therefore, the agreement for these cases is much better than the intrinsic accuracy of the SBV data.

## ii) Catalogue Augmentation

Catalogue augmentation occurs when measurements that did not correlate with the RSO catalogue — an uncorrelated target or UCT — are used to obtain an initial element set which leads to reobserving the object at a later time. With a series of observations — over several days — a reliable orbit is then established that can be used for reacquisition and catalogue maintenance. The key step in this process is determining an orbit of sufficient accuracy to be used for reacquisition, also known as initial orbit determination (IOD). IOD based only on angular measurements is notoriously difficult. The methods used today a derived from two methods, one developed by Gauss and augmented by Gibbs — the Gauss Gibbs method — and a second attributed to Laplace (Batton, 1987). These IOD methods are notoriously dependent on geometry and data noise. They are also suboptimal is that they use only three of the observed

points — generally chosen to obtain the longest time interval between the first and last. Therefore, the IOD process is done in two steps; first the IOD then followed by an iterated differential correction (including 3 sigma data screening). This leads to an optimal estimate of the orbit based on the available data.

To investigate what can be done with catalogue augmentation, short arcs of SBV data have been selected. Each one was processed to obtain 1) the initial orbit (using the Gauss Gibbs method), 2) the differential correction, and 3) an estimate of the prediction error of this corrected orbit 24 hours later. We chose 24 hours as the likely revisit time for the SBV when operated as a contributing sensor. Of course, the element set could potentially be handed off to another sensor for an earlier attempt at acquisition. We give in Table 3; the satellite Id, the action elements for the nominal orbit, and for the IOD orbit, and the prediction error after 24 hours.

| Table 3 Catalogue Augmentation Capability | | | | | | |
|---|---|---|---|---|---|---|
| Sid | Nominal Orbit | | | SBV IOD Orbit | | | 24 Hour Prediction Error (deg) |
| | a (km) | e | I(Deg) | a(km) | e | I(deg) | |
| 22195 | 12159.2 | 0.01366 | 52.68 | 12162.0 | 0.0142 | 52.66 | 0.84 |
| 21897 | 26554.5 | 0.7124 | 65.03 | 26554.4 | 0.7126 | 65.00 | 0.05 |
| 23656 | 42205.6 | 0.0022 | 0.579 | 42121.8 | 0.0030 | 0.564 | 1.09 |

We see that the SBV data can be used to reacquire UCTs within 24 hours We expect to demonstrate element set handoff and successful catalogue augmentation soon.

iii) Clusters

Clusters present a unique challenge to the space surveillance system. Many of the members of clusters are active payloads and therefore of high interest. Being active, they are manoeuverable, and orbit maintenance is correspondingly more difficult. There are at least 25 clusters of satellites in the geosynchronous belt. The primary difficulty is correctly associating an observation with an RSO. The three sources of error in this process are 1) the observation error, 2) the element set error, and 3) the orbit model error. Of course, the system feeds upon itself. If an observation is incorrectly associated, then the orbit resulting from combining it with the existing data will be degraded. Use of this degraded orbit will cause further incorrect associations, and so on. On the other hand, correctly associated high accuracy metric observations, combined with good orbit models, will give improved orbital elements, and increase the ability to correctly associate observations. Then, if an orbit manouevre takes place, as it often does in the geosynchronous belt, one can determine the manoeuver object with greater confidence, and concentrate tracking on it.

To illustrate the use of SBV for maintaining the orbits of clusters, we show multiple

measurements of a cluster. The one chosen is at 259 deg longitude. Figure 8,9 shows the frame sets on day 96318. We see that the SBV metric accuracy is sufficient to separate the four objects. By using tracking data from the SSN and the SBV these orbits are well determined. Continued observation by SBV of this cluster, coupled with analysis tools for clusters, will allow maintenance of all objects in this cluster.

The SBV can be used to correctly associate the observations and maintain the orbits of the geosynchronous clusters.

iv) Routine Space Surveillance

We has seen that the MSX/SBV can make accurate metric observations, and that these observations can be used to determine precise orbits, both by itself and combined with SSN data. We have seen that SBV data can be used to obtain useful initial orbits to support catalogue augmentation, that SBV data can be used to maintain the orbits of catalogued objects, and that it is sufficiently powerful to be used for maintaining the orbits of each object in a cluster. With these technology demonstrations, the remaining issue is the ability to operate the sensor for extended periods, to provide a continuous flow or data. To demonstrate this operation, a 12 hour data collection was planned. Experiment data was collected until an Attitude Processor reset occurred after more than 11 hours of operation. The statistics are given in figure 10. We see that the spacecraft and sensor operated nominally during for more the 11 hours. There is sufficient power, communications, data onboard data storage to support continuous operation. The data collected was of the consistent high quality obtained from shorter data collections. The spacecraft maintained pointing stability through out the experiment. The number of looks, i.e. frame sets, depends on the scheduling algorithm, the attitude dynamics for pointing the satellite among other factors. By using both signal processors -- only one was used during experiments to date -- and refining the scheduling algorithms optimizing the pointing -- after the Spirit III cryogen is all used restrictions on spacecraft pointing will be relaxed -- we believe that we can obtain more observations in a 12 hour interval than have been realized during this experiment. It is clear that the MSX/SBV can perform routine operational space surveillance.

5) Discussion

I) Implications for Future Space Surveillance

Space Based Space Surveillance is here. It has been demonstrated that space surveillance from a space based platform is possible. The predictions have been validated, and we can proceed to make the appropriate use of space based assets for space surveillance. It is clear that the current issues raised in above, can be addressed with this sensor, and in fact we are taking data now to this end. In the next few months, data will begin to flow to the SSC in an experimental way. In the longer view, we will see the MSX/SBV integrated into the SSN as a contributing sensor, and one can assess how the overall performance of the SSN will be changed.

ii) Lessons Learned

It takes a long time, much planning and hard work to make a system a complex as the MSX/SBV work. The success of the program, less than on year on orbit, is due to the vision of many people years ago that brought the MSX/SBV into being. Many of the lessons learned are given in figures 11,12 . It was essential to build on the experience of ground based space surveillance, not only to define the goals and identify the critical issues, but the exploit the experience and capability of existing facilities. There is great benefit of planning from the beginning, attention to detail. Simple things like common coordinate systems and consistent definition of interfaces. This program also depended on the cooperation between groups in the laboratory and between the laboratory and other organizations. It has been critical to establish good open working relationships across the program and at all levels.

iii) Remaining Tasks

The MSX/SBV system is working, but not as well as it could. We are still working to understand the operation of the sensor — how to set the signal processor parameters to obtain the data we want. The data analysis process can be improved to remove some bad data, to improve the correlation of observations with the catalogue — especially with clusters. The scheduler can be improved to get more observations, better distributed. Though the capability for catalogue augmentation is there, it must be carried through and actually bring objects into the catalogue. All the analysis given here is based on use of metric data. The use of photometric data for space object identification (SOI) needs to be exploited. In fact, the MSX has a complete suite of multispectral instruments from the UV to the LWIR. We have been archiving data for analysis, and we plan to demonstrate the SOI capability possible with a space based surveillance sensor. Then there are the additional issues of autonomous spacecraft operation for space surveillance. The SBV programmable Experiment Controller (EC) will allow future experiments in autonomous detection, tracking, scheduling, and catalogue maintenance. Clearly, we have just scratched the surface of space surveillance from space.

6) Conclusions

Expectations for the SBV have been exceeded for both metric and photometric accuracy, figure 13. Space Based Space Surveillance is here to be used in the most appropriate way. The vision of early planning for the SBV has been vindicated. *__We Did It!__*

84

References

Abbot, R.I., Gaposchkin, E.M., von_Braun, C.,1997, This proceedings

anon; 1991, "Midcourse Space Experiment Systems-Derived Requirements Document (SRD)" , DoD, SDIO, Washington DC. 20301-7100, 181 pp.

anon, 1992, "Midcourse Space Experiment Science Modeling Requirements Document (SMRD)". DoD SDIO, Washington DC, 20301-7100,

Batten, R.H., 1987, "Introduction to the Mathematics and Methods of Astrodynamics", AIAA Education Series, 796 pp.

Burnham, R., Sridharan R.,; 1997, "Geosynchronous Surveillance with a Space Based Sensor", in Advances in Space Flight Mechanics, 1966, Astronautical Sciences, ed. Powell, G.E., Bishop, R.H., Lundberg, J.B., Smith, R.H., pp 1683-1696.

Chow, J; and Harrison, D; 1994, "Space-based Visible (SBV) on the MSX Satellite",

Bergemann, R. 1995, in "MIT Lincoln Laboratory Technology in the National Interest", Lincoln Laboratory, Massachusetts Institute of Technology, Lexington MA, ed E.Freeman, 292 pp..

Buchman, K.; 1997; "Monthly Calibration Report", Millstone Hill, Lincoln Laboratory.

Gaposchkin, E.M.; 1995, "Space-Based Space Surveillance with MSX", in Spaceflight Mechanics 1995, Vol, 89, Advances in the Astronautical Sciences, ed Proulx, Liu, Seidelmann, Alfano, pp1681-1690.

Mill, J.D., O'Neil, R.R., Price, S., Romick, G.J., Uy, O.M.,Gaposchkin, E.M., Light, G., Moore Jr., W.W., Murdock, T.L.; 1994, "The Midcourse Space Experiment: Introduction to the Spacecraft, Instruments and Scientific Objectives, Journ. Spacecraft and Rockets, Vol 31, No 5, pp 00-907.

Peterson, M, 1996, APL Technical Digest, The Applied Physics Laboratory, Johns Hopkins, University, MD.

Sharma, J., von_Braun, C., Gaposchkin, E.M.,1997; This proceedings

Smith & Mansberger, 1997, This proceedings

von_Braun, C., Gaposchkin, E.M., Sharma, J.; This proceedings

## Infrared Focal Plane Arrays for Ground- and Space-based Space Surveillance

P. D. LeVan, K. A. Shrock (Phillips Laboratory), and J. E. Hubbs (Phillips Laboratory / Ball Aerospace)

**Abstract**: Several programs for infrared focal plane array (FPA) development, sponsored by the Ballistic Missile Defense Organization, and technically monitored by Phillips Laboratory, have a strong potential for space surveillance applications. For example, FPAs fabricated with impurity band conduction, arsenic-doped-silicon ("IBC silicon") are optimal for many applications in the MWIR, the LWIR, and even the VLWIR. The IBC silicon FPAs enjoy a high efficiency of conversion of incident photons into signal electrons, high pixel response uniformity, and an overall level of sensitivity approaching the background limit. This FPA technology has been sponsored by Phillips laboratory for both high and low background applications. More recently, LWIR HgCdTe FPAs have shown tremendous improvements, most pronounced for lower background applications, in both pixel response and dark current uniformity. "LW HgCdTe" may soon compete with IBC silicon for applications with wavelength response shortward of approximately 12 microns, given the higher operating temperature (40 Kelvin or high for LW HgCdTe vs. 10 Kelvin for IBC silicon). The results of recent characterizations carried out at Phillips Laboratory confirm the high levels of performance mentioned above. Also, IBC silicon detectors have recently been employed in a variety of space surveillance and related applications. An acquisition camera based on a 128x128 IBC silicon FPA was developed for the Phillips Laboratory 1.6 meter telescope as a pathfinder for the utilization of this technology for ground-based space surveillance. In addition, Phillips Laboratory sponsored the engineering proof of concept for, and export of, IBC silicon detectors for use with the European Space Agency's Infrared Space Observatory (ISO). These detectors were retrofitted into ISO, which is currently in orbit and acquiring celestial background data. Finally, IBC silicon FPAs have been chosen for both the multispectral radiometric and LWIR imaging sensors under construction for the new 3.6 meter telescope of the Phillips Laboratory Advanced Electro-Optical System.

### 64x64 MWIR & LWIR Dualband Focal Plane Array
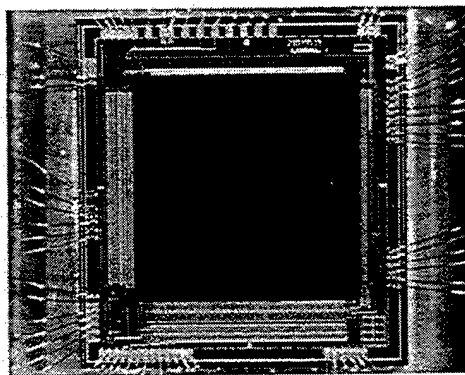


(This is the first-ever vapor phase epitaxy HgCdTe FPA to image simultaneously in these two wavebands.)

**Focal Plane Array (FPA) Performance Characterizations in the Phillips Laboratory IRREL**

The Infrared Radiation Effects Laboratory is a facility based at Phillips Laboratory and operated under contract by Ball Aerospace. IRREL characterizes state of the art focal plane arrays over a range of operational parameters, operating temperatures, and background levels. Infrared wavelengths from 1 to 23 micrometers. Characterizations can be done at FPA operating temperatures as low as 4 Kelvin, and at background levels as low as $10^9$ photons per second per square centimeter. The IRREL attain a range of background levels with a proper configuration of optical components. Also, IRREL can perform characterizations in ionizing radiation environments, with sources of Cobalt-60, linear accelerators, and flash x-rays. Characterizations are accomplished with the Mosaic Infrared Test System (MATS), a customized system capable of characterizing infrared FPAs developed under all current Air Force programs. MATS supplies the required clocking waveforms, bias voltages, and signal output conditioning, and interfaces to the device under test with device-specific wiring inside of a cryogenic test Dewar. MATS characterization includes detector spectral response, FPA responsivity, FPA noise, and conversion gain and linearity. MATS is supplemented with a spectral test station based on a Nicolet Fourier Transform Spectrometer that achieves a spectral resolution of 4 wavenumbers over the wavelength range from 2 to 25 micrometers. Finally, blackbody sources operating over the temperature range from 300 to 1300 Kelvin are used in conjunction with the MATS characterizations.

Recent IRREL characterizations include low background, LWIR HgCdTe FPAs (see below), impurity band conduction silicon FPAs, and GaAs/AlGaAs quantum well detectors. The recent IRREL characterization of low background, LWIR HgCdTe FPAs developed under the Phillips Laboratory LLUM program illustrate that this technology is reaching a level of maturity which should allow its use for lower-background system applications. In particular, the uniformity in both pixel responsivity (in the 5 to 10%, sigma over mean level) and dark current shows noteworthy improvements over that available previously.

Finally, one of the more recent IRREL characterizations of a dualband FPA that images simultaneously in both the MWIR and LWIR. This vapor phase-grown detector array and cryogenic multiplexer hybrid is the first ever of its type to provide this capability.
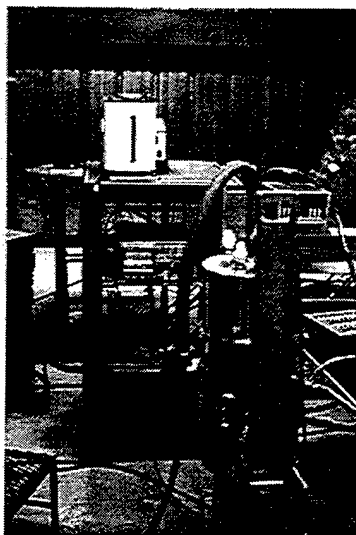


(See Reference 1)

88

**Applications of Impurity Band Conduction (IBC) Silicon Focal Plane Arrays (FPA)-
The Starfire Optical Range (SOR) LWIR Acquisition Camera**

This narrative briefly discusses a Phillips Laboratory internal design for a high sensitivity, large field of view infrared acquisition camera using a silicon IBC FPA. The acquisition of satellites with the 1.5 meter telescope of the Starfire Optical Range typically requires a sunlit target and dark sky However, the level of thermal radiation from such a satellite is often sufficiently high in the LAIR to permit detection with ground-based telescopes, irrespective of target illumination by the sun. The drawbacks of LAIR acquisition include the high levels of thermal radiation from both the telescope and the atmosphere, which lead to the following, (1), the "background signal" level usually exceeds the target signal level and must be removed on time scales over which it is relatively constant, and (2), associated with the background signal is a noise level that dominates all system noise sources. For our application, the background signal level at the detector array was in the mid $10^{15}$ photon sec$^{-1}$ cm$^{-2}$, for a one micron spectral bandpass.

The design of the camera posed several challenges related to the high levels of thermal background radiation. This was especially the case for an acquisition camera design, which has relatively large pixel fields of view (relative to the Airy diffraction disk) and correspondingly higher background signal levels. Yet another challenge is that the SOR 1.5 meter telescope with its slow f/217 optics; lower magnification was required for the acquisition mission. Also, chopping secondary mirror, the conventional method for removing background radiation, is not available on the 1.5 meter telescope. It is therefore necessary to incorporate a chopping mirror into the acquisition sensor for the removal of atmospheric and telescope background radiation. Finally, visible wavelength telescope in general have higher levels of background radiation than their infrared counterparts, making the background removal even more challenging.

The camera comprises a 128x128 pixel IBC focal plane array fabricated for use with high backgrounds (>$3\times10^{15}$ photons sec$^{-1}$ cm$^{-2}$). The FPA is operated in a vacuum vessel at cryogenic temperature, with cooling achieved with a commercial Gifford-McMahon cryocooler. The second cooling stage of the cryocooler cools both the FPA and a radiation baffle containing a spectral interference filter to 11 Kelvin. The first stage of the cryocooler maintains the camera's radiation shields and optical components near 80 Kelvin. The optical design employs a large, external germanium lens to image the f/217 telescope beam onto an 80 Kelvin field stop that is located behind the camera's zinc selenide vacuum window. The external germanium lens also image the telescope primary mirror onto a chopping mirror and collocated 80 Kelvin pupil stop. The field top is imaged onto the FPA with a small germanium lens located within the 11 Kelvin radiation baffle. A cold vignetting stop is located between the germanium lens and FPA, at the image of the telescope quaternary mirror, to eliminate the thermal background associated with telescope vignetting surfaces.

Our optical design for the acquisition camera maps a 128x128 pixel detector array onto a two milliradian patch on the sky. The optical design uses two aspheric lenses, one to re-image the field onto a cold field stop, and reimage the telescope pupil onto a cryogenic chopping mirror and collocated radiation stop. The second lens then re-images the field stop onto the detector array. Aberrations are kept lower than the diffraction blur over the entire two milliradian field of view.

In addition to providing a proof of concept for the LAIR acquisition of satellites at the SOR, a secondary benefit of the project was the exploration of novel techniques for the cancellation of thermal radiation from the telescope and atmosphere. In this sense the project was a pathfinder for LAIR imaging and radiometric sensors slated for the Phillips Laboratory Advanced Electro-Optical System. To the best of our knowledge, our sensor was unique in incorporating a cryogenic chopping mirror and radiation stop at the image of a ground-based telescope's primary mirror.

(See References 2 & 3)

**Applications of Impurity Band Conduction (IBC) Silicon Focal Plane Arrays -
The European Space Agency Infrared Space Observatory (ISO)**
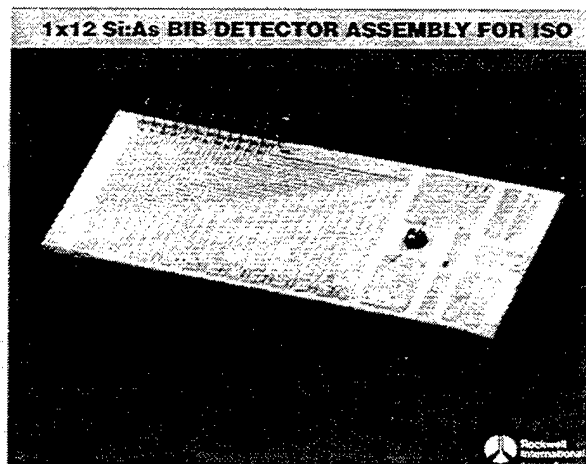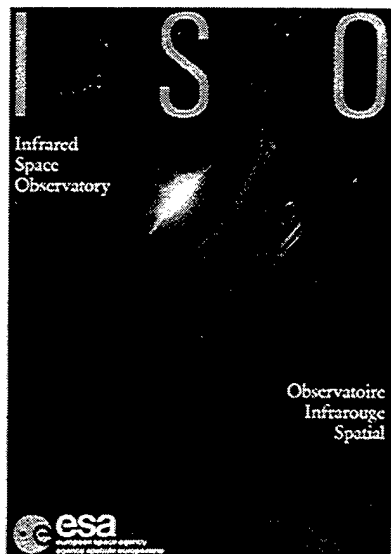


U.S. Impurity Band Conduction (IBC) detector technology offers dramatic improvements in sensitivity and ease of calibration to the European Space Agency's (ESA) Infrared Space Observatory (ISO), a satellite-based, cryogenically-cooled astronomical telescope. The ISO satellite is tasked to collect improved celestial background data that will benefit civilian infrared astronomy in the U.S. through NASA. (NASA had previously concluded negotiations with ESA for U. S. participation in the ISO mission, as did the DoD for its Strategic Scene Generation Model, of which the celestial background is a component.) ISO was launched in November 1995.

The details of this achievement follow. Phillips Laboratory, using its BMDO SHIELD (Silicon Hybrids with Infrared Extrinsic Long Wavelength Detectors) contract, sponsored the development of low-background, radiation-hardened, VLWIR detectors as a proof of concept for ISO. Rockwell International (Anaheim, CA) built these detectors. In addition to obtaining approval for export from several government agencies, Phillips Laboratory concurrently sponsored construction of the flight grade detectors, which were subsequently exported and retrofitted into the flight and flight spare spectrometer modules of the ISO spacecraft.

Phillips Laboratory has played a significant role over the years in the development of IR detectors with improved sensitivity and radiation hardness for space-based space surveillance. The attribute of radiation hardness is advantageous for spacecraft in the Earth's radiation belts, through with ISO will pass twice daily in its highly eccentric orbit. By contrast, the original detectors for ISO suffered from high susceptibility to single-event upsets, had a limited range of linearity, and an unstable operating point taxing to data calibration. The export of IBC detectors for ISO has also set a precedent for several exports of such detectors for use with ground-based telescopes. These exports protect the availability of the technology for future Air Force needs by extending the market to commercial users.

(See Reference 4)

**Applications of Impurity Band Conduction (IBC) Silicon Focal Plane Arrays (FPA)-**

## Conclusions

We summarize below the several applications of focal plane arrays with impurity band conduction silicon FPAs. Other applications employing this technology include the Midcourse Space Experiment (MSX), a BMDO satellite currently in orbit and collecting background phenomenology data. Future space-based missions baselining this FPA technology include the NASA Wide Field Explorer (WIRE) and Space Infrared Telescope Facility (SIRTF).

Also, IBC silicon focal plane arrays were chosen for two sensor currently under construction for the Advanced Elector-Optical System (AEOS). AEOS is an upgrade to the Air Force AMOS site to a 3.6 meter tracking telescope and facility. The AEOS radiometer comprises two 128x128 pixel, arsenic-doped-silicon (Si:As) FPAs manufactured by Rockwell International, for satellite radiometry to be acquired simultaneously in both LWIR and VLWIR wavebands. The AEOS Longwave Imager also comprises two Si:As FPAs for imaging simultaneously in the 8 to 9 micron and 10 to 13 micron spectral regions. Each of these AEOS sensors is beyond critical design review, and should be operational on Mount Haleakala by 1998 (see reference 5).

Finally, as described in the narrative above, IBC silicon detectors were exported by Phillips Laboratory to the European Space Agency for use aboard its Infrared Space Observatory (ISO), after sponsoring the development of proof of concept detectors at Rockwell International. ISO is a cryogenically-cooled telescope and sensor assembly that is currently in orbit and collecting celestial background data for the infrared astronomical community. The IBC silicon detector array is part of a spectrometer operating in the VLWIR. The ISO detectors are showing the effects of ionizing radiation as ISO passes through the radiation belts twice each day in its highly eccentric orbit; this performance degradation is under investigation.

Also, an LWIR acquisition camera was designed and integrated for the Phillips Laboratory Starfire Optical Range, to accomplish "dark" acquisition of satellites on a 24 hour basis. The camera comprises a 128x128 pixel extrinsic silicon FPA, of impurity band conduction type, and is designed for operation against the high backgrounds characteristic of ground-based LWIR imaging. In addition to demonstrating a proof of concept for acquisition of satellites, a secondary benefit of the camera was to explore novel techniques for the cancellation of thermal radiation from the telescope and atmosphere. In this sense, the program was a path finder for the LWIR imaging and radiometric sensors under development for AEOS.

## References -

1. Arrington, D.A, Hubbs, J.E., Gramer, M., and Dole, G., "Infrared FPA Characterizations at the Infrared Radiation Effects Laboratory (IRREL)", Phillips Laboratory Technical Report, PL-TR-96-1079, May 1996.

2. Cowan, W.D. et al., "Starfire Optical Range Long Wave Infrared Acquisition Camera; Initial Performance Report", SPIE Vol 2475, pp. 236-250, April 1995.

3. LeVan, P.D. et al., "128x128 Pixel Long Wavelength Infrared Acquisition Camera", SPIE Vol 2217, pp. 254-261, April 1994.

4. Valentijn, E.A et al., "Testing and Characterization of the Short Wavelength Spectrometer for ISO", SPIE Vol 2019, pp. 59-69, July 1993.

5. Vigil, M.L. et al., "Sensor Suite for the Advanced Electro-Optical System (AEOS) 3.6-Meter Telescope", SPIE Vol 2819, pp. 151-169, August 1996.

# HAYSTACK-PEGASUS DEBRIS MEASUREMENTS

Thomas J. Settecerri (Lockheed-Martin Space Mission Systems and Support)
Eugene G. Stansbery (NASA/JSC/SN3)
John Opiela (Lockheed-Martin Space Mission Systems and Support)
Mark Matney (Lockheed-Martin Space Mission Systems and Support)

## Abstract

A Pegasus launch vehicle Hydrazine Auxiliary Propulsion System broke up in orbit on
June 3, 1996. The U.S. Space Command Space Surveillance Network detected,
identified, and tracked nearly 700 objects related to this breakup. This vehicle had been in
orbit since May 19, 1994. This paper describes the post-processing analysis conducted to
characterize the Pegasus debris, their contribution to the environment, and the uniqueness
of this breakup.

## Introduction

On June 3, 1996, a Pegasus launch vehicle upper stage (International Designator 1994-
029B, U.S. Space Command Catalog Number 23106) broke up in orbit at 625 km. This
fourth stage was a Hydrazine Auxiliary Propulsion System (HAPS) that had been in orbit
since May 19, 1994. The HAPS was used for only the second time in support of the
STEP II mission. However, on this launch the payload failed to achieve its intended orbit
due to a premature shutdown of the main propulsion system. Some residual fuel remained
in the fourth stage. The HAPS orbit prior to breakup was at an inclination of 82.0
degrees, with a perigee of 586 km and an apogee of 821 km. The dry mass of the HAPS
was only 97 kg; yet by August 1996, the US Space Command Space Surveillance
Network (SSN) had detected, identified, and tracked nearly 700 objects related to this
breakup. Current NASA/JSC explosion and collision breakup models (EVOLVE[1]) predict
an order-of-magnitude fewer objects than were detected by the SSN. NASA Johnson
Space Center's Space Science Branch is closely analyzing data from the SSN to
characterize the breakup in terms of: size, inclination, altitude, flux, and number of
objects. NASA/JSC scheduled the Haystack radar to observe the HAPS debris cloud
during five opportunities on August 5 and 6, 1996. JSC uses the Haystack radar to
characterize the debris environment below 10-cm size because the SSN does not normally
catalog objects below this diameter. However, sizes down to 1 mm are a hazard to space
suits, and centimeter-size objects can severely damage the shuttle.[2]

## Measurements Plan

The first objective was to determine the optimum observation times to look for the HAPS debris. Measurements made by the SSN showed a narrow ring of debris orbiting Earth (figure 1). This ring would pass through the Haystack field-of-view twice a day. Further, figures 2 and 3 show that the optimum target altitude was from 300 to 1200 km; even though, it was suspected that some debris was thrown to 2500 km altitude and above. In figure 2, the data points are shown as apogee-perigee pairs. Data for these plots were generated from the SSN catalog for July 26, 1996. The SATRAK computer program, developed for US Space Command, was used to determine the optimum pointing angles (azimuth and elevation) and range window. Figures 4 and 5 depict the azimuth and elevation from the Haystack radar for 665 tracked objects for one window. Table 1 shows the orbit plane observation time windows and the pointing angles selected for data collection. Data was collected for a total of 17.2 hours on August 6 and 7, 1996; 14.2 hours were relevant to observing the HAPS debris cloud.
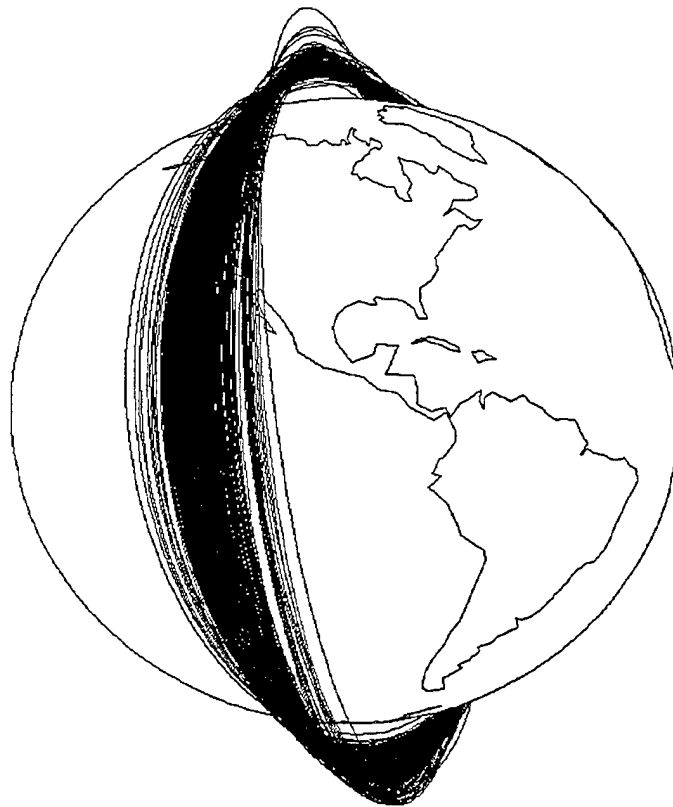


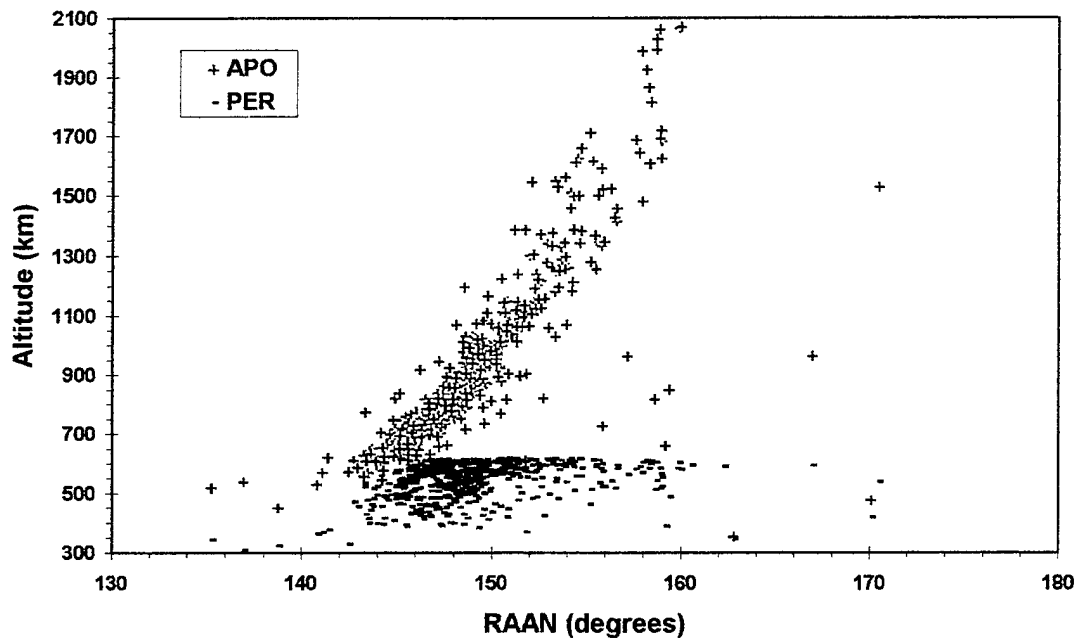Figure 1. SSN Cataloged Pegasus Orbits on 26 July, 1996.

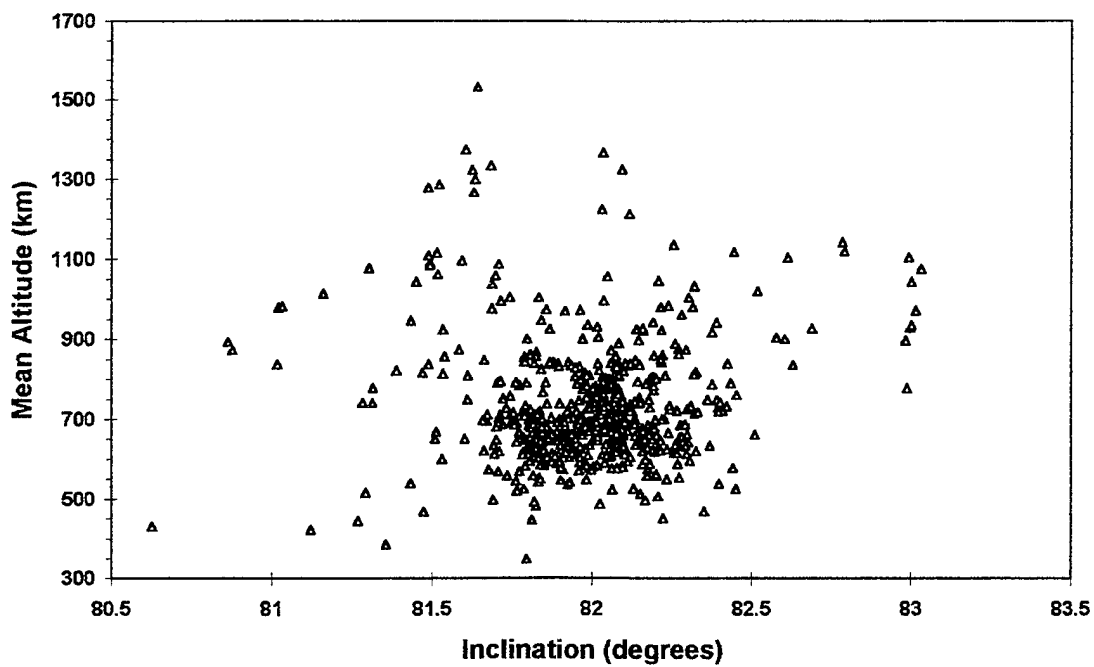Figure 2. Pegasus Catalog Debris, Altitude vs. Right Ascension



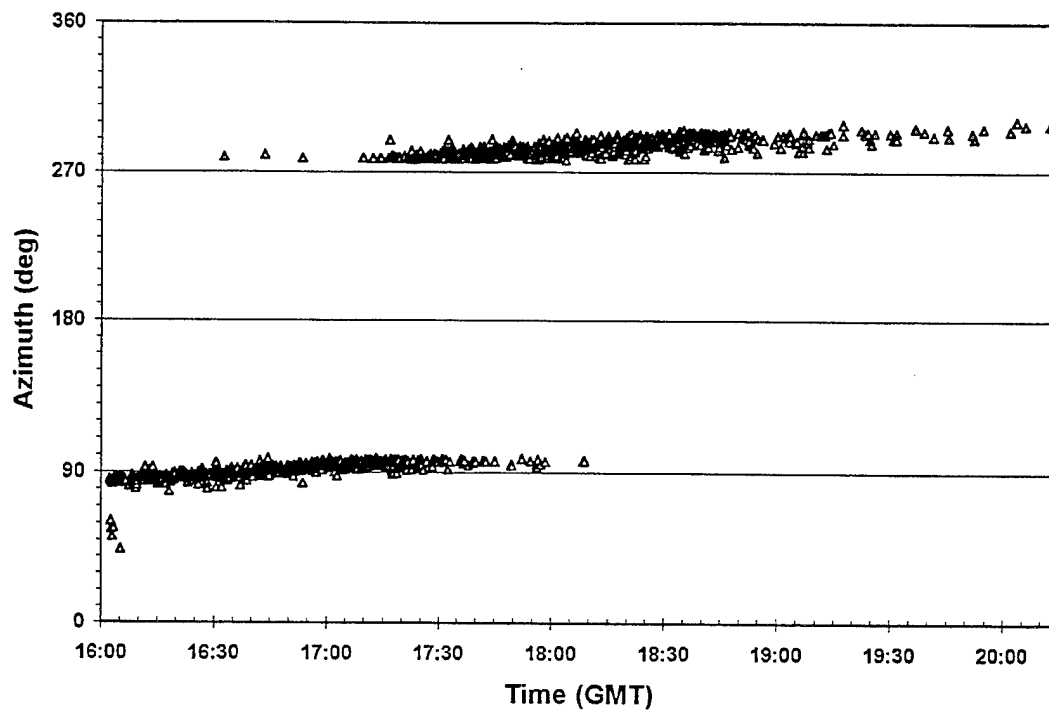Figure 3. Pegasus Catalog Debris, Altitude vs. Inclination

95

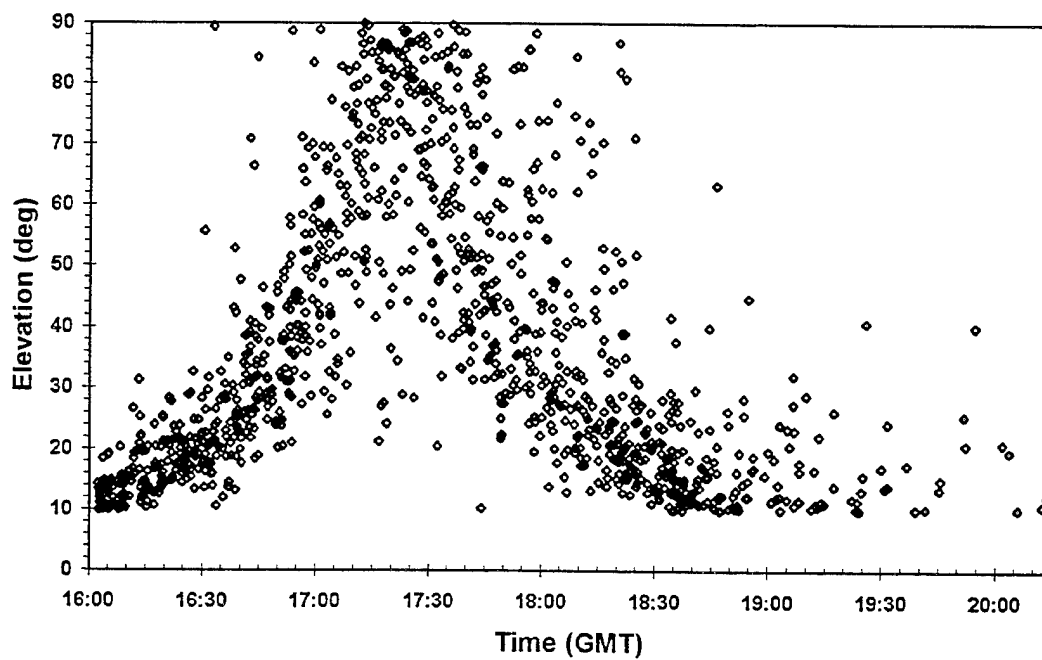Figure 4.  Pegasus Debris, Azimuth from Haystack Radar for August 4, 1996



Figure 5.  Pegasus Debris, Elevation from Haystack Radar for August 4, 1996

## Table 1. Haystack Pointing Strategy

| Pass | DOY | Time (GMT) Open | Close | Stare Strategy Time (HH:MM) / Pointing Angles | | | |
|---|---|---|---|---|---|---|---|
| 1 | 218 | 16:00:03 | 20:12:07 | 16:00 - 20:15 | | | |
|  |  |  |  | EL = 75  AZ = 90 | | | |
| 2 | 219 | 2:13:30 | 6:35:31 | 2:15 - 4:45 | 4:45 - 6:45 | | |
|  |  |  |  | EL = 20  AZ = 75 | EL = 20  AZ = 270 | | |
| 3 | 219 | 15:00:02 | 20:21:04 | 15:00 - 17:00 | 17:00 - 18:00 | 18:00 - 20:30 | |
|  |  |  |  | EL = 20  AZ = 90 | EL = 75  AZ = 90 | EL = 20  AZ = 290 | |
| 4 | 220 | 2:08:19 | 6:36:35 | 2:00 - 3:40 | 3:40 - 4:50 | 4:50 - 6:30 | |
|  |  |  |  | EL = 20  AZ = 75 | EL = 75  AZ = 75 | EL = 20  AZ = 270 | |
| 5 | 220 | 15:03:26 | 19:49:34 | 15:00 - 16:30 | 16:30 - 17:00 | 17:00 - 17:50 | 17:50 - 20:00 |
|  |  |  |  | EL = 20  AZ = 90 | EL = 75  AZ = 90 | EL = 75  AZ = 290 | EL = 20  AZ = 290 |

## Processing

The data was recorded on 8 mm tapes at Haystack and sent to JSC for processing. The JSC Orbital Debris Analysis System (ODAS)[3,4] is used to locate detection times on the 8mm tapes and record events to an optical storage disk. In subsequent processing, pulse data and event data are written to several Oracle database tables. ODAS processes each pulse to determine: range, range rate, amplitude, monopulse voltage ratios, and the noise floor (using a fading memory for each channel). The pulse data are then combined into an event where average RCS, estimated size, and orbital elements are computed. Each detection is checked to see if it correlates with an object in the U.S. Space Command catalog. The data is next analyzed to eliminate: sidelobe detections, detections that do not transit within the two-way half-power points of the main lobe, and events where the estimated path through the beam is not reasonable.

## Results

Figure 6 shows the signal-to-noise distribution. The integrated signal-to-noise ratio (SNR) data is sorted in descending order and plotted against the cumulative detections per hour. The dashed line is the theoretical false alarm rate based on the pulse repetition frequency and number of independent Doppler cells.[5] Notice that below an SNR of 10, the slope decreases. This is due to the fact that the noise threshold was set well above the noise floor by the operators at the Haystack radar facility. We expected the curve to look like figure 7 (data from FY94), where the threshold was set low enough to record more false alarms. Normally, Haystack records all detections above a 12-pulse integrated SNR of 5.0 dB and ODAS processes events above 5.5 dB. Then, for the final analysis an SNR threshold of 6.07 dB is used to display and report the results. A 12-pulse, 6.07 dB integrated SNR was selected so that only one false alarm per ten hours of observation time contributes to the final results. However, during this Pegasus debris campaign, 98 percent of the data had an integrated SNR greater than 9.0 dB.
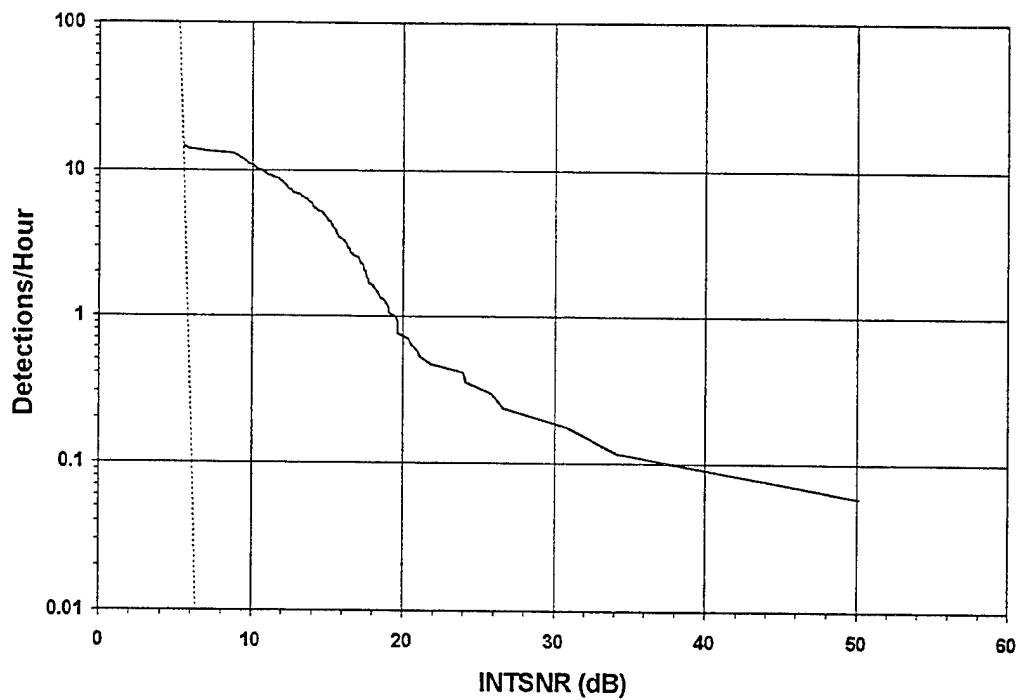
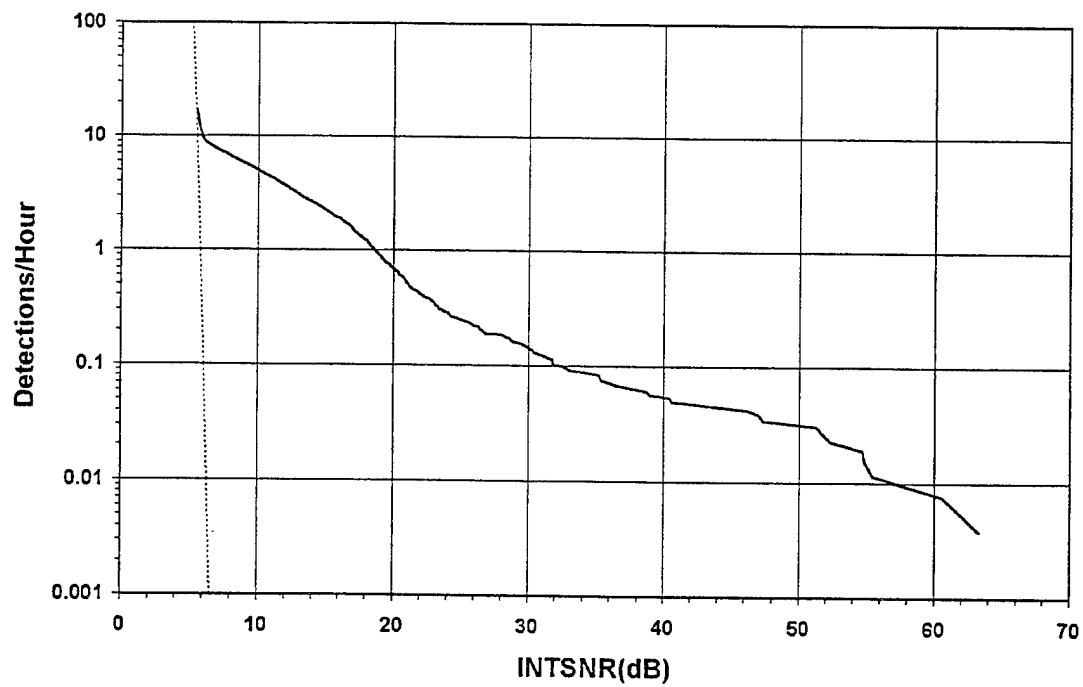Figure 6.  Signal-to-Noise Distribution



Figure 7.  FY94 Signal-to-Noise Distribution

After manual screening, figure 8 was created to examine the spread in altitude and inclination to determine which detections are most likely part of the HAPS breakup. We estimated that an explosion of this type could result in a ±2 degree spread in inclination. Also, the uncertainty of the range rate inclination is 3 degrees; so, a ±5 degree window was used to screen HAPS debris. Since, the initial inclination of satellite 23106 was 82.0 degrees, data between 77 and 87 degrees were included. From the initial 248 detections processed, 130 were considered to be HAPS fragments. Figure 8 shows a cluster of detections between 77 and 87 degrees. Just beyond those limits the data thins out until you reach 95 degrees, where the sun synchronous family of orbital debris is known to exist. Figure 9 is an expanded plot of the reduced/resulting data set shown with the catalog HAPS debris objects. The larger spread in inclination for the smaller Haystack debris fragments is consistent with an explosive breakup. The breakup models assume a velocity and mass distribution based on empirical data from sub-scale tests and radar measurements from Haystack. Smaller pieces may undergo a larger change in inclination, due to a force component that is normal to the velocity vector of the original satellite. This conclusion is validated by figures 10 and 11. Here, the USSPACECOM catalog sizes are plotted against both inclination and altitude. Both plots show that the smaller pieces have spread further in inclination and altitude than the larger objects. Figure 12 is a histogram of the detection rate for 100-km altitude bins. Also shown are similar data from FY94 and all detections from this staring campaign. Notice the huge increase below 800 km. The FY94 and the 'all detections' data sets show all inclinations greater than 42 and less than 138 degrees; whereas, the HAPS data includes only detections between 77 and 87 degrees inclination. Figure 13 shows the altitude plotted against the estimated diameter. The largest detection observed was 8.4 cm and the smallest was 2.1 mm.

JSC interest in this breakup stems from the fact that the initial dry mass was only 97 kg. Yet, assuming a modest density of 2.0 gm/cc for the entire satellite, the objects cataloged by USSPACECOM alone could total nearly 3000 kg. Figure 14 shows the difference between breakup models and actual measurements. This plot is a composite of the size distributions from three different models and radar measurements. The three different models[1] are: an on-orbit collision, a high-intensity explosion, and a low-intensity explosion. Each model assumes an initial mass of 97 kg. The Eglin data is provided by the SSN; JSC uses the NASA size estimation model to calculate size from the Eglin RCS data. From this curve it can be seen that the roll off is at about 15 cm, which is the nominal limit that the SSN catalogs. The lower Haystack curve is the size distribution for the 130 Haystack fragments. However, this data needs to be scaled because observations do not detect all possible debris pieces.

Two methods were used to scale the Haystack data. The first method resulted from several SATRAK runs of the USSPACECOM catalog elements set. Over a five day period (120 hours, encompassing the actual observations) the SSN cataloged HAPS debris objects were propagated through the Haystack beam at the same azimuth and elevation as the actual observations and using a .06-degree beam width. The percentage of catalog hits over 120 hours was then ratioed against the actual detections. For example, from a
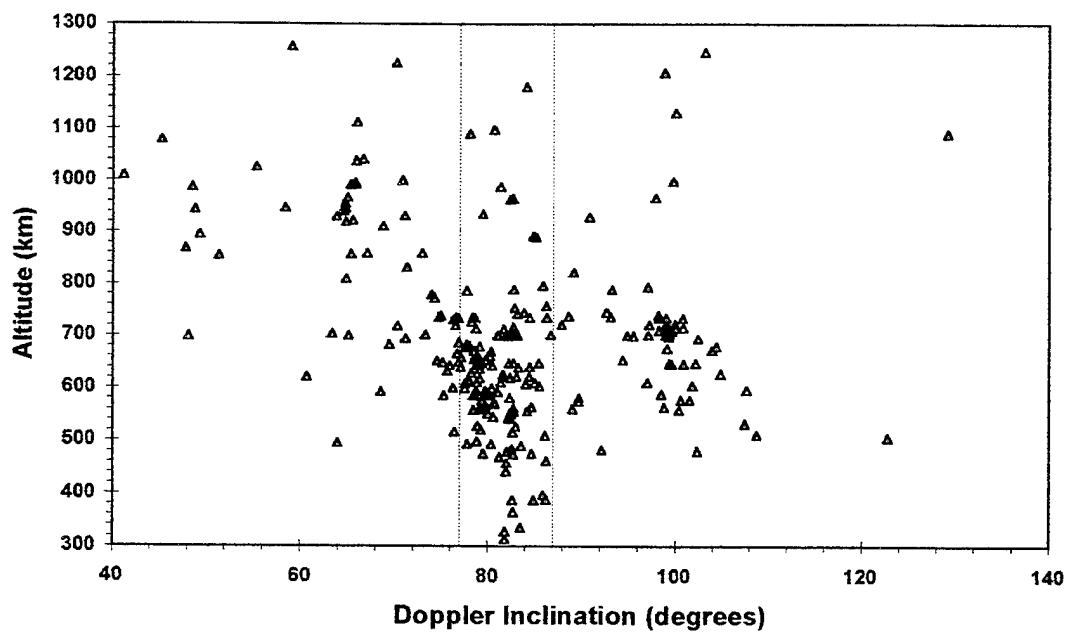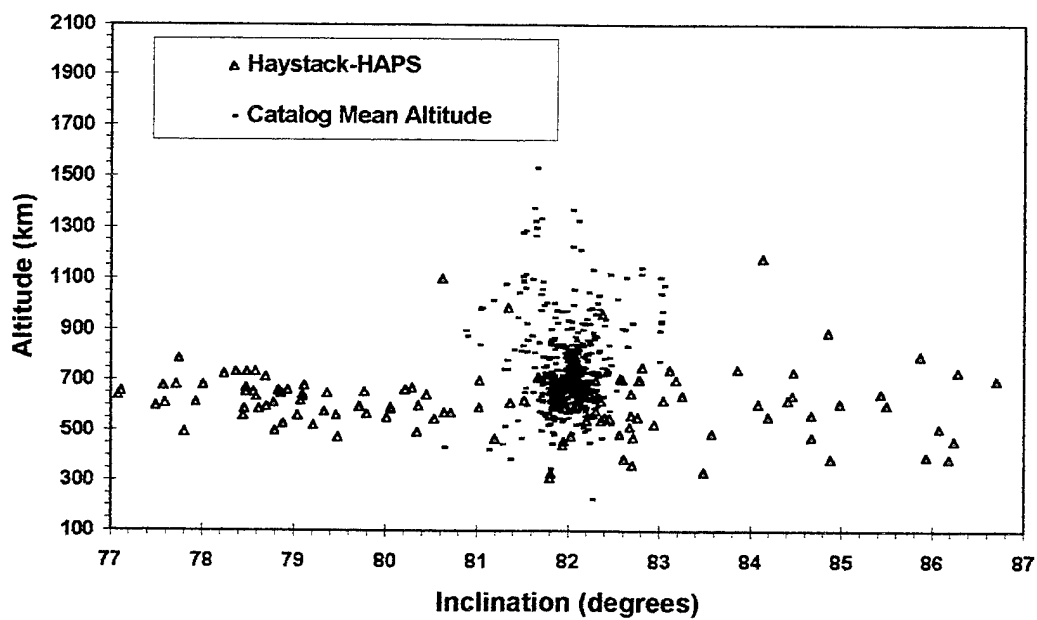
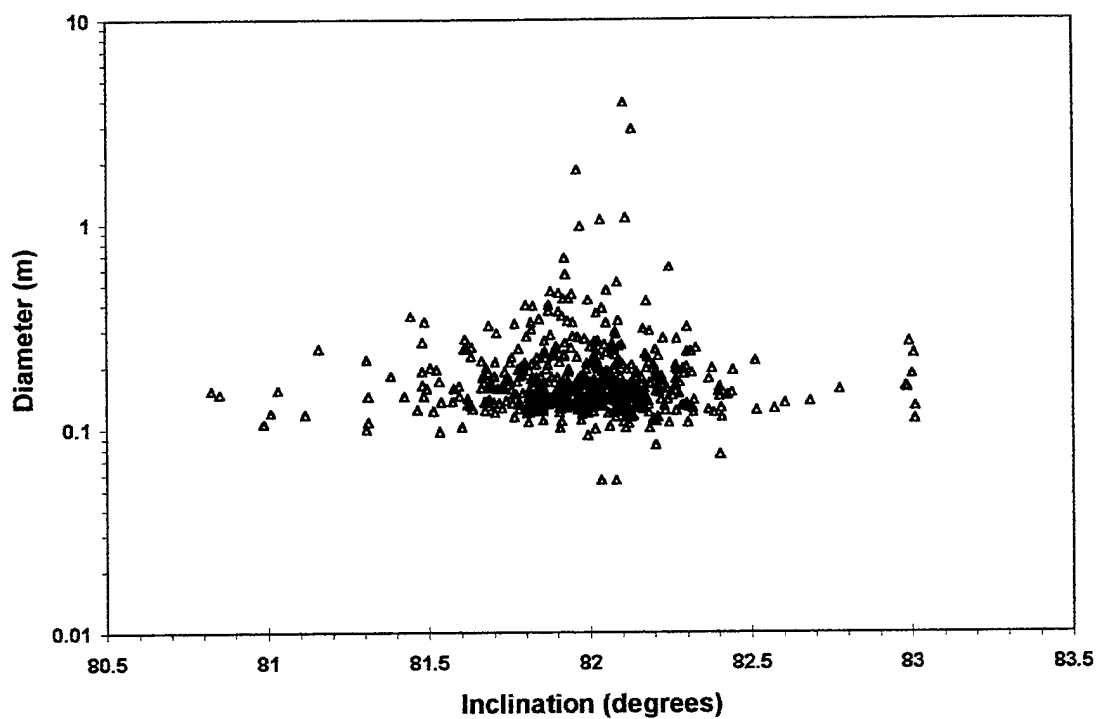Figure 8. Altitude vs. Doppler Inclination



Figure 9. Altitude vs. Inclination

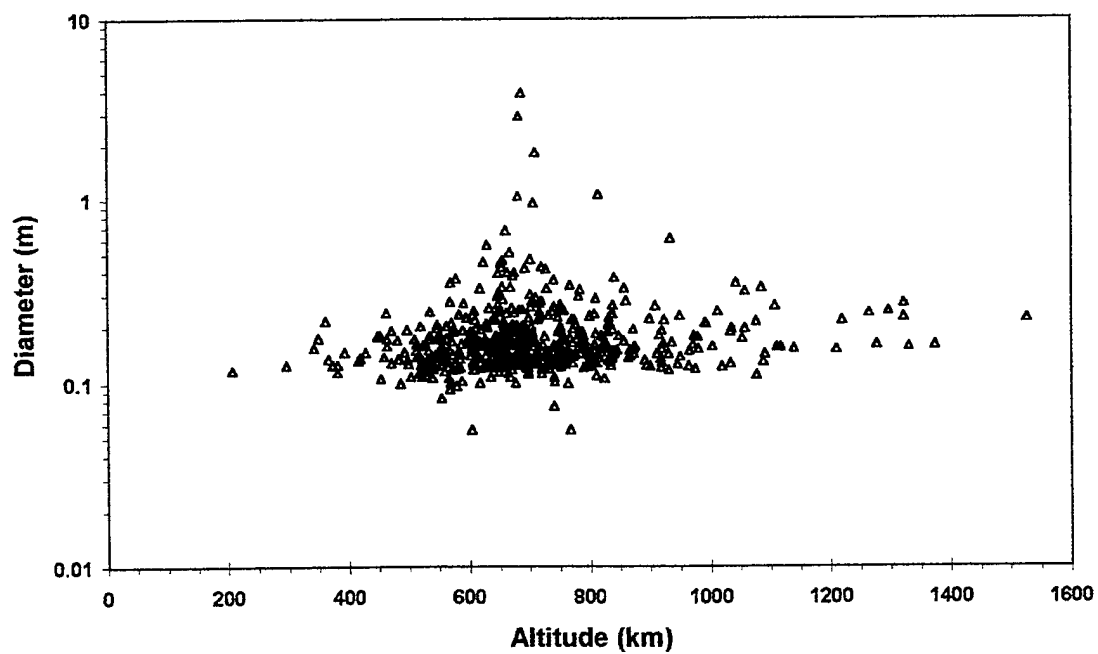Figure 10. USSPACECOM Catalog Data, Diameter vs. Inclination



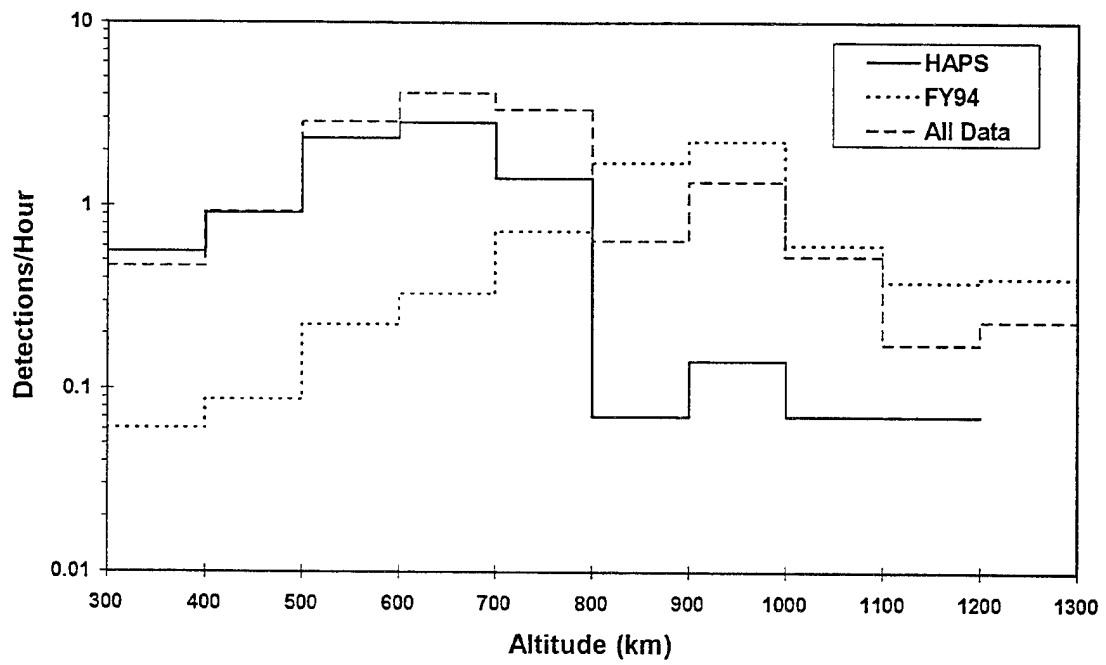Figure 11. USSPACECOM Catalog Data, Diameter vs. Mean Altitude
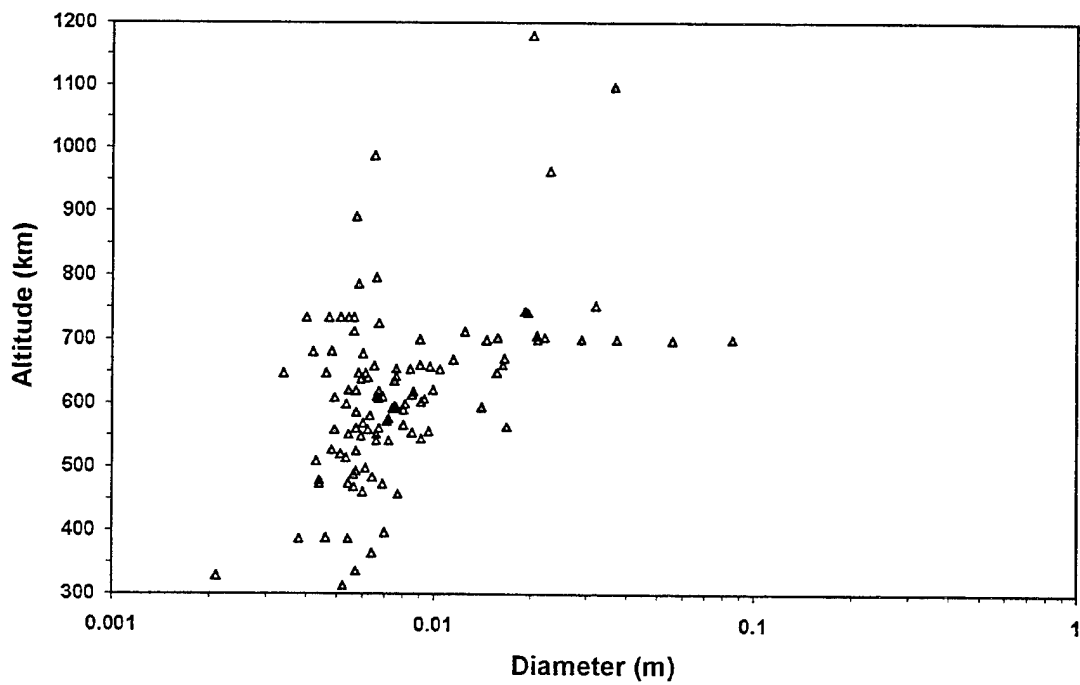
101

Figure 12.  Altitude Distribution



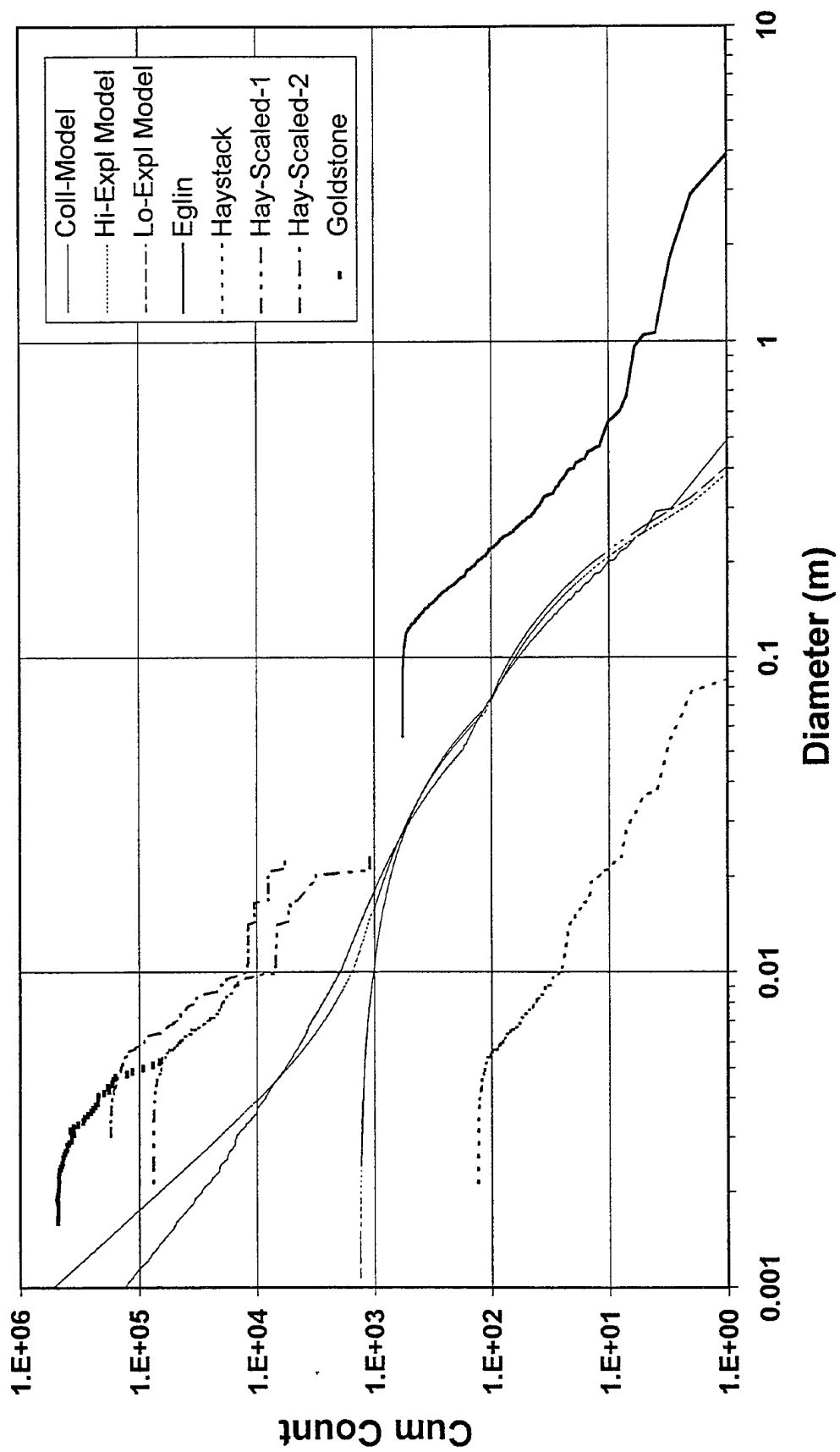Figure 13.  Pegasus-HAPS Altitude vs. Diameter

Figure 14. Size Distribution

SATRAK run, there were 138 detections (1.15/hour) from 665 total satellites. During one observation period of 1.346 hours (with Haystack beam pointed at the same azimuth and elevation), the radar detected 13 HAPS objects (9.66/hour). These 13 objects are then uniformly scaled to a population of 118 objects (9.66/1.15*13). Each pointing direction and staring duration is scaled independently and the results are combined to form a cumulative distribution. The resulting data is show as the 'Hay-scaled1' curve on figure 14. This method has two notable short-comings. First, the SATRAK runs are over a 5-day period and the resulting detection rate is an average. Second, all staring angles are combined.

The second method (labeled 'Hay-scaled2' on figure 14) uses a similar technique; but, computes the probability that each tracked object will pass through the radar beam for the specific time and antenna orientation. This computation is made by assuming that each tracked orbit represents many debris pieces with the same apogee, perigee, inclination, ascending node, and argument of perigee, but randomly distributed mean anomalies. Another assumption made is that the orbit parameter distribution of the tracked objects is characteristic of the orbits of smaller debris.

The Goldstone radar facility in California also provided JSC with debris staring data they had collected on October 8 and November 1. This data was scaled using the second method.

What stands out on figure 14, is the fact that the measured-scaled data is nearly an order-of-magnitude higher than any of the models discussed earlier. First, let's examine the Pegasus fourth stage. The HAPS stage contains propellant, pressurant, two attitude/control tanks, the main propulsion system, guidance and control electronics, and more. The tanks are made from a thin aluminum shell over-wound with graphite-epoxy. An internal explosion is highly likely to cause the composite material to unravel and breakup into long, narrow pieces.

Examination of the polarization information collected from the Haystack radar data supports this fragment shape. Both the principal and orthogonal polarizations (PP and OP) are recorded at Haystack. A comparison of the data from each detection is shown in figure 15. The histogram shown in figure 16 points out that most of the HAPS detections have a PP/OP ratio of one. A simple dipole is the most common shape that produces this ratio. The back-scatter return from a perfect dipole produces equal amounts of energy in both polarizations. Whereas, a spherical object returns primarily the PP energy. Figure 16 also shows FY 94 Haystack data for similar staring angles. Spanning the entire year, the PP/OP ratio is indicative of both spherical and dipole-shaped objects; whereas, the HAPS data points to debris that are primarily dipole-shaped. This fact could account for the vast difference between the actual HAPS mass and the estimated mass calculated from the radar measurements. Using a lower density and the volume of a dipole (rather than a sphere) would yield an estimated mass of debris fragments closer to the original 97 kg.
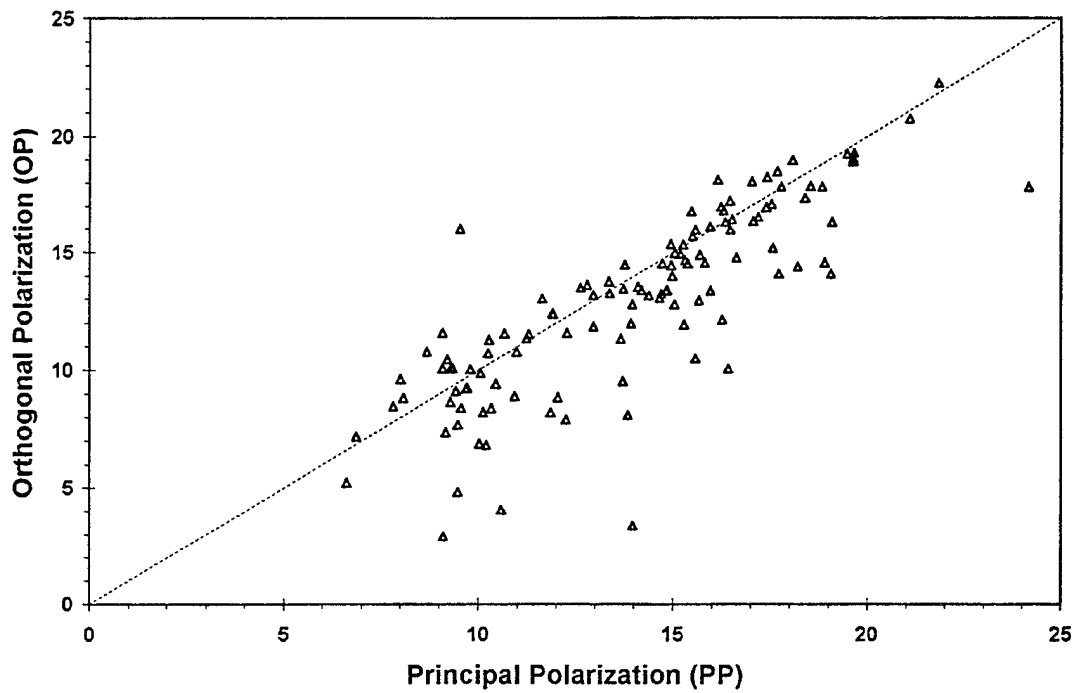
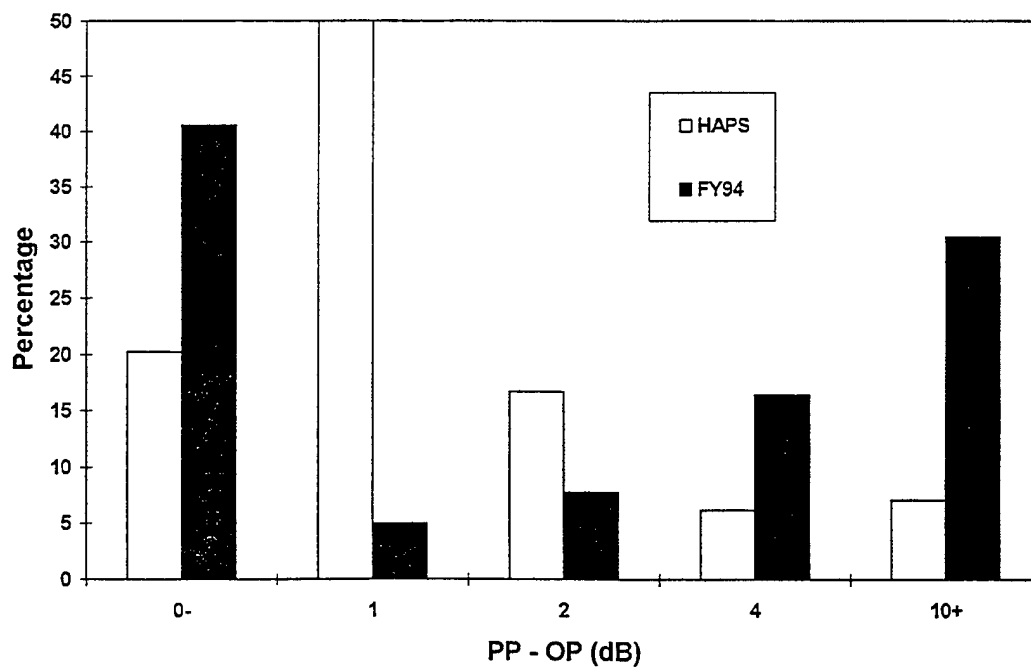Figure 15. Polarization Comparison



Figure 16. Polarization Histogram

Also, by assuming dipole-shaped fragments may account for the greater number of pieces detected than predicted by our models. Modeling to date, (figure 14) has assumed pressure vessels made from aluminum. An aluminum tank explosion would not be expected to breakup into many dipole-shaped pieces. Hence, both the mass anomaly and the unexpectedly high number of pieces can both be explained from the breakup of tanks over-wrapped with graphite-epoxy. JSC is in the process of updating their models and future results may produce better agreement.

**Post Mission Analysis**

It is unfortunate that the sensitivity threshold set at the Haystack was higher than requested. The result can be seen in figure 17, which is a comparison of this data with FY94 Haystack data. Readily apparent is the fact that we lost many detections below an integrated SNR of 9.0 dB. Using a simple model to fit the Haystack-Pegasus data to the FY94 distribution yields figure 18. The number of detections increased from 130 objects to 540. With more detections, the Haystack data and the Haystack-scaled curves would be smoother in figure 14. Also with more data, the slope of the Haystack-scaled curves would have been better aligned with the Eglin data.

**Conclusion**

The HAPS breakup greatly increased the debris environment below 700 km. This debris will remain in orbit for many years to come and will increase the risk to satellites in this altitude range. Initially, the high number of pieces observed was not expected from this breakup; whether, it was a high or low intensity explosion. However, newer models of composite tank explosions could explain this anomaly by taking into account a tank's specific composition and construction. The total mass of debris pieces can be better estimated by assuming dipole-shaped debris objects.

**References:**
1. Reynolds, R. C., "Documentation of Program EVOLVE; A Numerical Model to Compute Projections of the Manmade Debris Environment", System Planning Corporation Report OD91-002-CSP, February 1991.

2. Johnson, Nicholas, *Orbital Debris Quarterly News*, Volume 1, Issue 2, NASA Johnson Space Center, September 1966.

3. Stansbery, E.G., et. al. *Haystack Radar Measurements of the Orbital Environment; 1990-1994*, NASA/JSC Publication JSC-27436, April 20, 1996.

4. Stansbery, E.G., et. al. *Haystack Radar Measurements of the Orbital Environment*, NASA/JSC Publication JSC-26655, May 20, 1994.

5. Blake, L. V., "A FORTRAN Computer Program to Calculate the Range of a Pulse Radar." NRL Report 7448. August 28, 1972.
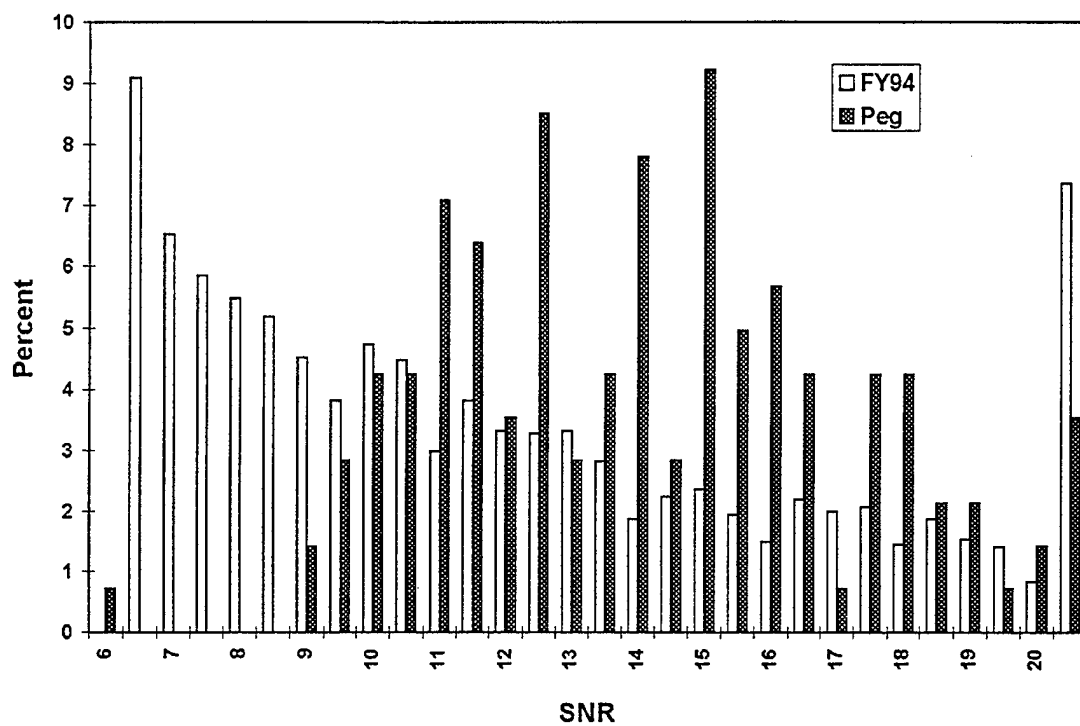
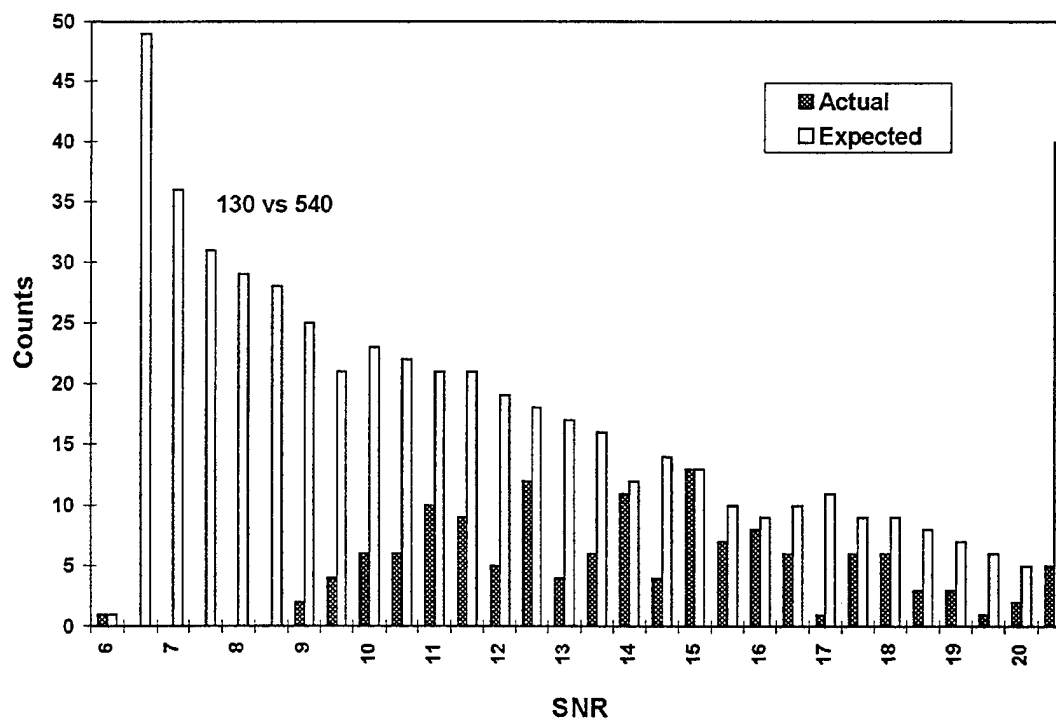Figure 17.  Signal-to-Noise Ratio Distribution 75° Staring Elevation



Figure 18.  Signal-to-Noise Ratio Distribution 75° Staring Elevation

# PAVE PAWS TASKING METRIC REPORT

D. Potter, J. Monti, P. Lipka
The MITRE Corporation

## Section 1

# Introduction

The Pave Paws Tasking Metric Tool (PPTMT) is a software application that develops intrinsic site metrics of space surveillance tasking performance using raw data from the Cape Cod Pave Paws site. This task was performed for the 6th Space Warning Squadron under the direction of ESC/TNS. The task included tool development, with interim prototype delivery to the site, and metric trends analysis of site-supplied data on an as-available time basis. The project was a one-year effort, culminating in delivery of the PPTMT and this report.

Pave Paws was optimized for its primary mission of missile warning. It therefore does not have a robust suite of software analysis tools to evaluate the space surveillance performance as are commonly available at dedicated space surveillance sites, such as Eglin or Millstone radars.

The PPTMT was designed to present orbit-class-based tasking trends of site activity as an off-line capability. To ensure that it would be easy for analysts to use, it was developed on a PC with a simple user interface.

Orbit class metrics are valuable because efficient tasking of the Space Surveillance Network relies heavily on results from studies that correlate the number of observations and sensors needed to maintain a satellite in a given orbit using general perturbations. Though existing Space Defense Operations System (SPADOC) tasking metrics provide insight into the percentage of completed taskings, they do not, as the PPTMT does, evaluate the site activity that occurs from working off the tasking list.

It is hoped that the PPTMT will be incorporated into an on-going process improvement as part of site operations. The tool also has the potential to be a springboard for exhaustively evaluating what conditions that prevent task achievement.

# Section 2
# Usability

## 2.1 Installation

The PPTMT installs on any PC with Windows 3.1 or Windows 95. Installation is easily done by running an executable program called setup.exe and making appropriate choices, which usually means selecting default options. After installation is complete, a typical Windows icon is available to run PPTMT.

## 2.2 Operation

The PPTMT icon can be mouse-clicked to start its operation. The tool's functionality makes use of a Microsoft Access database development environment. Visual Basic modules were written within Microsoft Access to process data quickly and be transportable for upwards Windows-compatibility.

## 2.3 Functionality

The "PPTMT Main Page" screen, shown in Figure 2-1, has seven buttons that represent user options.

- The top center button must be used first to load site-specific Satellite Tasking Program (SATLST) and Task List Program (TASKL) data files. (Appendices A and B, from other references, contain information about the data in SATLST and TASKL, respectively.)

Note that the listing from SATLST is a report of unclassified satellite characteristics from the SATCAT file.

The three buttons in the middle row are for three different queries that provide lists of tasking metric outputs based on the loaded data. Each tasking metric output is separated by orbit class for satellites in TASKL.

- The left button, "No Attempts," tabulates those tasks for which the site did not document any site-based activity, so there were no reports, misses, conflicts, or aborts.

- The center button, "No Reports," tabulates those tasks where the site underwent some activity that caused at least a miss, conflict, or abort, but did not have any reports.

- The right button, "Orbit Class Statistics" tabulates site activity for all tasks.

The bottom row of three buttons provides a listing of specific satellite identifiers (IDs) in orbit classes that correspond with queries previously selected in the middle row.

- The bottom left button lists satellite IDs that were "No Attempts" for a specific orbit class.

110

- The middle button is for "No Reports."

- The bottom right button will list every satellite ID in each and every orbit class. These lists provide the following associated data with each satellite ID:

- Radar cross section (RCS)
- Eccentricity
- Apogee
- Perigee
- Category
- Tasking suffix
- Time off element set
- Launch designation 1
- Launch designation 2

- Element set number (ESN)
- Epoch (EP) time seconds
- EP days
- Rev. No.
- Inclination
- Right Ascension
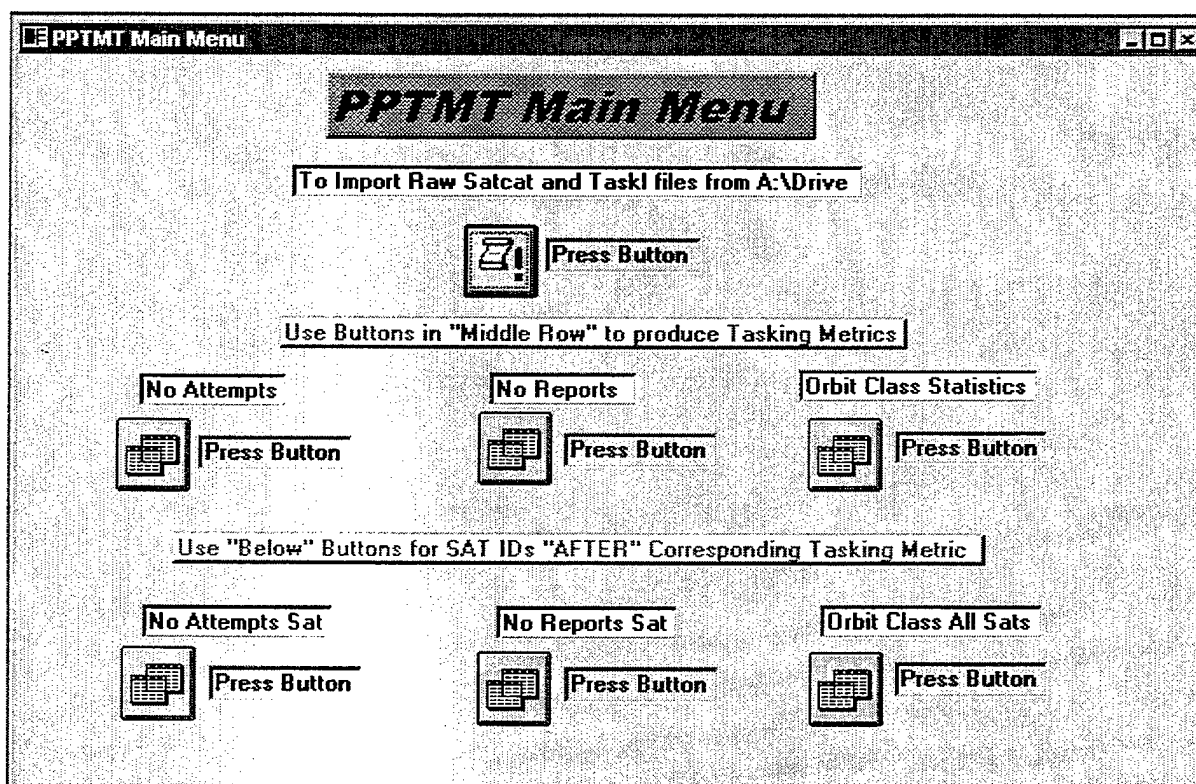- Mean Anomaly
- Mean Motion



**Figure 2-1. PPTMT Main Menu**

# Section 3

# Evaluation of Cape Cod Data

An evaluation was performed using PPTMT results from three different days of SATLST and TASKL data: 27 February, 15 April, and 16 April 1996. Results from SATLST and TASKL files of 30 July 1996 were similar, as determined during a site visit to deliver version 2 of PPTMT; however, this data was not released for more detailed analysis.

Though the tasking metric results from only four days of data provide limited insight, they yield noticeable trends that should be investigated, and indicate the value of longer term daily analysis.

## 3.1 Results from "No Reports" Query

The most revealing site-based tasking metric comes from the "No Reports" query. The metric trends show that orbit classes 10, 12, 37, 47, and 54 repetitively produce most of the misses and conflicts for tasks where no reports occur. Tasking requests are not achieved if no reports are provided.

Tables 3-1 through 3-5 present the metric trend for each orbit class. Column 2 of each table (Percentage of Tasks) shows the percentage of tasks requested in that specific orbit class where site activity occurred but no reports were provided. For example, in Table 3-1, only 9 percent of the tasks for orbit class 12 did not result in any reports on February 27. Fifty-two percent of the misses (column 3) and 40 percent of the conflicts (column 4) occurred in this orbit class during attempts to provide reports on these 9 percent of the tasks. In this case, the other 91 percent of the tasks in orbit class 12 provided at least one report and contributed the other 48 percent of misses and 60 percent of conflicts. (The percentage of aborts are not provided in these tables because they rarely occurred.)

The trends shown in Tables 3-1 through 3-5 show specific orbit class trends and, taken together, indicate overall orbit-based trends. Of the five cases, only orbit class 12 has a circular orbit. Though orbit class 10 has the same apogee as orbit class 12, it would not be considered to have a circular orbit. Table 3-2 shows that orbit class 10 has about one fourth of the tasking requests that do not result in reports, but contributes half the misses and over half the conflicts.

Orbit classes 37, 47, and 54 have similar perigees but are markedly different in apogee. A noticeable trend occurs with differences in apogee—increasing apogee causes an increase in the percentage of taskings that are not achieved since no reports are provided. The percentages of misses and conflicts also increase. Tables 3-1 through 3-5 show the continuing trend up to the largest apogee case, orbit class 54, where about three fourths of tasks do not result in reports and cause all of the misses and conflicts.

### Table 3-1. Orbit Class 12 "No Reports" Trend (Circular Orbit)

| Date | Percentage of Tasks | Percentage of Misses | Percentage of Conflicts |
|------|---------------------|----------------------|-------------------------|
| February 27 | 9 | 52 | 40 |
| April 15 | 6 | 42 | 28 |
| April 16 | 9 | 58 | 33 |

### Table 3-2. Orbit Class 10 "No Reports" Trend
### (Same Apogee but Smaller Perigee Than Orbit Class 12)

| Date | Percentage of Tasks | Percentage of Misses | Percentage of Conflicts |
|------|---------------------|----------------------|-------------------------|
| February 27 | 25 | 67 | 70 |
| April 15 | 31 | 36 | 60 |
| April 16 | 31 | 46 | 59 |

### Table 3-3. Orbit Class 37 "No Reports" Trend
### (Slightly Smaller Perigee and Much Larger Apogee Than Orbit Class 10)

| Date | Percentage of Tasks | Percentage of Misses | Percentage of Conflicts |
|------|---------------------|----------------------|-------------------------|
| February 27 | 22 | 100 | 50 |
| April 15 | 43 | 100 | 69 |
| April 16 | 57 | 100 | 86 |

### Table 3-4. Orbit Class 47 "No Reports" Trend
### (Similar Perigee and Larger Apogee Than Orbit Class 37)

| Date | Percentage of Tasks | Percentage of Misses | Percentage of Conflicts |
|------|---------------------|----------------------|-------------------------|
| February 27 | 63 | 100 | 100 |
| April 15 | 61 | 86 | 100 |
| April 16 | 67 | 92 | 94 |

### Table 3-5. Orbit Class 54 "No Reports" Trend
### (Similar Perigee and Larger Apogee Than Orbit Class 47)

| Date | Percentage of Tasks | Percentage of Misses | Percentage of Conflicts |
|------|---------------------|----------------------|-------------------------|
| February 27 | 60 | 100 | 100 |
| April 15 | 83 | 100 | 100 |
| April 16 | 71 | 100 | 100 |

In orbital terms, assuming similar perigees, higher apogees have greater eccentricities, resulting in faster velocities of the target past the radar. There are already known problems with detecting targets in highly elliptical orbits; these are supposed to be corrected in Vertical Release 96-1 by SCF 205-0124-95-072-PASMA, *Improved SSN STF Computation.*

Figures 3-1 through 3-3, which graph the magnitude of the "No Reports" site activity for all the orbit classes, present a different perspective for evaluation. Each orbit class is identified on the horizontal axis; the actual tally (not percentage) for each condition is on the vertical axis. Count represents the number of tasks that did not result in reports. The second row shows the number of misses; the third row shows the number of conflicts; and, fourth row the number of aborts (if there is a fourth row).

The "No Reports" percentages in Table 3-1 indicate that even though orbit class 12 looks best from a tasking-achieved perspective, more misses and conflicts occur in this class than any other. This trend, which holds true for all three days in Figures 3-1 through 3-3 is partly due to six analyst satellites that occur as "No Reports" for all three days. The IDs of these satellites were provided to the site analyst, Ms. Van Buskirk, per her request. The remaining satellites are in the catalog and none of them occurred repetitively; yet all were category 5, with tasking suffix G.

The cause of "No Reports" trends in orbit class 12 does not indicate what occurs in other orbit classes. For example, the "No Reports" trend in orbit class 47 shows that several catalog satellites occur repetitively. There is no parameter that indicates a specific cause; even the RCS values of the "repeat" satellites are in between the RCS values of satellites that do not occur repetitively. It is hoped that this trend is orbit-class based and confirms the site's difficulty in detecting highly elliptical targets that will be alleviated by the aforementioned SCF, *Improved SSN STF Computation.*

These figures show that there are tasking requests in many orbit classes that result in "No Reports" for all three days. The "No Reports" orbit classes that occur in these three days and as noted during the site visit for the 30 July 1996 data appear to fall in two distinct clusters if they are grouped by similar perigees and apogees. One cluster is composed of orbit classes 3, 6, 7, 9, 10 ,11, and 12, four of which are circular orbits. Another larger cluster is made up of orbit classes 24, 36, 37, 41, 46, 47, 52, 53, 54, 55, 56, 57, and 58, which have orbits with an apogee greater than 30,000 km and/or a perigee less than 575 km. Orbit classes not within these two clusters had minimal impact.

## 3.2   Results from "Orbit Class Statistics" Query

The "Orbit Class Statistics" query provides a high-level view of site activity. For example, the unusually high number of misses and conflicts in orbit class 12 are apparent by comparing to performance in other orbit classes. Orbit class 6 was similar to 12 in the number of tasking requests and resulting reports, but had many fewer misses and less than half the conflicts, as shown in Figure 3-4 for 15 April 1996.
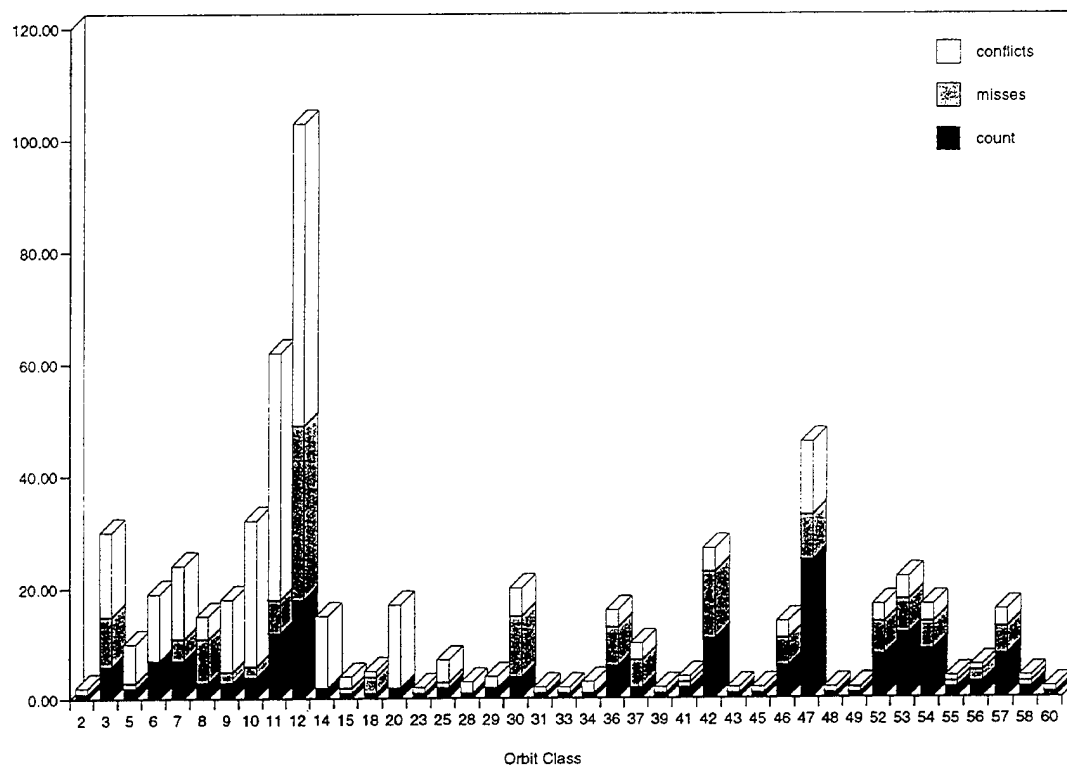
114

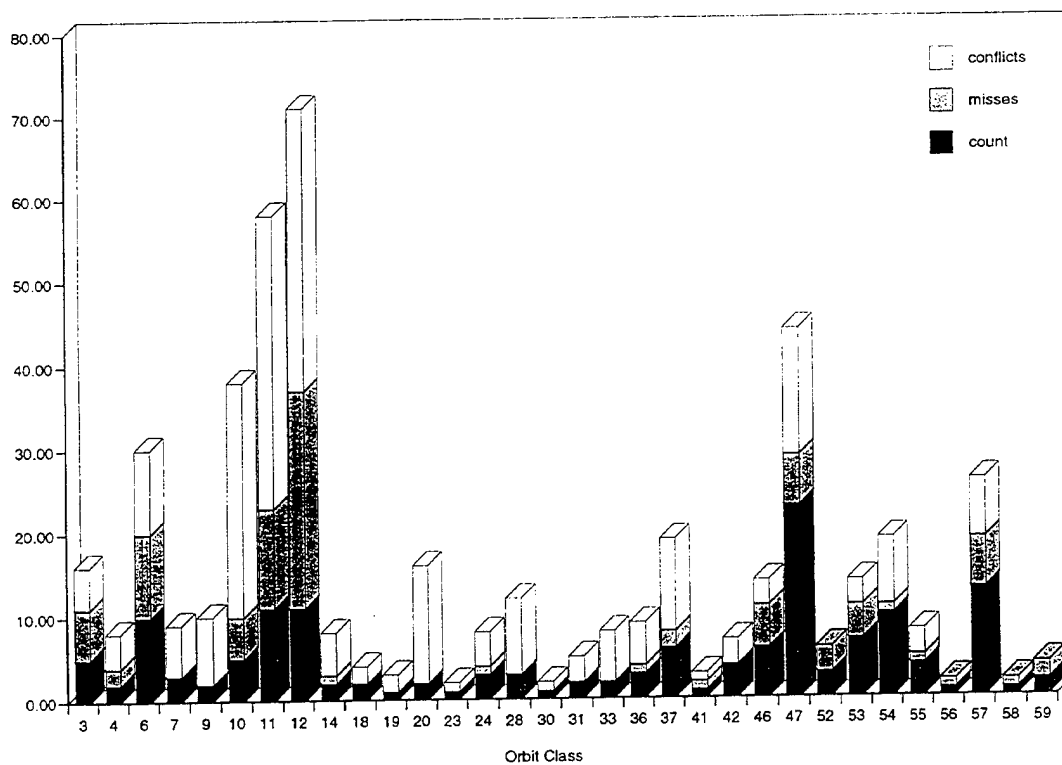Figure 3-1. "No Reports"- 27 February 1996
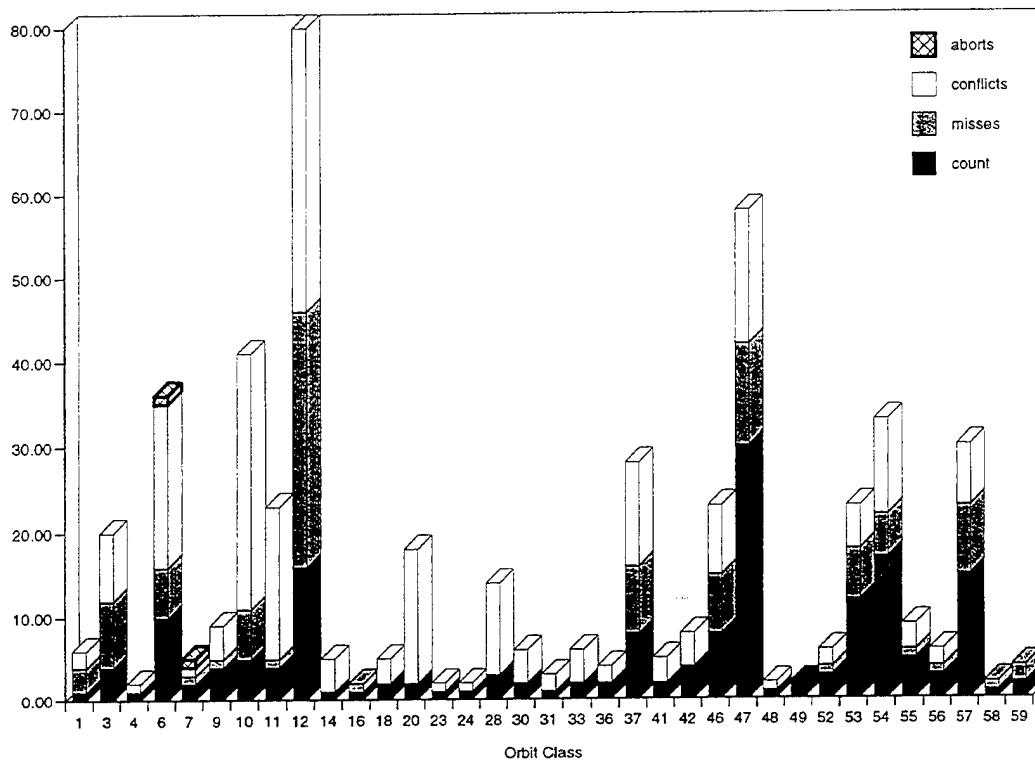


Figure 3-2. "No Reports" - 15 April 1996

115

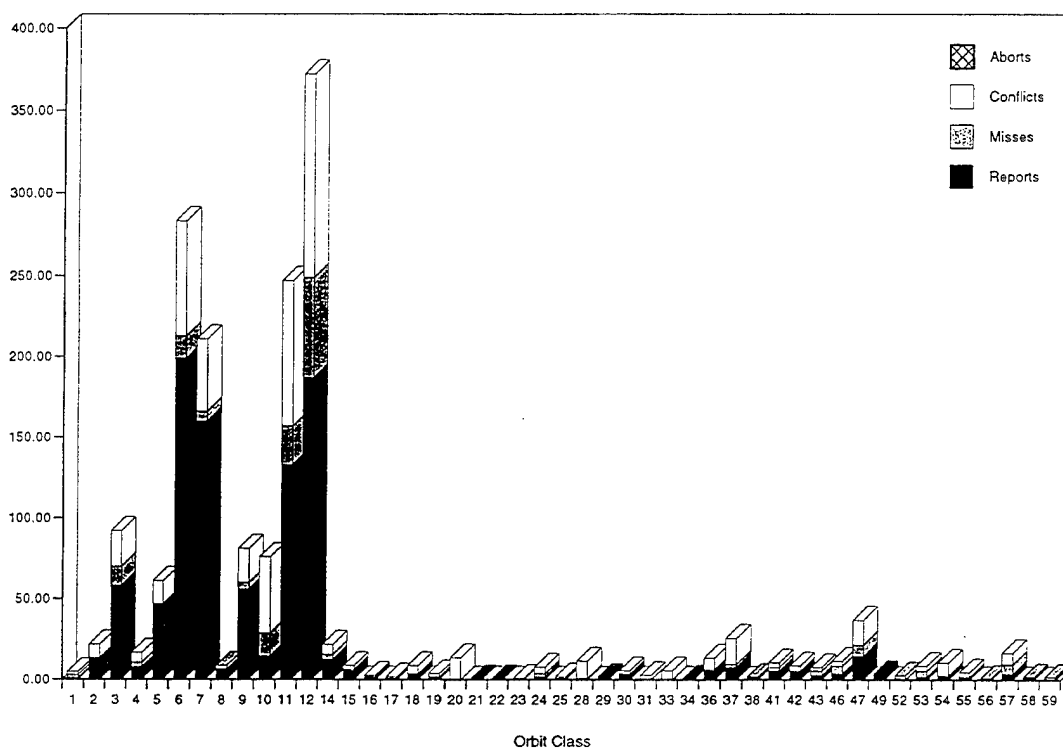Figure 3-3. "No Reports" - 16 April 1996



Figure 3-4. Orbit Class Statistics - 15 April 1996

116

## 3.3 Results from "No Attempts" Query

The "No Attempts" query indicates when the site does not respond to a task. From the four days of data, this happened infrequently. The highest daily tally was 14 "No Attempts" that occurred on 27 February 1996.

A time-consuming, previous investigation attributed nonacheivement of some tasks at the site to "No Attempts." The PPTMT results, however, show this is not happening now, even though the site is working off a bigger task load than at the time of the previous investigation.

## 3.4 Site Activity Summary

Each query of the PPTMT provides different insight into the site activity that occurs in response to tasking:

1. The "No Reports" query revealed that taskings resulted in several orbit classes to repeatedly undergo site activity that did not result in reports. This means tasking requests were not achieved. Five specific significant drivers are orbit classes 10, 12, 37, 47, and 54. Grouping all orbit classes by apogee and perigee that repeatedly have "No Reports" indicates there are two dominant clusters.

2. The "Orbit Class Statistics" query provides a high-level view of all site activity attempting to achieve the entire tasking list. This permits relative comparison between orbit classes and identification of the ones that are the worst performers.

3. Site non-responsiveness to a task occurs infrequently as shown by results from the "No Attempts" query.

# Section 4

# Conclusions and Recommendations

We consider the PPTMT project a major success. A valuable tool was provided to site analysts, and even a very limited analysis of site trends identified correctable problems.

The current functionality of PPTMT reveals trends in the "No Reports" query that indicate two dominant clusters to investigate.

1.  Hopefully, the cluster containing highly elliptical targets (apogees greater than 30,000 km and/or perigees less than 575 km) will be eliminated by the SCF titled, *Improved SSN STF Computation*, because the algorithm will correctly compute the short term fence and beam revisit rates tailored to each satellite's orbit.

2.  No specific SCF is planned that corrects the inability to track objects in the other cluster, but insight gained by using PPTMT will enable analysts to identify changes to mitigate this problem area. For example, six analyst satellites that caused many misses and conflicts in orbit class 12 were not tracked. If the site consistently cannot track these objects, analysts can request that SPADOC not task these objects, resulting in fewer misses and conflicts, and freeing time and energy to allocate to other taskings.

To increase the tasking response rate at the site, an evaluation should be done to find what conditions drive tasks not being achieved, concentrating on the troublesome orbit classes found by the PPTMT queries. It should consider the interaction of the tasker and site in recommending deletion of objects to be tasked and potential site modifications. The site should provide feedback to SPADOC on tasks considered technically unachievable (e.g. where the RCS is too small to be detected at range of target) or difficult to achieve, but for which the probability to detect can be increased (e.g. by providing more accurate orbit parameters) so that tasking requests can be adjusted to match sensor capabilities more closely. If the task appears achievable, the site should determine what is preventing it from being achieved. The reason may be non-optimum resource management, latent anomalies in sensor functionality, unresolvable sensor operational conflicts, etc.

PPTMT can be used not only to find general response inefficiencies, but to track performance and identify problems as they arise. Daily metric trends can be provided by using PPTMT after the site has finished responding to the tasking list each day. The trends will establish what a typical amount of sensor activity is. Large deleterious deviations from this should trigger investigation to determine whether the cause is due to unusual operational demands (tasking for a rarely requested object, an expedited change in site-configuration, etc.) or a specific site problem (such as equipment failure, a latent software anomaly, etc.)

As built, the PPTMT is an effective tool. Modifications could, however, provide more detailed insight into causes of inefficiencies. More specific causes of misses and conflicts should eventually be revealed by combining other types of data in PPTMT that have not been provided but reveals more details, such as higher priority activities where conflicts occur, situations where misses occur, and impact of data interdependencies on tasking throughput (e.g. effect of conflicts on misses). Such capabilities could be readily added by the MITRE team that built the original PPTMT tool.

# Appendix A
# Satellite Catalog File Lister (SATLST)

The appendix has been taken from Section 5 of the *Theory of Operation/Users Manual for Software Support Tools, Pave Paws Upgrade Program*, MU G432883-1 (Revision C, 8 July 1991), 21 April 1992, Raytheon Company.

## 5.6    Satellite Catalog File Lister (SATLST)

SATLST reads the reformatted Satellite Catalog and Produces a report of unclassified satellite characteristics.

This reformatted Satellite Catalog file is produced by the FMATER tool.  The SATLST run procedure gives the user the option to run FMATER prior to running SATLST.  If the user elects to run FMATER, after FMATER completes, the user must re-initiate the SATLST run procedure, answer 'N' to the FMATER prompt, and use the FMATER output as input.

The SATLST tool prompts for three inputs.  The first is the account where the input file exists, the second is the input file name, and the third is the option to review the submit file.

The submit file will attach and/or define all files needed, including the SATLST absolute from the library SSTLIB, and execute SATLST.

SATLST begins by opening the input file, reading a record, and opening the output file.  The remainder of events described will repeat until the input file end-of-file is reached

The first check made on the Satellite data is its classification.  If it is unclassified, a series of checks is done to see if it qualifies as an RWLIT candidate.  The criteria for RWLIT candidates are as follows:

| Avg. RCS | $\geq$ | 1 square meter | | |
|---|---|---|---|---|
| 20 deg | $\leq$ | Inclination | $\leq$ | 160 deg |
| 100 km | $\leq$ | Perigee | $\leq$ | 400 km |
| 600 km | $\leq$ | Apogee | $\leq$ | 2500 km |

If the satellite is determined to be an RWLIT candidate, the RWLIT field is flagged with a '*', otherwise it is left blank.  All of the data is written to an output record and formatted.  If the satellite classification is confidential or secret, the Launch designator is set to '**CCCC**' or '**SSSS**', respectively.  Then a check is done for an RWLIT candidate, the same way as the unclassified satellite.  Although, in this case, only the RWLIT field, sequence number, Satellite ID, and Launch Designator are written to the output record.

SATLST reads the next record from the input file (unless end-of-file is reached).  Once the end-of-file has been reached, the input and output files are closed.  Control is then returned to the SATLST run procedure which routes the output file and a dayfile of the procedure to the Wait Cue.

121

## 5.6.1    Preparation/Special Instruction

As mentioned earlier, the SATLST input file is produced by the FMATER tool.  Therefore, the option has been provided for the user to run FMATER prior to running SATLST.  If the option to run FMATER is selected, FMATER must complete execution and then SATLST will have to be re-initiated using the FMATER output file as input.

## 5.6.2    Inputs

User Specified –   Reformatted Satellite Catalog file (generated by the FMATER tool).

## 5.6.3    Outputs

LISTING –          The report of unclassified satellite elements characteristics.  An example of this file is shown in Figure 5.6.3-1.

DAYFILE –          The dayfile from the SATLST run procedure.

| 1RW | SEQ NO | SAT ID | LAUNCH DESIG | ESN | EPOCH TIME (SEC.) | EP DAY (DAYS) | TOES | REVN | INCLIN | RGHT ASC | ECCEN | ARG PERI | MEAN ANOM | MEAN MOTION | APOGEE ALT | PERIGEE ALT | RCS (M2) |
|---|---|---|---|---|---|---|---|---|---|---|---|---|---|---|---|---|---|
| | 251 | 746 | 64006A | 107 | 825076972.244 | 54.5019936 | -0. | 7226 | 60.87 | 112. | .3116660 | 309. | 27. | 8.85970 | 6562. | 413. | 2.5 |
| | 252 | 750 | 64006C | 280 | 825333310.178 | 57.4688678 | 0. | 58926 | 60.83 | 210. | .2361520 | 348. | 7. | 10.38949 | 4589. | 398. | .1 |
| | 253 | 753 | 63049F | 470 | 825033628.060 | 54.0003248 | 0. | 58409 | 90.09 | 61. | .0033695 | 308. | 52. | 13.50487 | 1096. | 1045. | .1 |
| | 254 | 801 | 64026A | 379 | 825261619.795 | 56.6391180 | 0. | 62357 | 90.52 | 289. | .0051459 | 298. | 61. | 14.08473 | 902. | 827. | 1.6 |
| | 255 | 805 | 64026B | 460 | 825141435.277 | 55.2480935 | 0. | 61648 | 89.88 | 136. | .0039333 | 316. | 44. | 14.10997 | 884. | 828. | .4 |
| | 256 | 806 | 64026C | 168 | 825069692.298 | 54.4177349 | 0. | 64976 | 90.80 | 15. | .0052092 | 306. | 54. | 14.57206 | 739. | 665. | .1 |
| | 257 | 809 | 64026D | 774 | 825307390.781 | 57.1688748 | 0. | 62136 | 90.53 | 291. | .0051241 | 34. | 326. | 14.04356 | 916. | 842. | .2 |
| | 258 | 812 | 64031A | 804 | 825293271.139 | 57.0054530 | -0. | 64215 | 99.84 | 242. | .0006220 | 90. | 270. | 14.21874 | 824. | 815. | .3 |
| | 259 | 813 | 64031B | 798 | 825336072.984 | 57.5008447 | 0. | 64169 | 99.85 | 244. | .0005681 | 131. | 230. | 14.21285 | 825. | 817. | .4 |
| | 260 | 815 | 64031C | 478 | 825352454.505 | 57.6904457 | 0. | 64341 | 99.83 | 300. | .0012765 | 75. | 285. | 14.24233 | 820. | 802. | 8.1 |
| | 261 | 829 | 64038A | 659 | 825076721.019 | 54.4990859 | 0. | 945 | 60.85 | 62. | .3070229 | 339. | 11. | 8.95084 | 6429. | 412. | 3.2 |
| | 262 | 831 | 64038C | 466 | 825071175.230 | 54.4348985 | 0. | 8574 | 60.75 | 180. | .2300864 | 43. | 333. | 10.52780 | 4439. | 392. | .2 |
| | 263 | 840 | 60007D | 379 | 825281132.175 | 56.8649557 | 0. | 86590 | 66.67 | 213. | .0143317 | 97. | 265. | 14.72784 | 753. | 551. | .0 |
| | 264 | 841 | 60007E | 486 | 825143908.536 | 55.2767192 | 0. | 86690 | 66.67 | 165. | .0136600 | 66. | 296. | 14.75737 | 739. | 547. | .0 |
| | 265 | 862 | 64047B | 486 | 824761301.185 | 50.8483933 | 0. | 3115 | 16.20 | 272. | .7125493 | 217. | 61. | 2.05084 | 38437. | 1144. | .9 |
| | 266 | 869 | 64049D | 175 | 825242590.301 | 56.4188692 | 0. | 15933 | 68.21 | 187. | .7086997 | 140. | 303. | 2.01492 | 38866. | 1335. | 5.7 |
| | 267 | 870 | 64051A | 168 | 825212078.613 | 56.0657247 | 0. | 59527 | 79.89 | 62. | .0099594 | 163. | 197. | 13.89368 | 1004. | 858. | .6 |
| | 268 | 871 | 64051B | 572 | 825065826.289 | 54.3729895 | 0. | 59828 | 79.89 | 6. | .0092899 | 29. | 332. | 13.94820 | 980. | 844. | 1.7 |
| | 269 | 876 | 64053A | 168 | 825310465.587 | 57.2044628 | 0. | 67052 | 65.06 | 102. | .0165888 | 270. | 88. | 14.58907 | 814. | 579. | 14.5 |
| | 270 | 877 | 64053B | 856 | 825299030.600 | 57.0721134 | 0. | 66740 | 65.07 | 283. | .0087818 | 279. | 80. | 14.54816 | 772. | 648. | 5.1 |
| | 271 | 893 | 64063A | 154 | 825077606.207 | 54.5093311 | 0. | 55211 | 90.14 | 236. | .0026537 | 140. | 220. | 13.55578 | 1072. | 1032. | 2.2 |
| | 272 | 897 | 64063B | 456 | 825335477.491 | 57.4939524 | 0. | 54878 | 90.14 | 233. | .0015965 | 296. | 64. | 13.52634 | 1074. | 1051. | .8 |
| | 273 | 898 | 64049E | 986 | 825347181.462 | 57.6294151 | 0. | 23095 | 68.20 | 192. | .7158832 | 144. | 298. | 2.00764 | 39166. | 1163. | 11.9 |
| | 274 | 899 | 64064A | 361 | 825286096.259 | 56.9224104 | 0. | 57707 | 79.69 | 326. | .0121586 | 146. | 215. | 13.79625 | 1055. | 876. | .9 |
| | 275 | 900 | 64063C | 988 | 825252652.158 | 56.5353259 | 0. | 55488 | 90.13 | 231. | .0026909 | 316. | 43. | 13.65051 | 1037. | 997. | .1 |
| | 276 | 901 | 64063D | 464 | 825111585.590 | 54.9026110 | 0. | 54845 | 90.14 | 232. | .0015184 | 298. | 62. | 13.53239 | 1072. | 1049. | 1.5 |
| | 277 | 902 | 64063E | 958 | 825280771.647 | 56.8607829 | 0. | 36050 | 90.14 | 233. | .0016083 | 314. | 46. | 13.52057 | 1077. | 1053. | .1 |
| | 278 | 903 | 64063F | 885 | 825111948.876 | 54.9068157 | 0. | 55496 | 90.12 | 225. | .0023260 | 292. | 68. | 13.66682 | 1029. | 994. | .0 |
| | 279 | 907 | 64064B | 164 | 825019061.736 | 53.8317331 | 0. | 57610 | 79.69 | 337. | .0123049 | 173. | 188. | 13.78487 | 1060. | 879. | 3.1 |
| | 280 | 932 | 64076B | 362 | 825194287.177 | 55.8598053 | 0. | 42250 | 81.34 | 183. | .1167632 | 322. | 31. | 12.56137 | 2352. | 526. | .7 |

**Figure  5.6.3-1    SATLST  Sample  Listing**

# Appendix B
# Task History List (TASKL)

The appendix has been taken from Section 5 of the *Theory of Operation/Users Manual for Software Support Tools, Pave Paws Upgrade Program*, MU G432883-1 (Revision D, 21 April 1991), 21 April 1992, Raytheon Company.

Cage Code   49956  
Doc. No.   MU G432883-1  
Rev. D      21 April 1991

## 5.10 Task History List (TASKL)

The TASKL tool reads the PAVE PAWS Task List File (TACT07) and produces two reports of Space Detection and Tracking System (SPADAT) Tasking statistics. As each satellite record is read from the TACT07 file it is written to the TASKL table. Once the reading of the TACT07 file is completed the TASKL table is sorted by Satellite ID in ascending order.

The first report created contains a sorted listing of all the Satellites in the TASKL table with its various tasking statistics. These tasking statistics include the tasking category and suffix as well as the number of aborts, reports, misses, and conflicts for each satellite for both the current day and prior day. The next report is the Exception List which contains a sorted list of all the satellites from the TASKL table that contain no reports for the current day. There will also be reports for all tasking sorted by category and suffix. Each category report will have a total of all tasking aborts, reports, misses, and conflicts for current day and prior day. The last report will contain a cumulative grand total of the above attributes for the entire tasking list.

### 5.10.1   Preparation/Special  Instructions

None.

### 5.10.2   Inputs

TACT07 -  Operator selected Task List File (TACT07).

### 5.10.1   Outputs

TASKLST - A report of Tasking Statistics. An example of the dayfile is shown in figure 5.10.3-1.

```
26 FEB 96                        *** TASKING TABLE SORTED BY SAT ID ***
PAGE   1

        SAT ID   CAT/SUF                      TODAY                                       YESTERDAY

    1    46       5G        ABT  0  REP  1  MIS  0  CON  0        ABT  0  REP  1  MIS  0  CON  0
    2    50       5G        ABT  0  REP  1  MIS  0  CON  1        ABT  0  REP  1  MIS  0  CON  1
    3    53       5G        ABT  0  REP  1  MIS  0  CON  0        ABT  0  REP  1  MIS  0  CON  1
    4    58       5G        ABT  0  REP  1  MIS  0  CON  0        ABT  0  REP  1  MIS  0  CON  1
         •                   •          •          •               •          •          •
         •                   •          •          •               •          •          •
         •                   •          •          •               •          •          •

26 FEB 96                        *** TASKING TABLE SORTED BY CAT/SUF ***
PAGE   2

    CAT/SUF      SAT ID                       TODAY                                       YESTERDAY


      2A         18362       ABT  0  REP  4  MIS  4  CON  3        ABT  0  REP  8  MIS  2  CON  2
      2A         19070       ABT  0  REP  9  MIS  3  CON  1        ABT  0  REP  3  MIS  9  CON  1
      2A         19223       ABT  0  REP  2  MIS  3  CON  2        ABT  0  REP  7  MIS  5  CON  0
      2A         19419       ABT  0  REP  6  MIS  4  CON  2        ABT  0  REP 10  MIS  3  CON  0
         •                    •          •          •               •          •          •
         •                    •          •          •               •          •          •
         •                    •          •          •               •          •          •
```

```
                                    ***CAT/SUFX SUMMARY***

                              TODAY                           YESTERDAY

        CAT/SUF      ABT    REP    MIS    CON      ABT    REP    MIS    CON
          2A          0      21     14      8        0      28     19      3


                                  ***CATEGORY STATISTICS***

                              TODAY                           YESTERDAY

        CAT      ABT    REP    MIS    CON      ABT    REP    MIS    CON
         1        0      4      0      2        0      0      0      0
         2        0     108    83     55        0     113     87     36
         3        0     264    77    300        0     258     69     321
         4        0     147    23     53        0     144     14     59
         5        1     652    42    254        0     662     45     276


        TOTALS    1    1175   225    664        0    1177    215     692
```

**Figure  5.10.3-1    TASKL  Report  Example**

125

# Glossary

| | |
|---|---|
| **abt** | abort |
| **alt** | altitude |
| **anom** | anomaly |
| **arg** | argument |
| **asc** | ascension |
| **cat** | catalog, category |
| **deg** | degree |
| **desig** | designator |
| **eccen** | eccentricity |
| **EP** | epoch |
| **ESC** | Electronic Systems Center |
| **ESN** | element set number |
| **ID** | identification |
| **inclin** | inclination |
| **km** | kilometers |
| **mis** | miss |
| **no** | number |
| **PC** | personal computer |
| **peri** | perigee |
| **PPTMT** | Pave Paws Tasking Metric Tool |
| **RCS** | radar cross section |
| **revn** | revolution |
| **SAT** | satellite |
| **SATCAT** | Satellite Catalog |
| **SATLST** | Satellite Tasking List |
| **SCF** | standard change form |
| **seq** | sequence |
| **SPADAT** | Space Detection and Tracking System |
| **SPADOC** | Space Defense Operations System |
| **SSN** | Space Surveillance Network |
| **STF** | Short Term Fence |
| **suff** | suffix |
| **TASKL** | Task List program |

Feasibility of Using GEODSS Data for Deep Space Anomaly Detection

C. C. Barnard, Daniel Eastman (Logicon RDA)

In cooperation with Phillips Laboratory Logicon RDA has examined the GEODSS data that has been archived by LL/MIT during the past three years. The purpose of this study is to determine if information could be obtained from the brightness data to aid in identification of the satellite, evaluate if the satellite is operating, or if it has changed its status. In the first phase of this effort the phase angle data was computed in two dimensions, longitude and latitude, and the data presented in three-dimensional graphs as a function of these two angles. The expectation was that characteristic signals or structure would be seen above the rms errors in the data. Unfortunately, these plots showed very little correlation and the rms fit to a quadratic surface was generally rather poor. This report addresses the question of whether the data contains a lot of 'noise' as a result of atmospheric and instrument variations, or is the variation in brightness caused by the features of the satellite to create a wide variation in the passive return as the illumination angle varies?

Under Phillips Laboratory funding over the past decade Logicon RDA has developed a very useful tool to simulate all aspects of system performance in the imaging of targets. This tool is called TASAT for Time domain Analysis Simulation for Advanced Tracking. TASAT is capable of modeling a variety of imaging systems engaging a variety of targets. It includes an extensively tested rendering package and uses detailed satellite models that are developed at the Satellite Assessment Center. It has as part of its code the ability to generate validated radiometrically correct imagery that has been anchored with experimental data. That capability has been used in this study to predict the passive return from GORIZONT-type satellites. Using a model available that had extremely fine detail to fractions of a meter, simulations were made of some of the GEODSS data and the results will be presented in this report. Another set of data was made available to us. This data was collected by Willet Beavers. He collected this data at the Fire Pond site outside Boston, Massachusetts, and took great care to accurately evaluate atmospheric and system variations to minimize noise in the data. This data is examined and presented in this report in a similar form as the GEODSS data, as three-dimensional graphs, and as a function of longitude and latitude phase angles.

TASAT is a very powerful computer software package with an extensive capability of modeling a complete active imaging system. For this application we are only concerned about modeling the passive illumination of a satellite. Of primary importance is the rendering routine and the detail of the satellite model. TASAT makes use of an extensive library of material properties including the Bi-directional Reflectivity Distribution Function (BRDF), reflectivities, and absorption. The render module and satellite model include information on surface roughness, shapes, and specular and scattered reflections. TASAT has a variety of options that have some effect on the imaging results. A parametric study was made to obtain the sensitivity of a few of the key options. The baseline case, BASE, models GORIZONT using a 256-square array size. Since a large number of runs will be needed to replicate the GEODSS data it may not be practical to run large 1024 array sizes demonstrated in case 'BIG'. With an array size of 256, computing time would be under an hour per case. All cases except 'AA2' use one ray per rendered pixel. Case 'AA2' will demonstrate the capability of using multiple rays in a pixel. An input file is used to define the quantum efficiency of the s-20 photomultiplier detector as a function of wavelength in all cases except 'FLAT'. One feature that was added to the Gorizont model is for the solar panel to automatically track the sun. This articulation is especially important at large longitude angles when the panels are turned to almost grazing angles and is used in all cases except 'NOART'. A summary of the case names and parameter studied is shown in Table 1. The key results from the image from each case is shown in Table 2. A copy of the TASAT rendering of the 1024x1024 case 'BIG' is shown in Figure 1.

Table 1. Parametric Run Names With Description of Parameter Examined

| Name | Parameters Changed |
|------|---------------------|
| BASE | 256 x 256 Array, One Ray/Pixel, S-20 QE, Solar Panel Articulated |
| BIG | 1024 x 1024 Array, One Ray/Pixel |
| FLAT | Flat Sensor Response, .40 - .90 Microns |
| NOART | No Solar Panel Articulation, No Solar Panel Texture |
| AA2 | Anti-aliasing, Up to Four Rays Per Pixel |
| MREFL | Multiple Reflections, Up to Three Reflections |
| DOWN5 | Satellite Pointed Down (South) From Nadir 5 Degrees |
| UP5 | Satellite Pointed Up (North) From Nadir 5 Degrees |

Table 2. Results of Parametric Run

| Name | S. Magnitude - Base | Peak/Base Peak |
|------|---------------------|----------------|
| BASE | 10.392517* | 1.0744165E-15* |
| BIG | 0.0040 | 0.09064 = 1.4502/16 |
| FLAT | -0.0616 | 1.3898 |
| NOART | 0.7033 | 1.0000 |
| AA2 | -0.0272 | 0.9990 |
| MREFL | -0.00192 | 1.1061 |
| DOWN5 | 0.0037 | 3.8794 |
| UP5 | 0.0106 | 2.1604 |
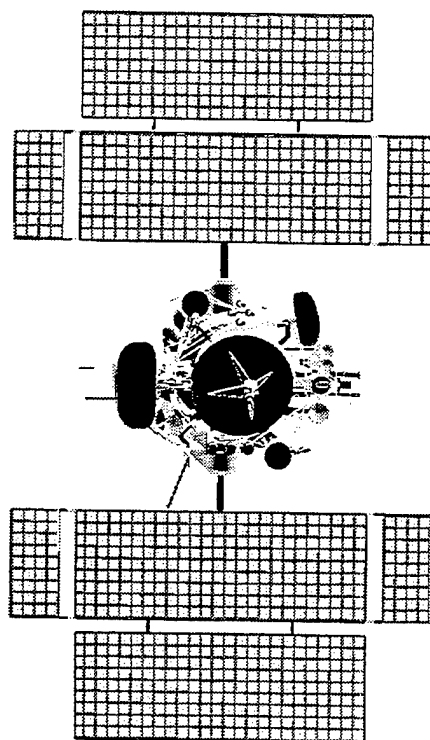


Figure 1. (BIG) 1024 x 1024 Rendering in TASAT

The second column in Table 2 is the difference in stellar magnitude from the baseline case. The third column is the ratio of the peak pixel to the baseline case. Note that for case BIG this ratio is shown adjusted by the difference in the area of the pixel (16). The examination of the above cases is a somewhat limited parametric study, but it does provide some confidence that the selected array resolution and other parameters should produce reasonably consistent results. We realize that there may be a case where multiple reflections, or a slight pointing change may result in a significant change in the stellar magnitude. A large number of renderings must be made with different longitude and latitude sun phase angles, and, based on the parametric studies, it is reasonable to proceed with the above simplifications to generate a full set of data that can be compared with the GEODSS data set.

A series of TASAT runs was made to predict the brightness at exactly the same illumination angles as the GEODSS data for three different Gorizont satellites: 20263, 20923, and 20953. Data for 20263 and 20953 were taken from the Diego Garcia site. 20923 data was taken from Maui. In order to present the TASAT computed magnitudes as 3-D graphs, the solar phase angle is split into the longitude and declination components. A spread sheet is used to compute this angle using the observer location, the satellite longitude, the date, and the time. The sun position is computed using a simple equation assuming circular earth orbit. This introduces some error as a result of the irregular elliptical orbit. TASAT uses a more exact computation of the earth and sun position as a function of date and time. The TASAT output includes the computation of the solar panel angle. The spread sheet also computes this angle which is not as accurate due to the simple model used. The difference of the solar panel angle from the two computations is directly related to the error in the spread sheet sun position. The largest error is about 6 degrees and most of the errors are less than 3 degrees.

The TASAT predictions are compared to the GEODSS data for satellite number 20263. Figure 2 is the TASAT results. The solid black squares are the TASAT magnitudes after normalizing to a 1 megameter range, consistent with the GEODSS data. The open squares are projections onto the three planes. The vertical drop lines connect the 3-D data points to the horizontal plane that locates the declination and longitude phase angle components for the point. Figure 3 shows the average GEODSS data superimposed with the best fit quadratic surface to the data. Note that the projected data for the TASAT magnitudes show a very compact curved line which suggests a strong dependency of magnitude to the longitude component of phase angle. Figure 4 is the difference from the TASAT magnitudes and the GEODSS data. In this plot negative numbers are points where the TASAT magnitude is brighter than the GEODSS data. Figure 5 is the difference from the GEODSS data and the quadratic fit surface where negative numbers are where the GEODSS magnitude is brighter than the fit surface. The range of the differences from the TASAT data is 6 magnitudes, the range from the fit surface is 4.5 magnitudes. A table showing a summary of the statistics of these fits will be presented after all the graphs.

Figures 6-9 show equivalent data plots for satellite 20923. Note that both Figures 6 and 7 show compact lines of projected points on the longitude component of the phase angle. The difference graphs are shown in Figures 8 and 9. In both the difference graphs a few points have a significant error, but many of the points form a tight group with errors less that a magnitude. This set of data shows some promise and note that this set is from Maui.

The results for satellite 20953 are shown in Figures 10 through 13. The difference plots are again at least as scattered as the data for 20263. Note that these two data sets were taken from Diego Garcia. A summary of the statistics from this data is shown in Table 3.
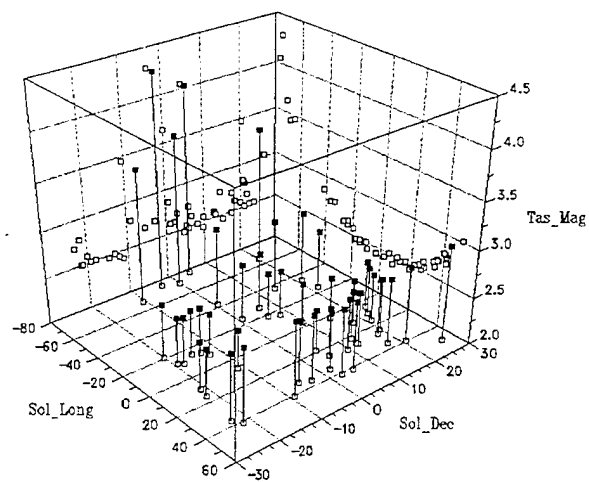
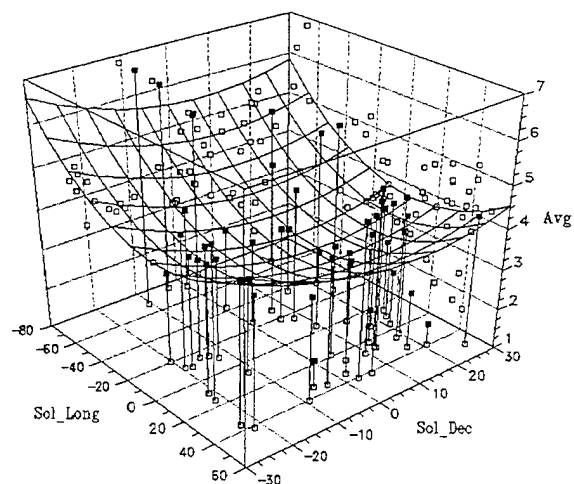Figure 2. 20263 TASAT Predictions



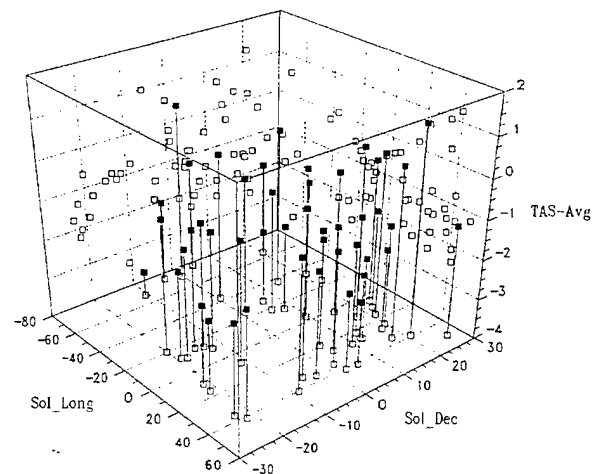Figure 3. 20263 GEODSS Average
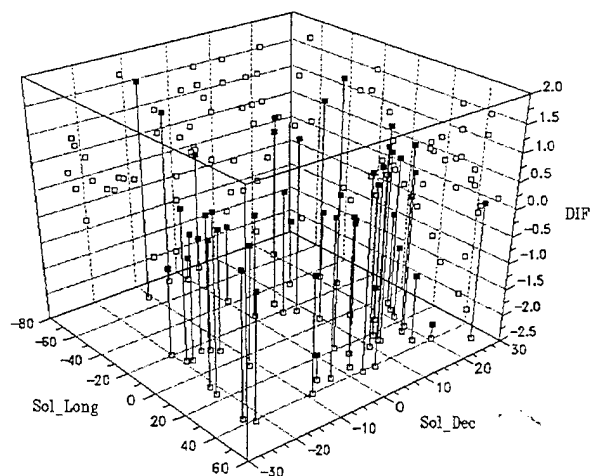


Figure 4. 20263 Diff. TASAT - GEODSS Avg.



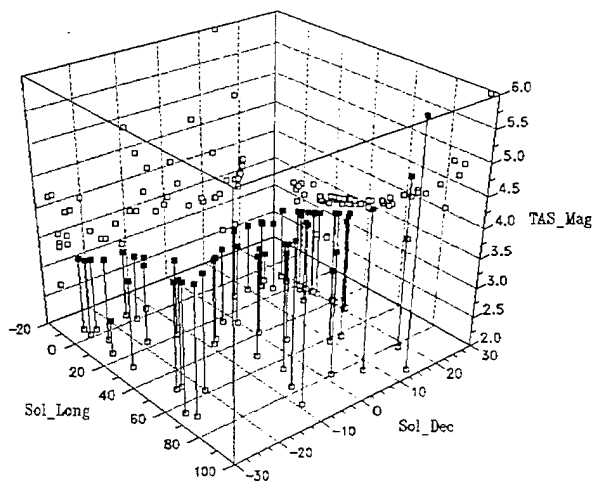Figure 5. 20263 Diff. GEODSS - Quad Fit



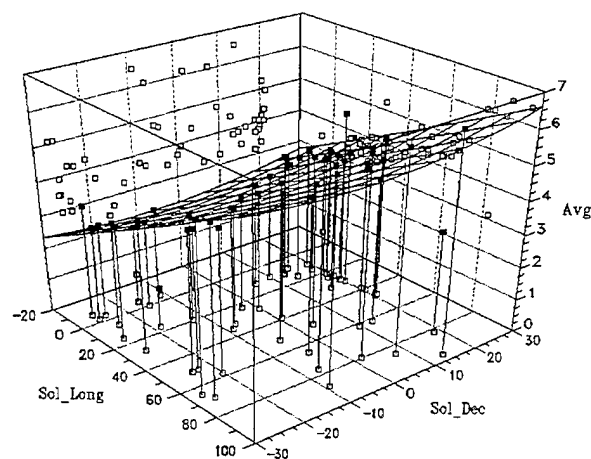Figure 6. 20923 TASAT Predictions
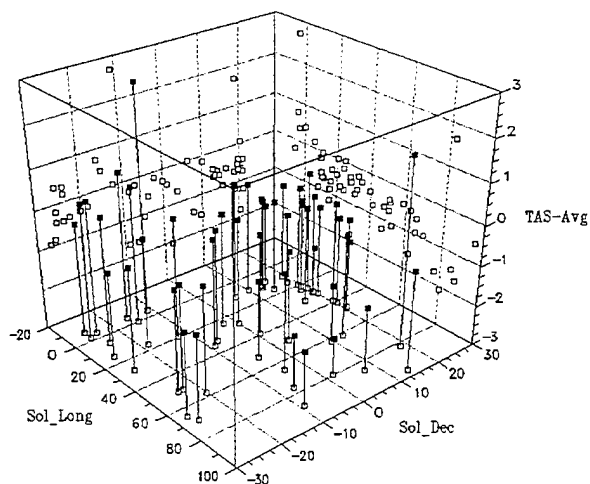


Figure 7. 20923 GEODSS Average
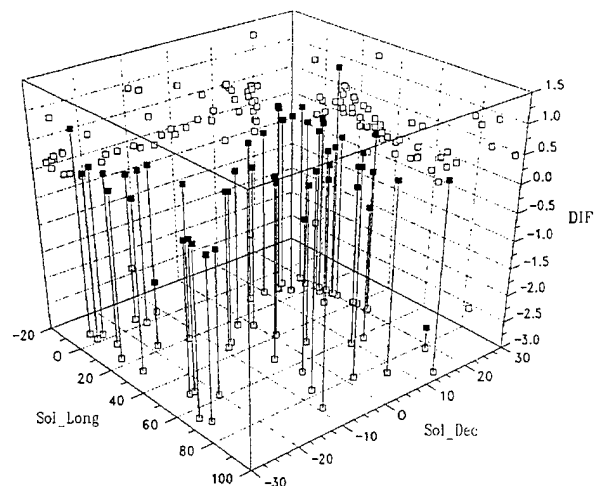
130

Figure 8. 20923 Diff. TASAT - GEODSS Avg.



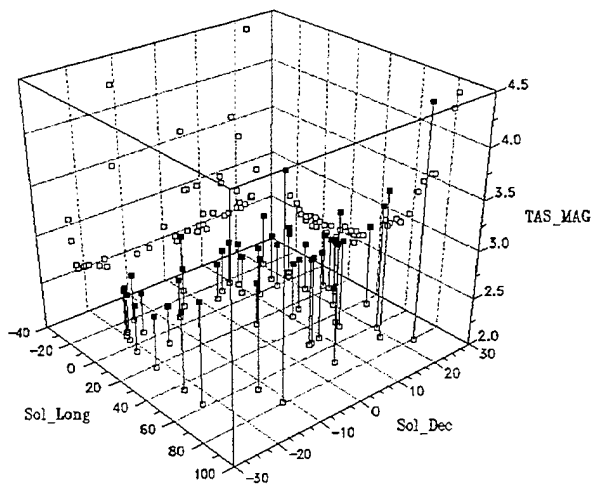Figure 9. 20923 Diff. GEODSS - Quad Fit



Figure 10. 20953 TASAT Predictions



Figure 11. 20953 GEODSS Average
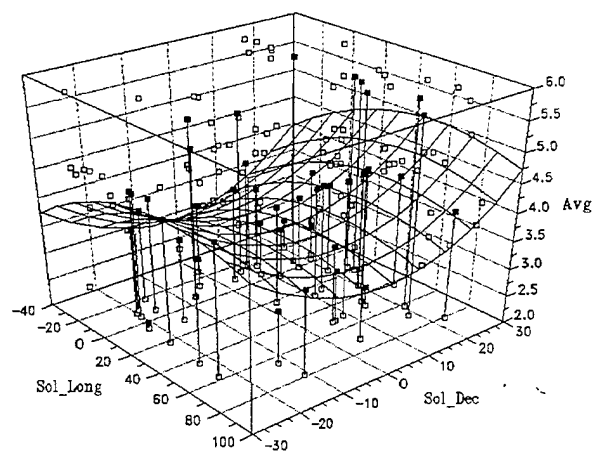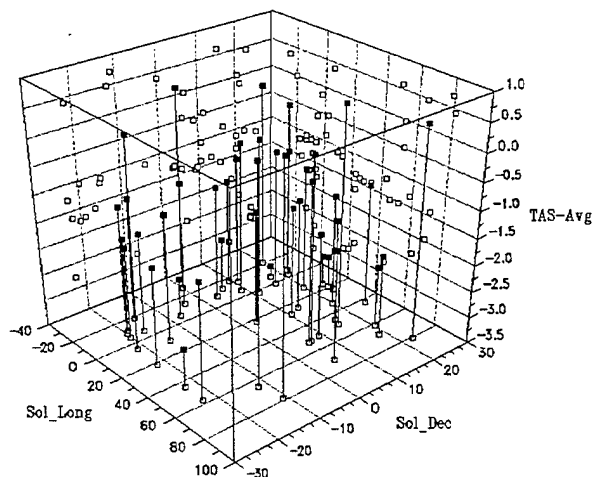


Figure 12. 20953 Diff. TASAT - GEODSS Avg.
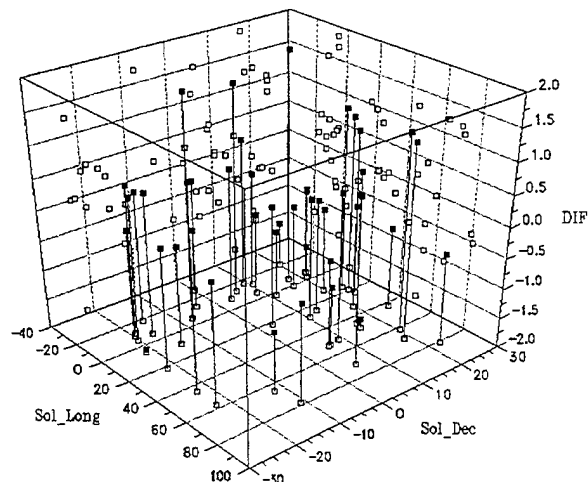


Figure 13. 20953 Diff. GEODSS - Quad Fit

131

Table 3. Statistics From Magnitude Differences

| Target | Data | Min | Max | Mean | St. Dev. |
|--------|------|-----|-----|------|----------|
| 20263 | GEODSS AVG | 1.55 | 6.825 | 3.699 | 1.091 |
| 20263 | QUAD DIFF | -2.234 | 1.644 | 0.0 | 0.957 |
| 20263 | TASAT DIFF | -3.380 | 1.255 | -1.143 | 0.984 |
| 20953 | GEODSS AVG | 2.10 | 5.75 | 3.962 | 0.972 |
| 20953 | QUAD DIFF | -1.950 | 1.864 | 0.0 | 0.904 |
| 20953 | TASAT DIFF | -3.258 | 0.710 | -1.2165 | 1.024 |
| 20923 | GEODSS AVG | 0.225 | 6.50 | 4.026 | 1.074 |
| 20923 | QUAD DIFF | -2.59 | 1.24 | 0. | 0.621 |
| 20923 | TASAT DIFF | -2.073 | 2.689 | -.481 | 0.792 |

The standard deviation of the fit data for 20923 is clearly better than that for the other two. Note that for 20953 the TASAT fit has a larger deviation than the GEODSS average data. This also suggests that the data from Maui, 20923, is better than the data for the other two taken from Diego Garcia. This is very strong evidence that the atmospheric conditions at Maui yield better quality data those that obtained at Diego Garcia. It would have been helpful if some measure of the atmospheric conditions were included in the raw data. This would have enabled a correlation of the difference to the atmospheric conditions. This could also enable the analyst to evaluate the reliability of each data point based on atmospheric conditions.

All three sets of TASAT difference data have a negative mean value indicating that the TASAT results are consistently a little brighter than the GEODSS data. This tendency for TASAT predictions to be a little brighter than measured satellite returns is not unusual. There have been reports that the material surfaces of a satellite in space are aged by micrometeorites, radiation, and vapor leakage, and that the brightness degrades as compared to satellite brightness when first launched. The table of material properties used in TASAT is occasionally updated as new reflectivity and BRDF data is made available.

Part of the difficulty with the analysis of this data is finding a way to display the data in a way that one of the best data processors, the eye, can visualize the data. One of the capabilities of PSIPLOT is to generate a surface to fit the data. This can also be used to generate a contour plot of the data. The next set of figures, 14 through 16, are graphs of the average GEODSS data for 20263, 20923, and 20953 using this format. Note that the thicker contour lines represent the lower, brighter, magnitudes.

The Beavers data is next examined to see if data collected with more rigorous control of noise will display characteristic patterns when presented in 3-D plots. The quadratic fit plots used for the GEODSS data did not help with visualizing any structure in the Beavers magnitude data. A variety of formats were tested for presenting this data. The selected format uses a surface fit to a uniform grid pattern. This surface is shown with a hollow grid pattern which does not block out the plotted points. After the surface is generated then a contour plot can be generated and displayed with the 3-D surface plot. Following is one of the plots for the M_V Beavers data collected for the Cosmos satellites, Figure 17, and an INTELSAT satellite, figure 18. The M_V data is taken using the standard astronomical V based and corrected to a standard distance of 36000 km.
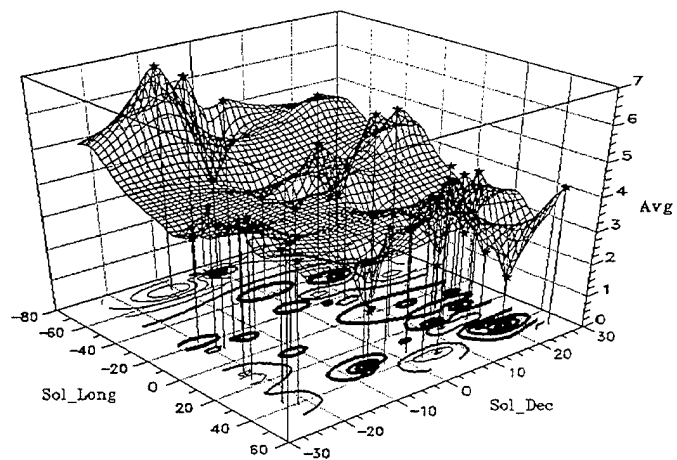
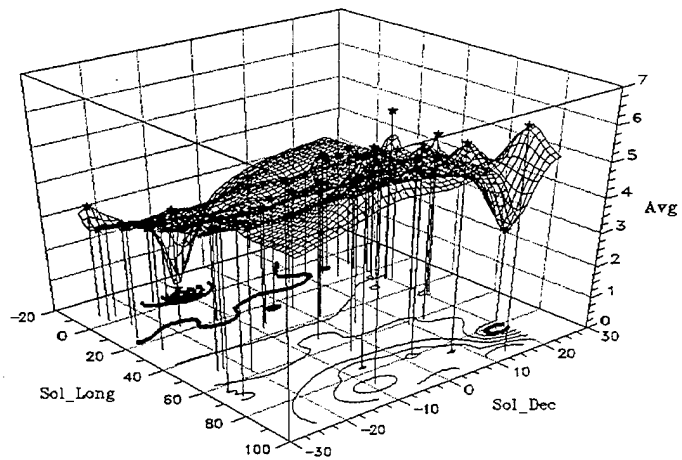Figure 14.  Surface Fit and Contour Plot for 20263 Average GEODSS Data



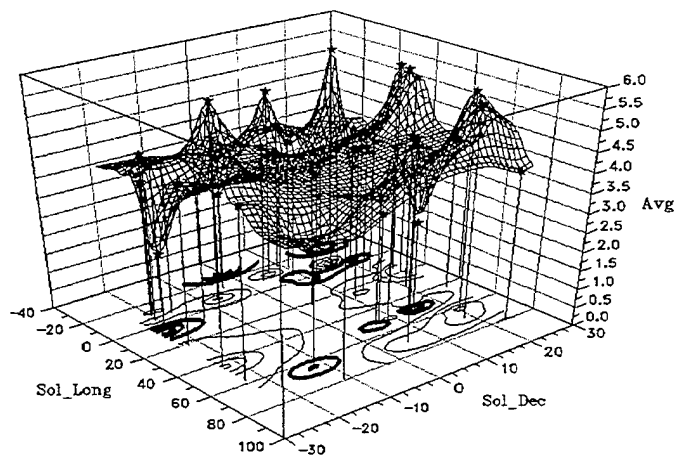Figure 15.  Surface Fit and Contour Plot for 20923 Average GEODSS Data



Figure 16.  Surface Fit and Contour Plot for 20953 Average GEODSS Data
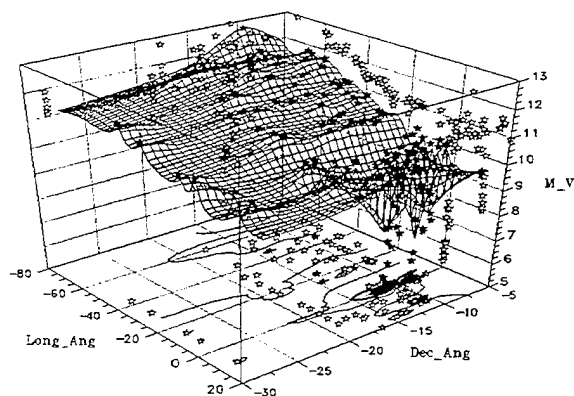
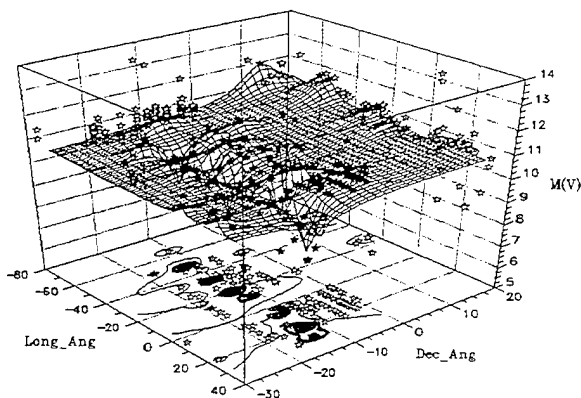133

Figure 17.  Surface Fit to 18384 COSMOS-1          Figure 18.  Surface Fit to 21653 INTELSAT-60

In order to compare data it would be helpful to show each of the magnitudes in the same phase angle component grid.  In Figures 19 through 23, each of the M(v) results are shown as contour plots using the same grid size.  The Cosmos results are shown in order of the longitude position which is included in each figure label.  Note that each of the Cosmos graphs show bright returns at about the same phase angles, -10 to +10 degrees longitude and -20 to 0. degrees declination.  22112 shows the most concentrated bright zone and it is at 0. degrees declination, a little higher than the others.  18384 shows a fairly close pattern of bright zones around -10. degrees declination.  The other two, 21789 and 20391, show a few bright zones between -10. and -20. degrees declination.  The position of these bright zones in the phase angle coordinates should be a good indication of the pointing direction of the satellite.  This data suggests that 22112 is pointed at a more northerly direction than the others.  21789 and 20391 appear to be pointed in a more southerly direction and the separate bright zones suggest that they may be pointing at different directions at different times.  Both 22112 and 18384 lack data points just above the bright zones.  The apparent concentration of this bright zone may be a result of the lack of data.  This data void makes comparisons of the data difficult and the above suggestions are not conclusive.

The bright zones from 21543, INTELSAT, are different from the Cosmos pattern.  The INTELSAT magnitudes form a trough-like pattern along a constant declination angle.  Note that this contour plot does not have vertical contour lines suggesting that the data points are flat or scattered along the longitude axis.  The vertical contour lines, and the projections onto the longitude plane in previous surface plots, suggest a strong dependency of magnitude to the longitude component for the Cosmos satellites.

The objective of this analysis was to determine if the GEODSS data, when examined using two-dimensional phase, contains characteristic signals or structure that can be used for identification or evaluation of operational status. The data presented in Table 3 indicates that for two of the cases studied, 20263 and 20953, the variation of the data did not decrease significantly when differenced by either the quadratic or TASAT data.  The results for satellite 20923 did show some reduction of the variation in the data when the quadratic or TASAT data was applied.  The difference plots for satellite 20263 in Figures 4 and 5 show scattered points that look more like random noise than a characteristic pattern.  The difference plots for satellite 20923 in Figures 8 and 9 show most of the points forming well-grouped projections on both planes.  There are several data points that are significantly separated from the group.  Unfortunately the data points are widely separated and it is not readily determined if these points are some kind of characteristic of the target or noise in the data.  The difference plots for satellite 20953 were shown in Figures 12 and 13.  The difference with the quadratic fit appears like random noise in both planes.  Many of the points in the TASAT difference plot are scattered like random noise.  Some of the points form a group between -1 and -1.5.  This suggests that some of the data is comparable to the TASAT predictions.  The many points outside the group appear more like scattered noise than characteristic signals.  Since the data is widely separated in phase

134

angle space there are few clustered points that would suggest a consistent localized signal. The surface fit combined with contour plots that were shown in Figures 14 through 16 help to visualize the data. Note that most of the brighter regions of the surface plots (dark rings in the contour plots) are generated by single data points. The sample of GEODSS data that was examined here does not show clear indications of significant signature data.

The results from examination of the Beavers data does show some patterns that suggest characteristic signature information. The contour plots in Figures 19 through 22 show characteristic bright zones in somewhat different locations in the two-dimensional phase angle space. This suggests the potential to evaluate the pointing direction of the satellite. Also the bright zone from the INTELSAT contour plot shows different characteristics than the four Cosmos contour plots.

These results show some potential for carefully obtained passive data to be useful for obtaining some information about the satellite. The GEODSS data as it currently is generated and saved is of limited use for this purpose. There is some potential for this data to be more useful with some upgrades to the data collection and storage. If the GEODSS process could be upgraded to mimic the process and quality of the Beavers data then the resulting data should be very useful for obtaining characteristic information. The quality of the data from Maui was better than the data from Diego Garcia. It is not certain if this data is better because of the atmospheric conditions at Maui or the operational system of data collection and storage.

One of the problems with this data is the uncertainty of the accuracy of each data point. It would be useful if some form of measure of uncertainty could be evaluated based on atmospheric conditions and stored with the data. Then the analyst could weight or discard the data points that have high uncertainty and then have more confidence that points that diverge from the majority of the data are characteristic features and not noise. Saving some form of uncertainty data would make this data more useful for this type of analysis and should not require a major change to the data collection process.

Some information on the atmospheric conditions could be obtained from the raw data. The first step in the data reduction process for this effort was to extract a mean, minimum, and maximum magnitude from the raw data. The raw data is a massive data file with each set containing about three minutes of data sampled at a rate of 100 Hz. Some indication of the reliability of the data could be obtained by examination of the data. High frequency variations are most likely atmospheric effects. Many of the data sets show flat lines with various levels of high frequency variation. This variation could probably be used to estimate the atmospheric turbulence, or $Cn^2$ profile. Some sets show a significant low frequency variation. Some show magnitude increases from a baseline magnitude which are probably caused by clouds. Some data shows time sections where the magnitude drops below a level baseline. These could be potential short duration glints, or are they clear sections in thin clouds? Even with this raw data it is not obvious when magnitude fluctuations are real variations in the satellite magnitudes, or variations in atmospheric conditions.
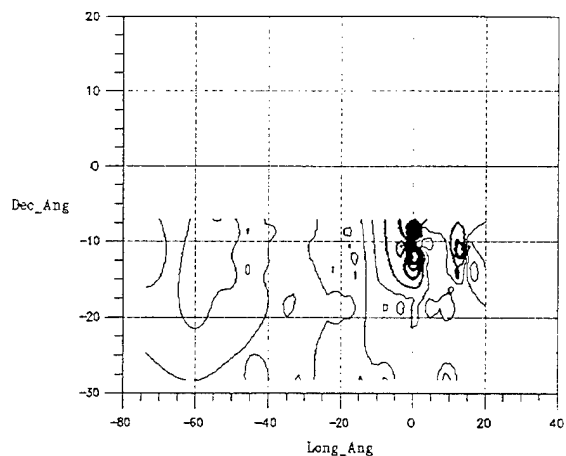
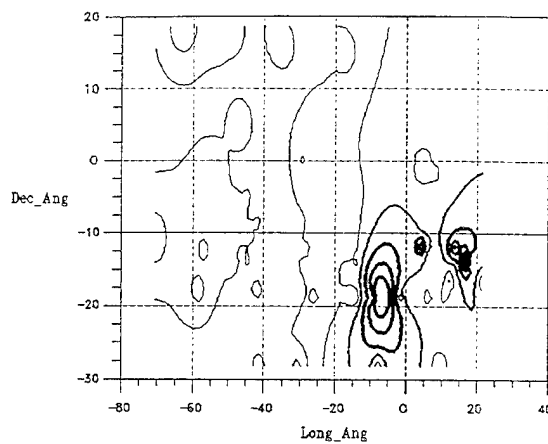Figure 19. 18384 at 12.03 deg Longitude



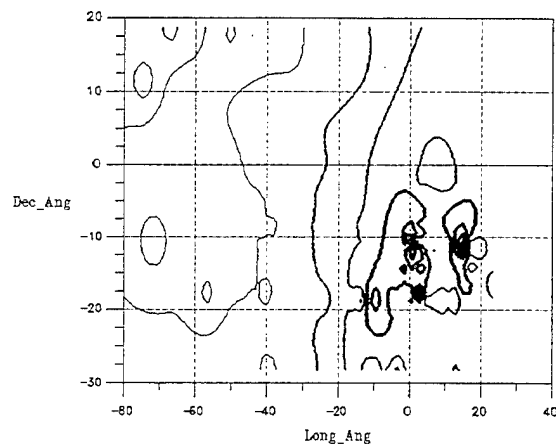Figure 20. 21789 at 13.94 deg Longitude
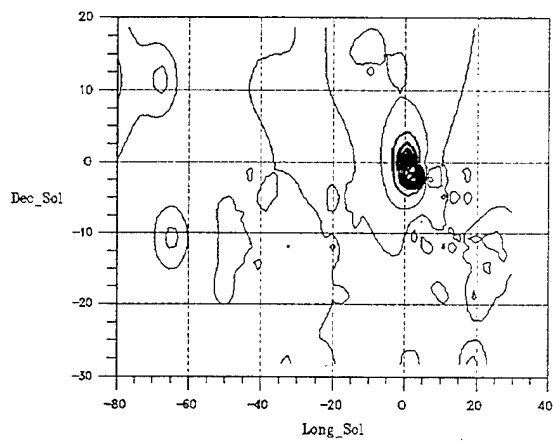


Figure 21. 20391 at 14.32 deg Longitude



Figure 22. 22112 at 24.75 deg Longitude



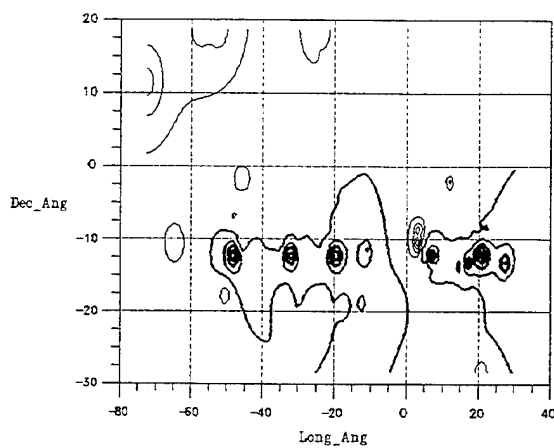Figure 23. 21653 INTELSAT at 24.51 deg Longitude

# REPORT DOCUMENTATION PAGE

| 1. AGENCY USE ONLY (*Leave blank*) | 2. REPORT DATE<br>27 March 1997 | 3. REPORT TYPE AND DATES COVERED<br>Project Report |
|---|---|---|

**4. TITLE AND SUBTITLE**

Proceedings of the 1997 Space Control Conference

**6. AUTHOR(S)**

L.B. Spence (Editor)

**5. FUNDING NUMBERS**

C — F19628-95-C-0002
PR — 77

**7. PERFORMING ORGANIZATION NAME(S) AND ADDRESS(ES)**

Lincoln Laboratory, MIT
244 Wood Street
Lexington, MA 02173-9108

**8. PERFORMING ORGANIZATION REPORT NUMBER**

STK-249 Volume II

**9. SPONSORING/MONITORING AGENCY NAME(S) AND ADDRESS(ES)**

ESC
Hanscom Air Force Base
Bedford, MA 01730

**10. SPONSORING/MONITORING AGENCY REPORT NUMBER**

ESC-TR-97-063

**11. SUPPLEMENTARY NOTES**

None

**12a. DISTRIBUTION/AVAILABILITY STATEMENT**

Approved for public release; distribution is unlimited.

**12b. DISTRIBUTION CODE**

**13. ABSTRACT (*Maximum 200 words*)**

The fifteenth Annual Space Control Conference (formerly called Space Surveillance Workshop) held on 25–27 March 1997 was co-hosted by MIT Lincoln Laboratory and Phillips Laboratory and provided a forum for space control issues. This *Proceedings* documents some of the presentations, with minor changes where necessary.

**14. SUBJECT TERMS**

**15. NUMBER OF PAGES**
143

**16. PRICE CODE**

| 17. SECURITY CLASSIFICATION OF REPORT<br>Unclassified | 18. SECURITY CLASSIFICATION OF THIS PAGE<br>Unclassified | 19. SECURITY CLASSIFICATION OF ABSTRACT<br>Unclassified | 20. LIMITATION OF ABSTRACT<br>Same as report |
|---|---|---|---|